ISSN 0038-531X

Russian Original Vol. 58, No. 4, April, 1985

October, 1985

SATEAZ 58(4) 243–338 (1985)

SOVIET ATOMIC ENERGY

АТОМНАЯ ЭНЕРГИЯ
(ATOMNAYA ÉNERGIYA)

TRANSLATED FROM RUSSIAN

CONSULTANTS BUREAU, NEW YORK

SOVIET ATOMIC ENERGY

Soviet Atomic Energy is abstracted or indexed in *Chemical Abstracts, Chemical Titles, Pollution Abstracts, Science Research Abstracts, Parts A and B, Safety Science Abstracts Journal, Current Contents, Energy Research Abstracts,* and *Engineering Index.*

Mailed in the USA by Publications Expediting, Inc., 200 Meacham Avenue, Elmont, NY 11003.

POSTMASTER: Send address changes to *Soviet Atomic Energy,* Plenum Publishing Corporation, 233 Spring Street, New York, NY 10013.

Soviet Atomic Energy is a translation of *Atomnaya Energiya,* a publication of the Academy of Sciences of the USSR.

An agreement with the Copyright Agency of the USSR (VAAP) makes available both advance copies of the Russian journal and original glossy photographs and artwork. This serves to decrease the necessary time lag between publication of the original and publication of the translation and helps to improve the quality of the latter. The translation began with the first issue of the Russian journal.

Consultants Bureau journals appear about six months after the publication of the original Russian issue. For bibliographic accuracy, the English issue published by Consultants Bureau carries the same number and date as the original Russian from which it was translated. For example, a Russian issue published in December will appear in a Consultants Bureau English translation about the following June, but the translation issue will carry the December date. When ordering any volume or particular issue of a Consultants Bureau journal, please specify the date and, where applicable, the volume and issue numbers of the original Russian. The material you will receive will be a translation of that Russian volume or issue.

Subscription (2 volumes per year)
Vols. 56 & 57: $560 (domestic), $621 (foreign)
Vols. 58 & 59: $645 (domestic), $715 (foreign)

Single Issue: $100
Single Article: $9.50

CONSULTANTS BUREAU, NEW YORK AND LONDON

c/b
233 Spring Street
New York, New York 10013

Published monthly. Second-class postage paid at Jamaica, New York 11431.

SOVIET ATOMIC ENERGY

A translation of *Atomnaya Énergiya*

October, 1985

Volume 58, Number 4 April, 1985

CONTENTS

	Engl.	Russ.
ARTICLES		
^{129}I Content in the Coolant of a Water-Cooled–Water-Moderated Reactor — L. I. Gedeonov, V. M. Gavrilov, V. K. Vinogradova, S. P. Rosyanov, and Yu. A. Shumov	243	221
RITM Facility for Testing Fuel Elements in Variable Power Regimes in the SM-2 Reactor — V. A. Kuprienko, A. V. Pershin, Yu. G. Spiridonov, V. Sh. Sulaberidze, and V. N. Shulimov	246	223
Heat Removal in Fast Reactor Cores — A. V. Zhukov, A. P. Sorokin, and N. M. Matyukhin	250	226
Interaction Forces and Deformation of Fast-Reactor Fuel Assemblies — Yu. I. Likhachev and L. V. Matveenko	259	232
Pulsational Characteristics of the Natural-Circulation Loop of a Large-Scale Model of a Light-Boiling Boling-Water Reactor — A. S. Babykin, B. F. Balunov, T. S. Zhivitskaya, E. L. Smirnov, V. I. Tisheninova, and N. G. Chernykh	265	237
Construction of a Model of the Process of Accumulation of Radionuclides of Corrosion Products on the Equipment in Nuclear Power Plants with Boiling-Water Reactors — S. A. Tevlin	272	242
Effect of the Solution Temperature on the Extraction Column Hydrodynamics — S. M. Karpacheva and O. K. Maimur	278	246
Solidification of Intermediate-Level Liquid Wastes with the Use of Inorganic Binders — A. S. Polyakov, M. I. Zhikharev, K. P. Zakharova, O. M. Khimchenko, T. T. Karpova, G. F. Surzhikov, V. L. Pankratov, V. P. Shelud'ko, and L. N. Shimarova	282	249
T-3M Tokamak Materials Testing Stand — A. A. Abagyan, A. A. Alferov, V. F. Babal'yants, D. G. Baratov, V. N. Dem'yanenko, S. B. Leonov, S. P. Maksimov, S. V. Mirnov, V. N. Mikhailov, V. V. Myalton, V. S. Semenov, M. M. Fiks, and V. P. Fokin	286	252
Single-Crystal Lithium Fluoride Detectors — A. I. Nepomnyashchikh, S. N. Mironenko, G. P. Afonin, and A. I. Selyavko	292	257
Use of Polarized Radiation for Increasing the Sensitivity of Multielement X-Ray Fluorescence Analysis — A. A. Ter-Saakov and M. V. Glebov	297	260
The Kerma-Constant and Kerma-Equivalent of a Radionuclide Source — V. P. Mashkovich	300	262

CONTENTS

(continued)

Engl./Russ.

Analysis of the Sensitivity of a Model of Terrestrial Food Chains — V. Ganushik, A. Mitro, T. Sabova, and O. Musatova	304	265
LETTERS TO THE EDITOR		
Stopping Power of Matter in Self-Similar Representation — S. A. Gerasimov	309	269
Method of Calculating the Stopping Cross Section of Nuclear Particles in Matter — V. F. Volkov and S. A. Gerasimov	310	270
Information System for Two RBT-10 Research Reactors — V. A. Kachalin, A. V. Kiselev, A. I. Kras'ko, V. G. Kusikov, Yu. F. Sviridova, and Yu. D. Federov	313	271
Method for Reprocessing Liquid Radioactive Wastes, Combining Selective Complexing and Ultrafiltration — V. A. Kichik, G. A. Yagodin, N. F. Kuleshov, and A. A. Svittsov	315	272
Emergency Shutdown of an Ambipolar Reactor — N. N. Vasil'ev and M. G. Kuznetsov	317	274
Yield of Fragments from Photodissociation of ^{242}Pu — Vo Dak Bang, Yu. S. Zamyatnin, Chan Dyk Tkhiep, Chan Dai Ngiep, Fan Tkhu Khyong, and Le Tkhi Kat Tyong	320	275
Determination of the Sensitivity of Thermoluminescent Detectors to Thermal Neutrons — Yu. N. Zhilov, V. G. Erkin, O. V. Lebedev, V. A. Kuchumov, and G. A. Tyurin	323	277
Radiative Capture Cross Section of ^{58}Fe at a Neutron Energy of 0.5-2.0 MeV — Yu. N. Trofimov	325	278
Total Neutron Cross Section of ^{101}Ru and ^{102}Ru in the Neutron Energy Range 0.01-1750 eV — V. A. Anufriev, S. I. Babich, N. G. Kocherygin, and V. N. Nefedov	326	279
An Integrated Benchmark for Attenuation of Neutrons with an Energy of 14 MeV by Lead Layers — S. Antonov, G. Voikov, K. Ilieva, and I. Iordanova	329	280
Detectors for Spectrometry of the X-Ray Emission from Germanium Obtained by the Hydride Method — G. G. Devyatykh, G. N. Flerov, Yu. A. Nechuneev, A. V. Gusev, Yu. P. Kharitonov, Yu. S. Tsyganov, and V. A. Gavva	331	281
Effect of Heat Release in the Coolant on the Stability of a Water-Cooled—Water-Moderated Reactor — S. I. Vdovin and E. F. Sabaev	333	283
Effect of Neutron Field Parameters on the Yield of ^{252}Cf — A. V. Klinov, A. V. Mamelin, and Yu. G. Toporov	335	284

The Russian press date (podpisano k pechati) of this issue was 3/27/1985. Publication therefore did not occur prior to this date, but must be assumed to have taken place reasonably soon thereafter.

^{129}I CONTENT IN THE COOLANT OF A WATER-COOLED–WATER-MODERATED REACTOR

L. I. Gedeonov, V. M. Gavrilov,
V. K. Vinogradova, S. P. Rosyanov,
and Yu. A. Shumov

UDC 621.039.534.23

Information on the ^{129}I content in the loop waters of nuclear power installations is required in order to understand the migration of iodine iostopes in the active zone of the reactor and to solve the problems of radiation safety [1].

^{129}I has a long half-life of $T_{1/2} = 1.7 \cdot 10^7$ years and a low energy of β-, γ-, and x-ray emission. In many cases, these properties of the radionuclide make it necessary to use the activation method for analyzing it with the use of the reaction $^{129}I(n, \gamma)^{130}I$, whose product is the γ-emitter with $T_{1/2} = 12.4$ h [2].

In this paper we describe the neutron-activation method and the results of the determination of the ^{129}I in the coolant of the first loop of the VVÉR-440 water-cooled–water-moderated reactor. The method includes several operations: extraction of the sample, separation of the iodine, irradiation of the separated preparation with neutrons, radiochemical purification of the iodine, and γ spectrometric analysis.

We extracted the coolant samples when the VVÉR-440 operated at 70% of rated power. We passed 900-1100 ml of the extracted sample, after introducing a stable carrier (1 mg KI), at a rate of 4 ml/min through a 100-mm-high column with a diameter of 10 mm, filled with AV-17 resin in a chlorine form with a grain size of 0.25-0.5 mm. Under these experimental conditions, the content of the radioactive iodine isotopes in the filtrate was equal to less than 1% initially. After this, we flushed the resin first with 10 ml of water and then with 200 ml of a 5% solution of sodium hypochlorite at a rate of 2-3 ml/min. We transferred the collected eluate into a separatory funnel and added nitric acid up to 2-3 M solution concentration. We added 20 ml of carbon tetrachloride and 20 ml of a 1 M solution of hydroxylamine chloride to the funnel. We shook the mixture in the separatory funnel for 2 min, during which time the carbon tetrachloride fraction with the extracted iodine separated from the water solution. We repeated the extraction with the addition of new portions of hydroxylamine (5 ml) and carbon tetrachloride (20 ml). We then combined the organic phases, flushed with a 10% solution of nitric acid, and then reextracted the iodine from them with a solution of sulfurous acid (10 drops of freshly prepared sulfurous acid per 20 ml of water).

To the reextract we added a solution of palladium chloride (5 mg), heated the mixture up to the formation of black particles, and let it stand for 10-12 h. After this, we washed the precipitate, precipitating out of the solution, with small quantities of a 1 M solution of hydrochloric acid and then with alcohol and transferred it to a quartz ampul. We dried the precipitate in the ampul at 333-343°K, sealed the ampul, and irradiated it.

We irradiated the ampul with neutrons with a total flux of 10^{12} $sec^{-1} \cdot cm^{-2}$ for 18 h. After the irradiation, we flushed the ampul successively with nitric acid (1:1) and water and placed in into a Teflon vessel with 20 ml of a 5% solution of sodium hypochlorite, to which we added 10 mg of potassium iodide and 5 mg of potassium bromide. After the ampul was crushed the palladium iodide precipitate dissolved, and 3-4 min later the solution separated from the fragments of the quartz ampul. We washed the fragments of the ampul and the walls of the vessel with water. We then transferred the combined solutions into the separatory funnel and introduced into it concentrated nitric acid (until a solution concentration of 2-3 M was attained), 5 ml of the hydroxylamine solution, and 20 ml of carbon tetrachloride.

We extracted the iodine, and then reextracted it. We repeated the extraction cycle once again. We heated the reextract obtained the second time in order to remove the excess sulfur dioxide, and then we cooled and passed it through a chromatographic column with a diameter

Translated from Atomnaya Énergiya, Vol. 58, No. 4, pp. 221-223, April, 1985. Original article submitted July 11, 1984.

0038-531X/85/5804-0243$09.50

of 10 mm, filled with AV-17 resin in NO_3 form with a layer 100 mm high. The solution was passed at a rate of 1.5-2 ml/min. We washed the column with the resin with 270 ml of a 2 M solution of potassium nitrate. The latter fraction with a volume of 20 ml contained the iodine. To this fraction, after adding nitric acid, we added 10 ml of a 0.05 M solution of silver nitrate. We washed the silver iodide precipitate with a 1% solution of nitric acid and a small quantity of water. We subjected the dry precipitate to γ-spectrometric analysis. We evaluated the iodine yield based on ^{131}I, contained in the coolant sample or introduced into the control water solution.

We measured the γ-emission spectra of the separated samples on a γ spectrometer with a 60-cm^3 Ge(Li) detector and an AI-1064 analyzer. The duration of the measurements of the spectrum, depending on the activity of the sample, was equal to 20-40 min. We determined the ^{129}I content in the sample being analyzed under the assumption that it is a point source using the formula

$$p = \frac{A}{\Phi (1 - e^{-\lambda t}) \Sigma},$$

where p is the ^{129}I mass, in g; I is the activity of ^{130}I in the analyzed sample, calculated at the moment the irradiation stops, in sec^{-1}; Φ is the average neutron flux density, $cm^{-2} \cdot sec^{-1}$; Σ is the macroscopic cross section for the reaction forming ^{130}I, in $cm^2 \cdot g^{-1}$; λ is the decay constant of ^{130}I, sec^{-1}; and t is the duration of the irradiation, sec. In the calculations, we used the following values of the decay constant and the macroscopic cross section of the ^{130}I-forming reaction: $\lambda = 1.558 \cdot 10^{-5}$ sec^{-1}; $\Sigma = 140$ $cm^2 \cdot g^{-1}$.

We took the value of the average neutron flux density with a relative error of 10% from the specifications of the sample irradiated in the reactor. The relative error in the computed value of the activity of ^{130}I in the sample was equal to 15%. Table 1 shows the results of the analyses of samples of a control solution with ^{129}I and samples of coolant from the first loop of the VVÉR-440.

The average content of ^{129}I in the control solution, calculated from six parallel determinations, was equal to $(8.3 \pm 0.7) \cdot 10^{-9}$ g/liter with an error of $0.3 \cdot 10^{-9}$ g and a rms relative error of ≅4%. The average ^{129}I content in the coolant during the period of observations corresponded to the value $(5 \pm 3) \cdot 10^{-10}$ g, which is many times smaller than the established concentration of this radionuclide in water in open reservoirs.

The average ^{131}I content in the coolant during the same period was equal to $1.0 \cdot 10^4$ Bq/liter with a relative rms error of 40%. A comparison of the data presented gives the ratio of the number of atoms $^{129}I/^{131}I = 2.2 \cdot 10^2$. If the fluctuations in the ratio are insignificant, then this value can be used to make approximate calculations of the ^{129}I content in the coolant from the results of the determination of the ^{131}I content.

The penetration of the radionuclides into the coolant is determined by two processes: accumulation of radionuclides under the jackets of the fuel elements and leakage of gas from under the jackets into the coolant.

The number of atoms N_1 of some radionuclide under the jackets of the fuel elements is determined by the relation

$$N_1 = \frac{g}{\lambda + \varphi} \left[1 - e^{-(\lambda + \varphi) t} \right], \quad (1)$$

where g is the number of atoms of the radionuclide, entering under the jacket of the fuel elements per unit time from the fuel tablets; φ is the leakage factor, showing the fraction of the atoms of a given radionuclide from its total quantity N_1 which escapes from the fuel elements into the coolant per unit time; λ is the radioactive decay constant of the given radionuclide; and t is the time measured from the beginning of the accumulation-leakage process. For ^{129}I $\lambda \approx 1.24 \cdot 10^{-15}$ sec^{-1} and with the usually observed values of φ [3] the condition $\varphi >> \lambda$ holds. Equilibrium appears approximately after 200 h with $\varphi = 10^{-5}$ sec^{-1}; approximately after 20 h with $\varphi = 10^{-4}$ sec^{-1}; and after 2 h with $\varphi = 10^{-3}$ sec^{-1}. In the chain of isobars with a mass of 131, forming as a result of the fission of uranium by thermal neutrons, the longest-lived nuclides are ^{131}I ($T_{1/2} = 8.05$ days) and ^{131}Tl ($T_{1/2} = 30$ h). For ^{131}I $\lambda \approx 1 \cdot 10^{-7}$ sec^{-1}, i.e., as also for ^{129}I the condition $\varphi >> \lambda$ holds, and equilibrium under the fuel-element jacket appears after the same time intervals.

It follows from the analysis performed that with an insignificant rupture of the seal of the fuel element the ratio of the number of atoms of ^{129}I in it to the number of ^{131}I

TABLE 1. Results of the Determination of ^{129}I in Water Samples

Sample	^{129}I content, ng/liter
Control solution	$9{,}0 \cdot 10^{-9}$
Same	$7{,}4 \cdot 10^{-9}$
» »	$7{,}6 \cdot 10^{-9}$
» »	$8{,}8 \cdot 10^{-9}$
» »	$8{,}2 \cdot 10^{-9}$
» »	$8{,}5 \cdot 10^{-9}$
Coolant (extracted on Dec. 6, 1977)	$1{,}3 \cdot 10^{-10}$
Coolant (extracted on Dec. 7, 1977)	$4{,}4 \cdot 10^{-10}$
Coolant (extracted on Dec. 8, 1977)	$3{,}2 \cdot 10^{-10}$
Coolant (extracted on Dec. 12, 1977)	$13 \cdot 10^{-10}$

atoms will increase. With a large break in the seal, this ratio becomes practically constant. It is evident that the number of atoms of the radionuclides escaping per unit time from the fuel element into the coolant is

$$Q = \varphi N_1 = g \frac{\varphi}{\lambda + \varphi}. \tag{2}$$

Under equilibrium conditions, in the first loop,

$$Q = (\lambda + h) N_2, \tag{3}$$

where N_2 is the number of atoms of the radionuclide in the coolant; h is a constant describing the removal of the radionuclide by the coolant system.

From the relations presented it is easy to obtain a value for the number of atoms of radionuclide per unit volume of coolant:

$$n = \frac{gh}{V(\lambda + \varphi)(\lambda + h)}, \tag{4}$$

where V is the volume of water — the coolant in the first loop.

For iodine radioisotopes, we shall study the case when 10^{-5} sec$^{-1} \leq \varphi \leq 10^{-3}$ sec^{-1}; $h \approx 10^{-5}$ sec^{-1}. In this case, the relations $\lambda \ll \varphi$; $\lambda \leq h$ hold for both ^{129}I and ^{131}I. From here follows

$$n_{131} = \frac{g_{131}}{Vh_1}; \quad n_{129} = \frac{g_{129}}{Vh_1}. \tag{5}$$

The values of V and h_1 are determined by the operational conditions and the VVÉR-440 construction. The values of n_{131} and n_{129} for the first experiments were determined as shown above.

It is unlikely that significant quantities of the weakly volatile (compared to iodine) tellurium would penetrate into the coolant. Under this assumption, using the formula (5) we can estimate not only the ratio of the iodine isotopes in the coolant n_{129}/n_{131}, but also the ratio of the intensity with which they enter the coolant from the jacket of unsealed fuel elements.

The first experiment performed in this work on the comparison of the concentration of iodine isotopes in the coolant encompassed as yet an insignificant time interval and revealed a large nonsystematic spread in the results of the observations. A further increase in accuracy of the determinations over long time intervals could permit estimating the ^{129}I content in the coolant from the concentration of ^{131}I in the coolant.

LITERATURE CITED

1. Radioactive Iodine in the Problem of Radiation Safety [in Russian], Atomizdat, Moscow (1972).
2. D. Aumann, H. Faleschine, and L. Freedmann, "Determination of ^{129}I and ^{127}I of natural levels by neutron activation analysis," Radiochem. Acta, 27, No. 4, 209-215 (1981).
3. V. V. Gerasimov, A. I. Kostrovich, and O. I. Martynova, Water Regime of Nuclear Electric Power Plants [in Russian], Atomizdat, Moscow (1976).

RITM FACILITY FOR TESTING FUEL ELEMENTS IN VARIABLE POWER REGIMES IN THE SM-2 REACTOR

V. A. Kuprienko, A. V. Pershin,
Yu. G. Spiridonov, V. Sh. Sulaberidze,
and V. N. Shulimov

UDC 621.039.54

One of the chief problems originating with a change of the requirements for the operting conditions of nuclear power stations with water-cooled–water-moderated reactors (VVÉR) in the power generation system is the assurance of the necessary durability of the fuel elements in conditions of repeated changes of the power level at a rate of 1-6% per minute [1]. This problem incorporates a number of special problems on the investigation of different aspects of the behavior of fuel elements. These include the study of the temperature conditions and mechanism of gas release from the fuel for the purpose of creating reliable methods of forecasting these characteristics in the stated operating conditions.

In order to solve the problems posed, the RITM facility was developed, with a gas system for regulating the power of the fuel elements. Systems with absorbed gas are used widely in reactor technology [2, 3]. The defining criterion for choosing a system with ^{3}He was the relative simplicity of controlling the thermal-neutron flux density in the cells of the irradiation facility (IF) by a change of pressure of the absorbing gas.

The RITM installation consists of the IF itself, a closed circuit of the absorbing gas, and a test rig for measuring the parameters of the fuel elements being tested. The IF (Fig. 1) is a multitube channel which allows the simultaneous irradiationof three fuel elements and which is provided with a thermometric unit for measuring the thermal power of the fuel-element assembly. The fuel elements are placed in individual cooling channels joined by inlet and outlet collectors. The coolant distills at a temperature of $\leqslant$335°K and is under a pressure of 5 MPa. The thermal insulation of the IF cells from the reactor coolant is provided by annular spaces, created by the double walls of the descending and ascending tubes. At the core height (350 mm), annular hermetically sealed voids are located around each cell and they are joined by means of impulsive tubes with the absorbing gas circuit. The thickness of the gap is 2.5 mm and the total volume of the voids is 600 cm^3. The IF is installed in the reflector of the SM-2 reactor and is connected to the low-temperature water loop.

The absorbing gas circuit (Fig. 2) is designed for the generation of a vacuum or a ^{3}He pressure up to 3 MPa in the annular voids, purification of the gas from hydrogen and tritium, and monitoring and maintenance of the specified pressure. The circuit comprises the absorbing gas source, membrane-type blowers (large and small), ^{3}He purification unit, means for monitoring the pressure, and a shut-off equipment. The ^{3}He source is a cylinder with a volume of $4\cdot10^4$ cm^3 filled with the gas under a pressure of 0.6 MPa. A receiver, with a volume of $6\cdot10^3$ cm^3, ensures the necessary operative reserve of gas for generating the required pressure in the IF. The designs of the large and small blowers are identical. Inside the protective housing a circular, flat membrane box is installed (with a diameter of 1.0 and 0.6 m), welded from two plates with a thickness of 1 mm of OKh18N10T steel. The opening of the membrane box is controlled by the pressure of nitrogen fed into the protective housing and monitored with a rheostat-type indicator. The volumes of the completely open membrane boxes of the large and small blowers amount to $6\cdot10^3$ and $1.7\cdot10^3$ cm^3, respectively.

A vacuum pump and a cylinder with highly pure helium are provided for purging the circuit and IF voids. An interchangeable purification unit is provided for the removal from the ^{3}He of the hydrogen and tritium accumulated in it. The unit consists of a main filter with a volume of 1000 cm^3 and a monitor filter with a volume of 200 cm^3. The absorbing capacity of the main filter, determined in labortory investigations, amounts to $3\cdot10^4$ cm^3 of hydrogen. Zirconium chipping previously annealed at a temperature of 1320°K and a vacuum of ~1.5 Pa is used as the absorber. The working temperature of the filters, 623-673°K, is achieved by

Translated from Atomnaya Énergiya, Vol. 58, No. 4, pp. 223-225, April, 1985. Original article submitted August 13, 1984.

 0038-531X/85/5804-0246$09.50

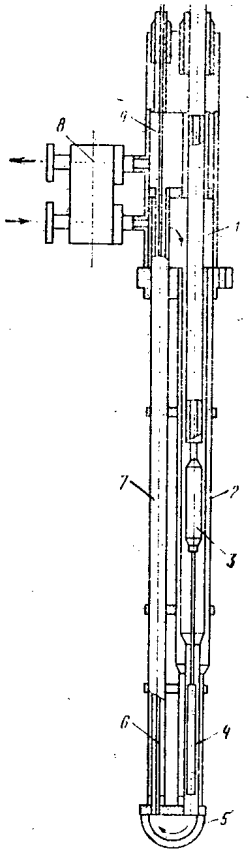

Fig. 1. Irradiation facility: 1) inlet collector; 2) descending tube; 3) pressure transducer; 4) fuel element; 5) common collector; 6) direct-charge detector; 7) ascending tube; 8) thermometric unit; 9) outlet collector.

asjusting the power of the electric heaters. The monitor filter serves to determine the completeness of the hydrogen and tritium absorption in the main filter. The requirement for sufficiently complete purification of the helium in the filter with its continuous or periodic operating conditions limits the maximum rate of increase of power of the fuel elements. It amounts to 12% per min in the range 0.5-1.0 of the nominal value with adjustment of the power of each fuel element individually, and 4% per min in the case of simultaneous power adjustment of three fuel elements.

The main drawback of the system with ^3He is the possibility of the discharge of radioactive tritium into the servicing compartments. For the purpose of reducing the probability of this hazard, the maximum hermetic sealing of the absorbing gas circuit is provided. This explains, in particular, the rejection of a scheme using blowers with an external drive mechanism and the development of hermetically sealed blowers of the membrane type. Operative monitoring for hermeticity of the IF voids and the circuit is effected by means of manometers. The pressure of the gas in the IF voids is monitored with MÉD-type manometers with continuous recording of the readings. The circuit is tested periodically by filling it with high-purity helium under elevated pressure.

The test rig for measuring the parameters of the experimental fuel elements is designed for recording the readings of a differential multijunction thermoelectric transducer, from which the coolant heating in the IF is determined, for regulating the power of the electric heater installed in the thermometric unit of the IF, for recording the readings of the direct-charge detectors (DCD) located in the IF, and also the pressure and temperature transducers installed in the fuel elements. The measurements are made by means of a potentiometer or a digital voltmeter. Provision is also made for recording the readings of the thermoelectric transducers by secondary instruments of the KSP type. The coolant flow rate through the IF is measured with a conventional loop flowmeter.

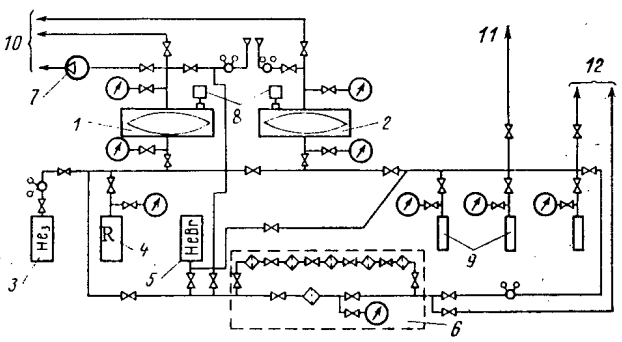

Fig. 2 Fig. 3

Fig. 2. Diagram of the RITM gas test rig: 1) large blower; 2) small blower; 3) cylinder with ^3He; 4) receiver; 5) cylinder with highly pure helium; 6) helium purification unit; 7) vacuum pump; 8) indicators; 9) IF voids; 10) ventilation; 11) to vacuum pump of the impulsive channel test rig; 12) to special ventilation.

Fig. 3. Orientation the the channel relative to the reactor core: 1, 2, 3) cell numbers; 4) IF void with ^3He.

TABLE 1. Relative Variation of U_{DCD} in Adjacent Cells in the Case of Their Successive Filling with ^3He up to a Pressure of 1.1 MPa, %

Cell	No. of experiment		
	1	2	3
1	*	−9	−16
2	−9	*	−14
3	−6	−3	*

Note. The filled cells are marked with an asterisk.

The regulating characteristics are investigated by means of DCD installed in the descending tubes instead of the fuel elements. The DCD emitter is made of rhodium wire with a diameter of 0.5 mm; the length of the active part is 50 mm. The DCD current is assessed by the voltage drop (U_{DCD}) in a standard resistance of 10 kΩ. The scheme of arrangement of the cells of the IF relative to the core of the reactor is shown in Fig. 3. The ^3He pressure was varied in one, two, and three cells simultaneously. The relative changes of the thermal neutron flux density in the cells with the simultaneous filling of the annular voids of the IF with helium are shown in Fig. 4, and for successive filling of each of them in Fig. 5.

The simultaneous filling of the IF voids with ^3He at a pressure of 2.6 MPa led to a reduction of the thermal neutron flux density in the cells to 0.2-0.3 of the nominal value (in the absence of absorber). The relative changes of the neutron flux density for each cell are different. The maximum variation was observed in cell 1 and the least in cell 3, the nominal value of the neutron flux density in which was a factor of approximately 1.7 higher than in cells 1 and 2.

The results of the measurements confirm the effect of the absorber in the annular void of each cell on the others (see Table 1). Cell 1 was subjected to the greatest effect and cell 3 to the least. This is explained by the mutual positioning of the cells and their orientation relative to the reactor core.

The absence of a relation with a constant exponent index (see Fig. 4) is due to the presence of the perturbing action of the strong absorber, varying the intensity of the neutron field at the site of location of the IF. In the case of separate filling of the cells with ^3He up to a pressure of 1.1 MPa, the experimental results can be described by an exponential relation with an error of ±5% (see Fig. 5).

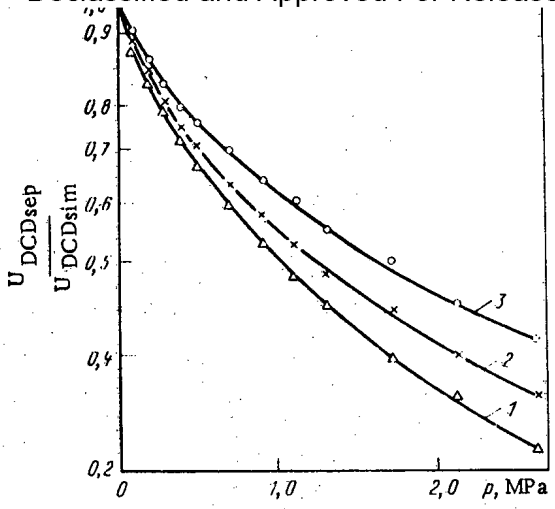

Fig. 4

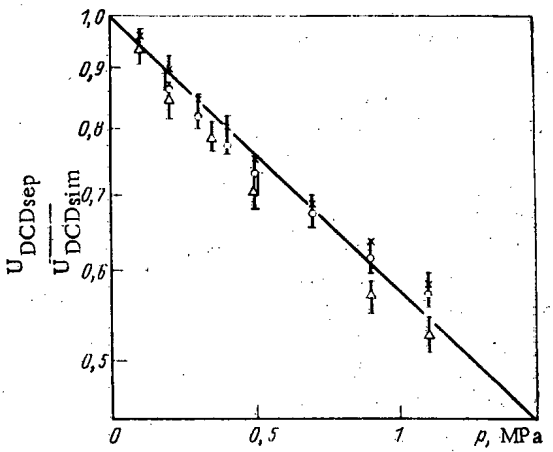

Fig. 5

Fig. 4. Relative change of neutron flux density in the IF cells in the case of their simultaneous filling with ^3He; 1) cell 1; 2) cell 2; 3) cell 3.

Fig. 5. Relative change of neutron flux density in the IF cells in the case of filling each cell individually with ^3He: Δ) cell 1; ×) cell 2; o) cell 3.

The mutual effect of the cells during pairwise filling of the annular voids is intermediate between that observed in the case of simultaneous filling of all the voids with ^3He and filling each of them individually.

The experiments showed that the presence of the absorber in all the annular voids of the IF at a pressure of 2.6 MPa has no appreciable effect on the reactivity and shows no effect on the reactor control system.

The RITM facility allows tests of model fuel elements to be conducted in conditions satisfying the requirements on the maneuvering units of nuclear power stations both with respect to depth and speed of control. Coupling of the facility to the low-temperature water loop of the SM-2 reactor is the first stage of its operation. At this stage, a study is being planned of the gas release in the fuel elements irradiated in conditions with repeated power variations.

LITERATURE CITED

1. Yu. K. Bibilashvili and A. V. Medvedev, At. Tekh. Rubezhom, No. 7, 3-11 (1979).
2. G. T. Potapenko, At. Tekh. Rubezhom, No. 6, 22-32 (1975).
3. V. N. Andreev, P. M. Egorenkov, V. I. Kolyadin, et al., At. Energ., 51, No. 5, 302-304 (1981).

HEAT REMOVAL IN FAST REACTOR CORES

A. V. Zhukov, A. P. Sorokin,
and N. M. Matyukhin

UDC 621.039.517.5

One of the most important efforts of the USSR power program is being directed toward the acceleration of the construction and mastery of sodium-cooled fast reactors, which offer the prospect of the development of a nuclear power fuel base [1-3]. The results of the operation of the first USSR fast reactors, the BR-5 and BR-10, at 5 and 10 MW respectively [2] and the BOR-60 pilot reactor at 60 MW [4] enabled us to proceed to the mastery of the high-power BN-350 [5] and BN-600 [6] fast reactors which are being successfully used today at the Shevchenko and Beloyarsk nuclear power plants. At the present time a series of still larger fast power reactors is being developed (the BN-1600 and others). Ensuring their high efficiency and reliability presents an important problem whose solution is determined largely by the level of the thermophysical design basis of reactors.

Fast reactors are characterized by high neutron and thermal fluxes, deep fuel burnup, high pressure of gaseous fission products in the fuel elements, and high temperaure of the fuel and cladding. The characteristics of the core physics and geometry (Fig. 1) and the appreciable uncertainties in the geometric parameters of the fuel element assemblies (FEA) present a problem which penetrates more deeply into the essence of thermophysical processes and the knowledge of new phenomena corresponding to the contemporary level of knowledge of reactor thermophysics. The study of the interchannel hydrodynamic and thermal interaction, heat transfer during variable energy release by the initial thermal parts, deformed fuel element lattices, and in atypical channels under asymmetric heat loads, in finned fuel element systems is a far from complete list of present practical reactor construction problems which are of decisive importance for thermophysical study and design of fast reactors.

A complete and rigorous account of the above factors in thermal-hydraulic calculation is a very complicated problem. A thermal-hydraulic calculation must furnish a large amount of complex and highly reliable information, particularly on local hydrodynamic and thermal characteristics. On the one hand, it is necessary to avoid large margins of the fuel element and coolant temperatures (they limit the power and efficiency of the installation); on the other hand, exceeding the admissible local temperature can disable the reactor.

One of the basic problems of a thermal-hydraulic calculation of fast reactor FEA is that of finding on the basis of the reactor core design parameters (the energy release, the total flow rate of the coolant, etc.) the thermal-hydraulic characteristics which determine its operating ability. These include the maximum temperature of the fuel element cladding and the FEA jackets and the maximum temperature inhomogeneities around the perimeter of the fuel elements and FEA jackets.

In order to find a reliable thermal-hydraulic design of contemporary high-flux fast reactors (BN-350, BN-600) many experiments were performed and new methods of calculating the local characteristics of FEA were developed.

Research at the FÉI included studies of the mechanism of interchannel mixing, complex longitudinal-transverse flow in reactor elements, the characteristics of the hydrodynamics and heat transfer in systems of parallel fuel elements and in atypical channels (peripheral zones of FEA), the temperature distributions in symmetrical and distorted fuel element lattices during constant and variable energy release under stabilized hydrodynamic and thermal conditions, etc., which form a basis for calculating local thermal and hydrodynamic characteristics of fast reactor FEA.

Some of the questions listed include a wide range of problems, and in essence determine the further development of the thermal physics of reactors in general. For example, the question of the temperature distribution in atypical (peripheral) FEA channels and in distorted fuel element lattices, including local overheating of fuel elements because of the

Translated from Atomnaya Énergiya, Vol. 58, No. 4, pp. 226-232, April, 1985. Original article submitted May 18, 1984; revision submitted August 2, 1984.

 0038-531X/85/5804-0250$09.50

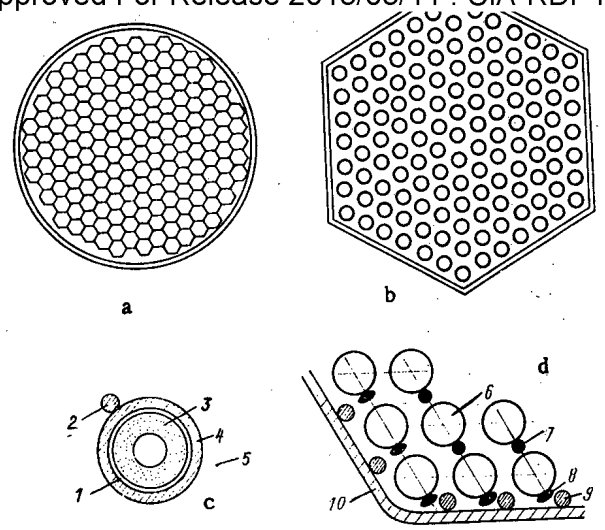

Fig. 1. Schematic diagram of a) cross section of core; b) a fuel element assembly (FEA); c) a fuel element; d) pheripheral region of FEA of a fast reactor; 1) gas gap; 2) wire winding; 3) nuclear fuel; 4) cladding; 5) coolant; 6) fuel element; 7, 8) wire and ribbon windings; 9) displacer; 10) FEA jacket.

shape of the channels, because of single and group displacements of fuel elements, because of the blockage of through FEA cross sections, and for other reasons, related to the problem of the reliability and increase of reactor power will obviously be solved as reactor construction develops. At the present time these problems for fast reactors are being successfully solved by the collaboration of specialists of the Comecon countries.

Methods of mathematical modeling of coolant velocity and temperature distributions in fast reactor FEA are being actively developed. A set of programs has been written for calculating the local thermal–hydraulic characteristics of FEA (TEMPR), the average characteristics along channels (TEMP-M, CORA) and over the volume of FEA (UGRA, PROTVA). These programs can be used to solve a broad class of practical problems of the thermal–hydraulic design of fast reactor FEA, and give the information necessary for an analysis of the operating ability of FEA elements. These programs take adequate account of the effect of various factors on the temperature and velocity distributions in FEA; they have been tested on a large amount of experimental material, and offer an effective method for performing thermal–hydraulic calculations [7-10].

The initial problem of the thermophysical calculation of fast reactor FEA is the proper choice of the geometrical parameters of the FEA. Unfortunately, some authors perform a thermal calculation of fast reactor FEA by assuming an idealized arrangement of the fuel elements at the nodes of a regular triangular lattice [11]. In doing this they assume that the boundary fuel elements are in contact with the hexagonal jacket through the spacing wire winding, and that the remaining fuel elements are uniformly distributed over the cross section of the hexagon, forming nominal computational cells of a definite area. The possible deviations of the through cross section of a cell from its nominal value are taken into account by overheating factors as a random quantity. In a variant of this model it is assumed that, all other things being equal, there is one cell or a group of cells in a FEA in which three fuel elements are brought into contact with one another along the whole length through the spacing wire winding, and the cell formed with a minimum area of the through cross section is taken as the computational cell.

Investigations of the distribution of the through cross sections of cells performed on mock-up assemblies showed that the actual pattern of the fuel element spacing in a bundle differs from idealized concepts. Fuel elements have a certain freedom of radial displacement, and for a number of reasons are bowed, shifted within the limits of the possible gap, so that the rods no longer form an ideal lattice, but are distributed along the radius and height of the assembly in accordance with Weibull's law.

Thus, the random character of the fuel element arrangement makes it essential to choose a valid computational model of FEA geometry. The statistical model of the geometry of a fuel element bundle, which is being developed at the present time and is realizable by using the Monte Carlo method [7], gives a valid representation of FEA geometry and significantly refines the overheating factors. This model is themost physically well founded and promising for the thermophysical calculation of fast reactor FEA. The values of the temperature distribution calculated with the TEMP-M program using the statistical model of the geometry of the BN-600 reactor FEA differ appreciably from the values calculated with other models of the geometry of fuel rod bundles (Fig. 2).

A fast reactor core is a large and complex system of FEA which in turn have a complex structure (Fig. 1a, b, c). In view of this, the thermal–hydraulic design of a reactor core is divided into several steps.

In the first step, performed at the design survey stage (optimization of parameters), the flow rates of the coolant through the FEA and the average temperature rises of the coolant in a FEA are determined [9]. The next step is the calculation of the thermal–hydraulic characteristics of individual FEA and fuel elements [10]. At this step the geometrical characteristics of a FEA, the distribution of flow rates of the coolant over the FEA channels, taking account of the interchannel hydrodynamic interaction, the distributions of the temperature rises of the coolant over the FEA channels, taking account of the interchannel thermal interaction, the "wall–fluid" thermal heads, and the maximum temperature nonuniformities around the perimeter of the fuel elements are calculated. The effect of various factors on the temperature distribution is taken into account, and the maximum temperature of the fuel element cladding is determined. Since the temperature rise of the coolant in reactor FEA is large (~200°C), the accuracy of the determination of the maximum fuel element cladding temperature depends largely on the accuracy of the calculation of the distribution of the temperature rise of the coolant over the FEA channels. The important question here is the individual approach to the calculation of typical central, lateral, and corner fuel elements of hexagonal FEA. Since the temperature distributions of these fuel elements differ substantially, appropriate computational formulas must be used for each category of fuel elements [8].

A fast reactor FEA is a system of parallel interconnected channels. There is greater mass transfer between channels than in isolated channels; the effect of random geometrical deviations (bowing, displacement of fuel elements) on the development of flow rates, the effect of helical spacing fins of the fuel elements on the interchannel intermixing and the degree of turbulence of the flow, the nonuniformity of the distribution of the coolant over cells of different geometries (central peripheral cells), and other factors determine the hydrodynamic pecularities of interconnected channels in comparison with isolated channels.

The use of methods and formulas derived for isolated channels to make hydraulic and thermal calculations of interconnected channels can lead to large errors. Special methods must be developed which take account of the peculiarities of interconnected channels.

Interchannel heat and mass transfer is a decisive factor in shaping thermal and hydrodynamic patterns in a fast reactor core [12]. Helical wire windings on fuel elements lower the temperature in the region of "hot spots," and thus permit an increase in reactor power. No contemporary method of thermal–hydraulic design of a reactor can avoid taking account of this factor, which is important in considering processes both within a fuel element bundle and in the reactor core as a whole (interaction between FEA). Taking account of heat and mass transfer between cells in the so-called subchannel method of calculation is a substantial contribution to the thermophysical basis of fast reactor cores [10].

According to the subchannel method, a fuel element assembly is divided into a series of parallel channels, and conservation of mass, momentum, and energy equations are solved for them. This gives the coolant velocity and temperature rise distributions along the channels.

The systems of conservation equations formulated by various authors differ in the completeness and accuracy with which the physical effects and mechanisms of interchannel interaction are taken into account. Consequently, the programs of the subchannel calculation (in which the conservation equations are solved) differ in the class of solvable problems and the acuracy of the description of the thermal–hydraulics.

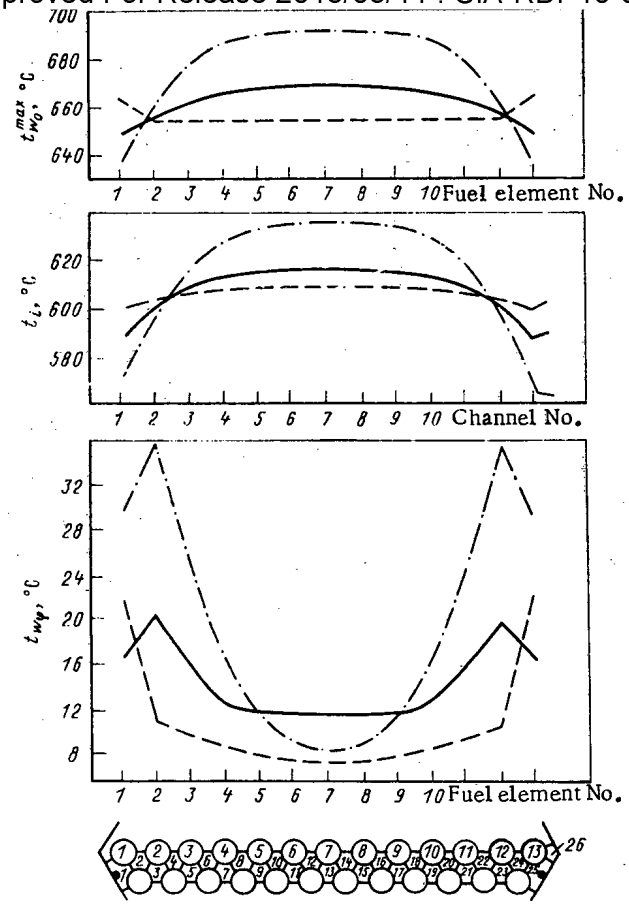

Fig. 2. $t_{w_0}^{max}$) Distribution of maximum temperature of inner surface of fuel element cladding over the cross section of a FEA; Δt_i) temperature rise of coolant; $\Delta t_{w\varphi}$) temperature nonuniformity around perimeter of fuel elements: ——) statistical calculation; —·—) "tight" bundle model; ---) "separated" bundle model; ●) displacer.

An analysis of the methods and programs of the subchannel thermal–hydraulic calculation of fast reactor FEA led to correct formulations of the subchannel method [13] and the development of the TEMP and CORA programs. Considerable attention was paid to the thermal–hydraulic calculation of FEA in the peripheral region, which is the most dangerous from the point of view of temperature nonuniformities [8]. The peripheral fuel elements are surrounded by cells with a different geometry. As a result of the fact that a different amount of coolant flows in the cells, its temperature varies substantially around the perimeter of the peripheral fuel elements (Fig. 3).

Liquid metals have large thermal conductivities and small volumetric heat capacities. As a result of the large temperature rise of the coolant and high heat-transfer coefficients, the surface temperature of fuel elements washed by metals is determined mainly by local heating of the coolant, and not by local heat-transfer coefficients. This applies particularly to peripheral fuel elements around whose perimeter the temperature rise of the coolant differs appreciably.

The tolerances in the dimensions of fast reactor FEA having small-diameter fuel elements and relatively small lattice pitches are commensurate with the transverse dimensions of the cells surrounding the fuel elements, and this has an appreciable effect on the displacements and the temperature rises of the fuel elements, even when spacing wire windings are used on them [14]. These questions are especially important for peripheral fuel elements on which the wire winding has a diameter half that for the central fuel elements. Thus, the peripheral fuel elements can be displaced along the perimeter of the jacket by at least half the gap between fuel elements.

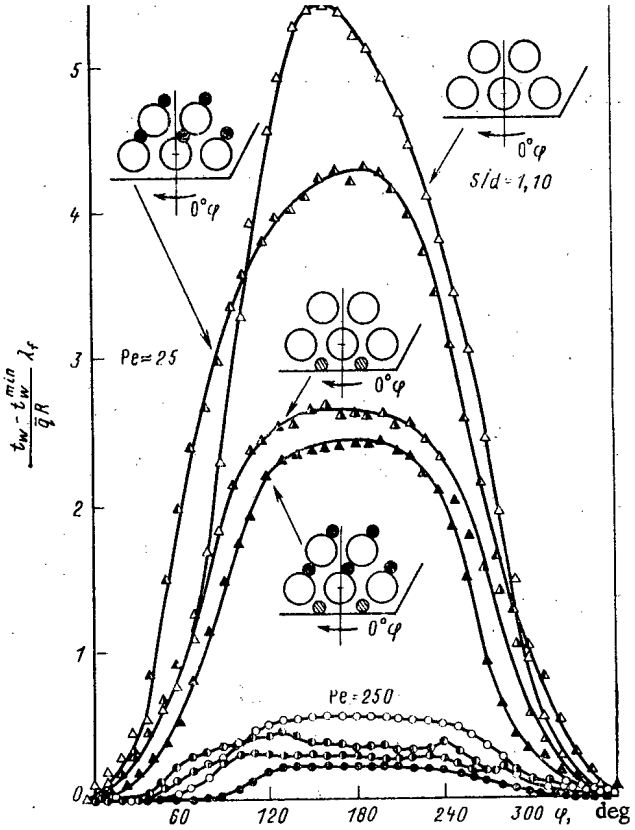

Fig. 3. Temperature distribution of lateral fuel elements in models of fast reactor FEA with smooth fuel elements without displacers (△, ○), with finned fuel elements without displacers (▲, ◐), with smooth fuel elements and displacers (▲, ◑), and with finned fuel elements and displacers (▲, ●).

Studies of the temperature distributions in FEA in which the fuel elements had been displaced furnished important experimental and computational material as applied to characteristic limiting cases of lattice deformation (single and group displacement of fuel elements in various directions and by various distances up to contact of the fuel elements with one another and with the FEA jacket), and have determined relations for maximum temperauture nonuniformities in deformed fuel element lattices (Fig. 4). We have to complete experiments in this field, correlate the results, and incorporate them into programs in order to develop a universal procedure for calculating hot spots.

Heat transfer in peripheral channels frequently occurs under unstabilized conditions. The length of the initial thermal region depends on the equivalent thermal conductivity and the relative pitch of the fuel element lattice, the diameter of the displacers, the size of the gap between the fuel elements and the FEA jacket, and other factors. In using formulas for the heat-transfer coefficients and the temperature nonuniformities around the perimeter of peripheral fuel elements, it is necessary to keep in mind the relative length of channels for which the formulas are recommended.

Fins on fuel elements improve heat transfer to liquid-metal coolants by promoting intermixing of the coolant over the cross section of the FEA, but on the other hand they produce a local increase in the temperature of the fuel element cladding.

Thus, the hydrodynamic and heat-transfer peculiarities in fast reactor FEA are mainly associated with the peripheral rows of fuel elements and the use of sodium as a coolant. These peculiarities are the following:

the temperature nonuniformities around the perimeter of the peripheral fuel elements are an order of magnitude larger than for central elements;

there are large nonuniformities of the coolant flow rates around the perimeter of the peripheral fuel elements;

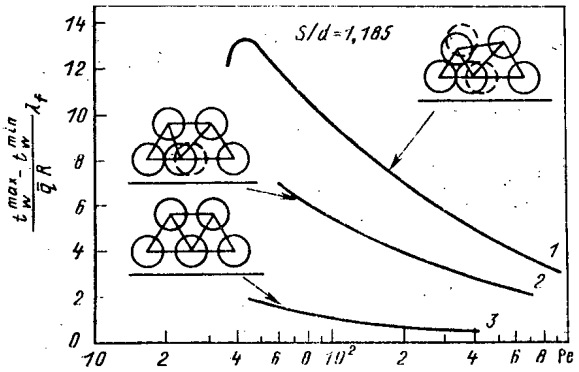

Fig. 4. Maximum temperature nonuniformities of an unfinned lateral fuel element of a FEA without displacers: 1) displacement of a group of fuel elements; 2) displacement of a single fuel element; 3) nominal geometrical conditions.

interchannel intermixing has a decisive effect on the velocity and temperature distributions in FEA;

the deformation of the fuel element lattice has a rather large effect on the velocity and temperature distribution;

heat transfer in the peripheral channels of FEA occurs under unstabilized conditions.

In the last few years a great deal of attention has been paid to the solution of the following problems of the thermophysics of fast reactor FEA.

Study of Blockages of Through Cross Sections of Reactor FEA. The information available at the present time [15] indicates that a through cross section of fast reactor FEA can become partially or completely blocked (Fig. 5a). This can lead to local boiling of the coolant and the subsequent rupture of the fuel elements, which in turn can increase the blockage and cause an accident.

Blockages can arise as a result of oxide contaminants in the coolant. The spacing lattices and the wire winding on the fuel elements promote the accumulation of foreign material, which initiates the formation of a blockage. Fuel element failure due to fabrication defects, structural defects, and improper operating conditions can also lead to blockage.

Blockages are classified as local and global, in the central and in the peripheral regions of the FEA, solid or porous, two-dimensional or three-dimensional, active (energy releasing) and nonactive, etc.

Many investigations have shown that a stable recirculating flow exists beyond a complete blockage in rod assemblies with a relative pitch of more than 1.1 (Fig. 5b). The divided flow is united at the end of the recirculating flow, where a stagnation zone is formed [15, 16]. The length of the recirculation zone is estimated as 1.3-2.6 diameters of the blockage for a central blockage, and 1.3-4.8 diameters of the blockage for a lateral blockage (Fig. 5b). The wake area beyond the blockage is 5-10 times longer than the recirculation zone.

Recent research on the local hydrodynamic characteristics of a blocked model fast reactor FEA [17] (relative pitch of smooth rods 1.17, hexagonal jacket, 55% blockage of through cross section in the center) furnished rather detailed information on the physical pattern of flow in the region of the blockage. The recirculating flow zone has the shape of the frustum of a cone whose height is the length of the recirculation zone, and whose base is a circle with a diameter of three rod lattice pitches and an area 3/4 the area of the blocked cross section of the FEA.

In the central part of the FEA the length of the recirculation zone is ~1.7-1.9 times the diameter of the blockage. In intermediate fuel elements the recirculation zone varies around the perimeter of the fuel elements, decreasing in the direction from the inner part of the FEA toward the periphery; in the region of a lateral fuel element the recirculating flow exists only over a relatively small part of the perimeter facing the inner part of the FEA; in the region of a corner fuel element there is practically no recirculation.

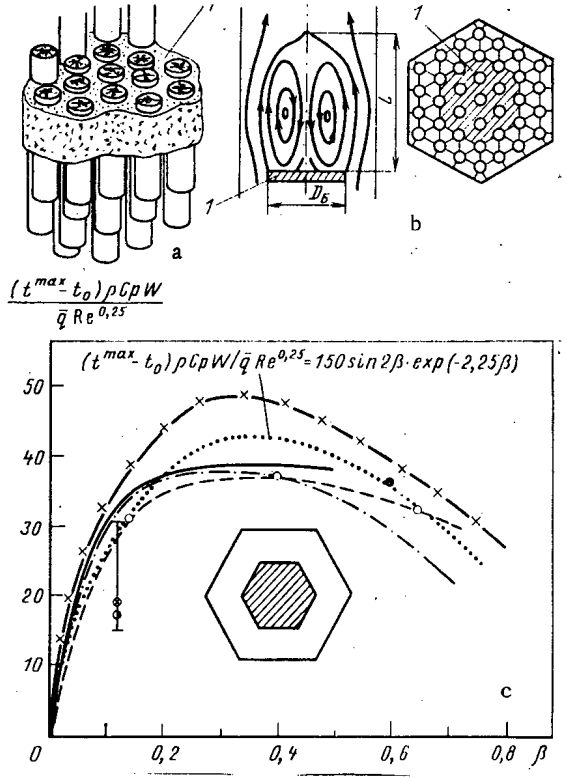

Fig. 5. Schematic diagram of a) blockage of through cross section in a FEA, b) recirculation zone beyond central blocked part of through FEA cross section, and c) dependence of maximum overheating of coolant beyond complete blockage on the fraction of the through cross section of the FEA shut off, according to data of various authors: 1) blockage; t_0) temperature of coolant at entrance to blocked zone; ×, •, o, ⊗, ◑) experimental data [15]; ---, —·—, ——, -×-) calculated relations [15]; ···) our generalized relation.

If the fraction of the cross section of a FEA which is blocked is increased to the value $\beta = 0.7$, the flow rate of the coolant through the FEA is decreased no more than 15%. The maximum overheating of the coolant beyond the blockage occurs for $\beta \cong 0.3$ (Fig. 5c). On the basis of correlated data Bogoslovskaya et al. [15] derived formulas for estimating the flow rate and overheating of the coolant in blocked FEA as a function of the degree of blockage of the cross section. The temperature rise of the coolant beyond a lateral blockage is 1.5-2 times larger than the temperature rise for a central FEA blockage of the same size. This is a result of the smaller mass and heat transfer beween the wake area and the outer flow for a peripheral blockage than for a central blockage.

The Use of Counter Wire Windings on Fuel Elements. The USSR work program for fast reactors [2] provides for further development of thermal-hydraulic research on the optimization of temperature conditions in fast reactor cores.

The nonuniform energy release over the cross section of fast reactor FEA, particularly FEA near a baffle, the formation of hot spots as a result of systematic and statistical inhomogeneities of the fuel, tolerances in fabrication and arrangement of the fuel elements in the lattice and deformation of the lattice during reactor operation (bowing, displacement, swelling of fuel elements under deep burnup, etc.) necessitate the flattening of the temperature over the cross section of a FEA. A promising method for doing this is to use counter windings on the fuel elements. With these windings heat and mass transfer are greater than with unidirectional windings, and there is a certain decrease of the hydraulic resistance of a FEA [18, 19].

The temperature distributions in model assemblies with unidirectional and counter windings were compared [18]. Two variants of counter helical fins were used: an alternation of

smooth and finned fuel elements, with counter windings on neighboring fuel elements, and counter ribbing over neighboring rows of fuel elements. The comparison showed that counter windings decreased the nonuniformities in the heating of the coolant in a FEA by a factor of 2-2.5. The temperature nonuniformities of boundary fuel elements were also very much smaller.

The distribution of the liquid temperature over the radius of a FEA for the same energy release in a central fuel element is more uniform for counter windings; the heating of the coolant in the surrounding fuel elements of the cells is ~60% lower and in the next row of cells higher than for unidirectional ribbing on the fuel elements. This indicates more intense spreading out of the heat for counter windings on the fuel elements, which may have an important application for decreasing the temperature nonuniformities in FEA.

Temperature Fluctuations in the Sodium Stream at the Outlet of Fast Reactor FEA (mixing of sodium streams with different temperatures above the core). A study of temperature distributions and fluctuations at the outlet of fast reactor FEA is necessary because of the urgency of questions of the thermal stability of FEA and structures above the core, and also because it is necessary to develop methods of monitoring the coolant temperature at the FEA outlet, i.e., to diagnose processes occurring in reactor cores when the operating parameters deviate from nominal or in emergencies.

The solutions of these problems require the study of the laws of intermixing of coolant streams with different temperatures at the outlet of a FEA and the generation of thermal noise; the laws of the spreading of a hot spot over the core; the laws of behavior of the temperature of a FEA cap when there is a sudden change of the temperature conditions, etc.

The results obtained can be used to solve problems related to the construction of temperature-sensitive elements and their optimum disposition above the core; to solve problems related to the diagnosis of the overheating of a FEA or a group of FEA (formation of a global hot spot), to the blockage of part of the through cross section of a FEA (formation of a local hot spot), to different heat outputs of the fuel elements, etc.; for the reliable monitoring of the temperature distribution in reactor zones when as a result of the alternation of zones of energy release and breeding there is an increased probability of temperature drops in a zone in comparison with a uniform core; in obtaining input data for developing methods of calculating the thermomechanical durability of FEA and structures above the core. The statistical characteristics of temperature fluctuations are being studied primarily in order to judge the local aspect of the process of mixing sodium streams at a FEA outlet.

Effect of Different Heat Outputs of Fuel Elements. An increase of the heat output of one or three fuel elements in a FEA with wire windings leads to a certain increase in the fuel element temperature and the maximum dimensionless nonuniformity around the perimeter of the fuel elements with an increased output [20]. For the alternation of energy-releasing and non-energy-releasing rods in a FEA with wire windings mocking up fast reactor FEA, the dimensionless temperature nonuniformities around the perimeter of fuel elements may be increased by a factor of 1.2-1.4

Recent experimental research on temperature distributions in FEA in which the energy release varied over the FEA cross section [18] showed that the temperature nonuniformities around the perimeter of fuel elements of FEA with an energy release which varied over the cross section were 50-60% higher than for a constant energy release. In view of this, the question of temperature nonuniformities around the perimeter of fuel elements when the energy release varies over the FEA cross section is very urgent and requires further study.

NOTATION

s, pitch of fuel element lattice; d = 2R, outside diameter of fuel element; s/d, relative pitch of fuel element lattice; t_w, temperature of fuel element surface; t_w^{max}, t_w^{min}, maximum and minimum temperatures of fuel element surface on the part under consideration; t_i, temperature rise of coolant in cells; $\Delta t\varphi = t_w^{max} - t_w^{min}$, temperature nonuniformity around fuel element perimeter; λ_t, ρ, C_p, thermal conductivity, density, and specific heat of coolant; D_b, diameter of blockage; Re, Pe, Reynolds and Peclet numbers calculated for coolant velocity w averaged over FEA cross section and hydraulic diameter of central cells of FEA; β, ratio of blocked through cross section to total through cross section of FEA.

LITERATURE CITED

1. A. I. Leipunskii, O. D. Kazachkovskii, and I. I. Afrikantov, Sodium-Cooled Fast Reactors [in Russian], Proc. Third Int. Conf. on Peaceful Uses of Atomic Energy, Vol. 6, New York (1965), p. 45.
2. O. D. Kazachkovskii, A. G. Meshkov, F. M. Mitenkov, et al., "Program and state of work on fast reactors in the Soviet Union," At. Energ., 43, 343 (1977).
3. M. F. Troyanov, "Development of the scientific-technical bases of fast power reactors," At. Energ., 50, No. 2, 102-109 (1981).
4. O. D. Kazachkovskii, N. V. Krasnoyarov, V. A. Afrikantov, et al., "Principal results of the operation of the BOR-60 reactor," in: Collection of Papers of Second Symposium of COMECON Countries on: "State and prospects of experiments on the construction of nuclear power plants with fast reactors" [in Russian], Obninsk: ONTI FÉI, Vol. 1 (1975), p. 356.
5. A. I. Leipunskii, F. M. Mitenkov, V. V. Orlov, et al., "Experience in startup and adjustment operations and power startup of BN-350 reactors," ibid, p. 307.
6. A. I. Leipunskii, I. I. Afrikantov, I. S. Golovnin, et al., "A nuclear power station with the BN-600 reactor," At. Energ., 25, 503 (1968).
7. G. P. Bogoslovskaya, A. V. Zhukov, A. P. Sorokin, et al., "Temperature field in heat-liberating piles of fast reactors," At. Energ., 55, 281 (1983).
8. A. V. Zhukov, N. M. Matyukhin, and E. Ya. Sviridenko, "Temperature distributions and heat transfer in peripheral zones of hexagonal fuel element assemblies of fast reactors," Vopr. At. Nauki Tekh., Ser. Reaktorostr., No. 4(18), 5 (1977).
9. V. I. Subbotin, M. Kh. Ibragimov, P. A. Ushakov, et al., Hydrodynamics and Heat Transfer in Nuclear Power Installations (Fundamentals of Calculation) [in Russian], Atomizdat, Moscow (1975).
10. A. V. Zhukov, A. P. Sorokin, P. A. Ushakov, et al., "In-channel thermohydraulic calculation of nuclear reactor fuel element assemblies," At. Energ., 51, 307 (1981).
11. G. B. Usynin, A. S. Karabasov, and V. A. Chirkov, Optimized Models of Fast Reactors [in Russian], Atomizdat, Moscow (1981).
12. A. V. Zhukov, N. A. Kotovskii, L. K. Kudryavtseva, et al., "Interchannel interaction in fast reactor fuel element lattices," in: Thermophysics and Hydrodynamics of Fast Reactor Cores and Steam Generators, Vol. 1 [in Russian], KAÉ ChSSR (1978), p. 132.
13. A. V. Zhukov, Yu. N. Kornienko, A. P. Sorokin, et al., "Methods and programs of subchannel thermal-hydraulic calculation of fuel element assemblies with allowance for interchannel interaction of coolant," Analytical Survey [in Russian], OB-107, Obninsk: ONTI FÉI (1980).
14. A. V. Zhukov, N. M. Matyukhin, and E. Ya. Sviridenko, "Experimental study of the effect of lattice deformation on the temperature distribution of peripheral fuel elements," in: Thermophysical Research, Part 1 [in Russian], FÉI, Obninsk (1980), p. 27.
15. G. P. Boroslovskaya, A. V. Zhukov, A. P. Sorokin, et al., "Investigation of thermal-hydraulic characteristics of fuel element assemblies with a partially blocked through cross section," Analytical Survey [in Russian], OB-146, Obninsk: ONTI FÉI (1982).
16. P. A. Ushakov, Yu. S. Yur'ev, and A. P. Kolmakov, "Velocity, pressure, and temperature distributions in fast reactor fuel element assemblies for blockage of a through cross section," in: Heat and Mass Transfer VI [in Russian], ITMO Akad. Nauk BSSR (1980), Vol. 8, p. 173.
17. A. V. Zhukov, N. M. Matyukhin, and K. S. Rymkevich, "Effect of blockage of through cross section of a model of a fast reactor fuel element assembly on the distribution of coolant velocity," Preprint FÉI-1979, Obninsk (1983).
18. O. D. Kazachkovskii, A. V. Zhukov, N. M. Matyukhin, et al., "Intensification of heat and mass transfer in fast reactor fuel element assemblies with counter windings for nonuniform heat release over the cross section of the assembly," Preprint FÉI-1396, Obninsk (1983).
19. A. V. Zhukov, N. M. Matyukhin, K. S. Rymkevich, et al., "Comparison of coefficients of interchannel intermixing for different methods of spiral ribbing of rods," Preprint FÉI-1158, Obninsk (1981).
20. A. V. Zhukov, N. M. Matyukhin, E. Ya. Sviridenko, et al., "Temperature distributions in deformed lattices of fast reactor fuel elements with uniform heat loads," Preprint FÉI-909, Obninsk (1979).

INTERACTION FORCES AND DEFORMATION OF FAST-REACTOR FUEL ASSEMBLIES

Yu. I. Likhachev and L. V. Matveenko

UDC 621.039.546.8

The inhomogeneous expansion of fuel-assembly casings due to nonuniform temperature and neutron fields in the cores of fast reactors at large fluxes results in significant distortion of the fuel assemblies, which leads to their mechanical interaction in the core. To ensure safe operation of the core, it is necessary to know the kinetics of variation in the elastic deformation of the casings and the interaction forces between fuel assemblies.

Note that the casing of the control and safety system is of significantly greater rigidity than the fuel-assembly casings, and is made from low-expansion and low-creep matrial. In addition, nonuniformity of the neutron and temperature fields is observed around the units of the control and safety system, which influences the distortion of the neighboring fuel assemblies. With frequent reloading of the core, when the individual spent fuel assemblies are replaced by fresh ones, which are straight and unswollen, inhomogeneous three-dimensional interaction between the fuel assemblies arises close to the replenished units.

At present, computational programs for taking account of all the above-noted inhomogeneities are at the disposal of these developing fast reactors. According to the available data, these programs are based on the use of two methods: the method of gap iteration, for example, DDT (German Federal Republic [1]), and the HARMONIE energy method (France [2]). The two methods entail the use of a high-speed computer with a large operative memory, since a large number of laborious operations must be performed. This complicates their practical application. In addition, in the opinion of researchers, the convergence of the methods cannot be established theoretically, but only on the basis of experience in using the algorithms.

At the Physical and Energy Institute, a mathematical model and method of calculation for fuel-assembly deformation in the core of a fast reactor in a three-dimensional formulation have been developed. The equilibrium equations for the fuel-assembly system in the core are equations ensuring that the flexural forces acting on the assembly are equal to the uniformly acting contact forces on the faces of the assembly in contact with adjacent fuel assemblies. This system of equations is nonlinear, since the flexural forces act on the fuel assembly only on contact with the adjacent fuel assemblies, which means that the equation needs an additional coefficient equal to zero in the absence of contact and unity otherwise.

The search for the equilibrium position of the fuel-assembly system is based on Lagrangian variational principles [3], when the equilibrium equation is replaced by the condition for a minimum of the system's potential energy, under the condition of compatibility of the deformation.

In the present case, this entails that the fuel-assembly cross sections do not overlap. The following assumptions are made here: the fuel assembly is hinged to the upper and lower plates of the delivery collector; contact forces are directed perpendicular to the faces (frictional forces are neglected); torsion of the rod is not considered; contact may occur along a plane (the distance piece at the face of the fuel assembly in the upper part of the casing) and in the middle of the core length; creep deformation is taken into account according to aging theory.

Thanks to the linear dependence of the radiational-creep rate on the stress, solving the creep problem reduces to solving a series of elastic problems with reduced elastic moduli, decreasing as the number of displacements per atom increases [4, 5]. Taking the radiational swelling into account reduces to summing the distortions due to nonuniformity of the swelling deformation over the fuel-assembly cross section with the temperature distortions [4, 5].

The potential energy of the system is the sum of the potential-energy values of the individual fuel assemblies, which consist of the energy of fuel-assembly flexure on account

Translated from Atomnaya Énergiya, Vol. 58, No. 4, pp. 232-237, April, 1985. Original article submitted July 23, 1984; revision submitted November 15, 1984.

0038-531X/85/5804-0259$09.50

of the reaction forces from the adjacent fuel assemblies and the flexural energy of the fuel-assembly faces under the action of contact forces at the level of the planes and in the middle of the core. The potential energy is described by a function of the displacement of the fuel-assembly faces, and the dependence of the forces on the displacement is assumed to be linear, taking account of the variability in the reduced elastic modulus over the length of the fuel assumbly.

The flexural energy of the faces is expressed in terms of their rigidity k_1, k_2 and the flexure of the faces at two levels δ_i (i = 1, ..., 12)

$$u_{\text{flex}} = \sum_{1}^{6} k_1 (\delta_i)^2 + \sum_{7}^{12} k_2 (\delta_i)^2,$$

where δ_i (i = 1, ..., 6) denotes the flexure of the faces of a hexahedron at the level of the planes; δ_i (i = 7,..., 12) denotes the flexure of the faces at the level of the center of the core; k_j (j = 1, 2) is half the rigidity of the face at the given level.

The energy of rod flexure with a variable elastic modulus over the length may be determined in terms of the displacement from the initial position of the rod with respect to the X and Y axes at the level of the vertices δ_x^1 and δ_y^1 and at the level of the center of the core δ_x^2 and δ_y^2, where contact with the adjacent fuel assemblies is observed. The energy of rod flexure will be

$$u_{\text{flex}} = n_1 [(\delta_x^1)^2 + (\delta_y^1)^2] + n_2 [(\delta_x^2)^2 + (\delta_y^2)^2] + n_3 (\delta_x^1 \delta_x^2 + \delta_y^1 \delta_y^2),$$

where n_1, n_2, n_3 are coefficients expressed in terms of the fuel-assembly rigidity in flexure

$$n_1 = \frac{k_{22}}{2(k_{11}k_{22} - k_{12}^2)}; \quad n_2 = \frac{k_{11}}{2(k_{11}k_{22} - k_{12}^2)};$$

$$n_3 = \frac{k_{12}}{2(k_{11}k_{22} - k_{12}^2)};$$

k_{11}, k_{12}, k_{22} are Maxwellian influence coefficients.

Since the flextural forces under whose influence the rod axis is shifted by δ_x^1, δ_x^2, δ_y^1, δ_y^2 are uniformly acting contact forces on each fact, and the latter, in turn, are linear functions of the face flexure, the displacement of the rod axis is expressed in quadriatic form in terms of the displacement coordinates of the face centers at the two levels, which corresponds to a (12 × 12) matrix

$$\begin{aligned} u = &\sum_{i=1}^{6} k_1 (\delta_i)^2 + \sum_{i=7}^{12} k_2 (\delta_i)^2 + \\ &+ n_1 [(k_{11}k_1\alpha_1 + k_{12}k_2\alpha_2)^2 + (k_{11}k_1\alpha_3 + k_{12}k_2\alpha_4)^2] + \\ &+ n_2 [(k_{12}k_1\alpha_1 + k_{22}k_2\alpha_2)^2 + (k_{12}k_1\alpha_3 + k_{22}k_2\alpha_4)^2] + \\ &+ n_3 [(k_{11}k_1\alpha_1 + k_{12}k_2\alpha_2)(k_{12}k_1\alpha_3 + k_{22}k_2\alpha_4) + \\ &+ (k_{11}k_1\alpha_3 + k_{12}k_2\alpha_4)(k_{12}k_1\alpha_3 + k_{22}k_2\alpha_4)], \end{aligned} \tag{1}$$

where

$$\{\alpha\} = \begin{Bmatrix} \alpha_1 \\ \alpha_2 \\ \alpha_3 \\ \\ \alpha_4 \end{Bmatrix} = \begin{cases} \sqrt{3}/2\,(\delta_2 + \delta_3 - \delta_5 - \delta_6) \\ \sqrt{3}/2\,(\delta_8 + \delta_9 - \delta_{11} - \delta_{12}) \\ \delta_1 + 1/2\delta_2 - 1/2\delta_3 - \delta_4 - \\ \quad - 1/2\delta_5 + 1/2\delta_6 \\ \delta_7 + 1/2\delta_8 - 1/2\delta_9 - \delta_{10} - \\ \quad - 1/2\delta_{11} + 1/2\delta_{12}. \end{cases}$$

Taking account of the large number of rods in the core, minimization of this quadratic form becomes difficult. Reducing the quadratic form in Eq. (1) to the sum of squares entails passing from the original basis to one whose elements are eigenvectors of the energy matrix.

Flexure of the hexahedral faces under the action of contact forces at the two contact levels may be characterized by 12 two-dimensional radius vectors, each of which runs from the initial position of the center of the face to the position of the center of the face after flexure. The set of these 12 two-dimensional vectors is regarded as a vector in 24-dimensional space – the space of deviations M. Formally expanding this space to complex form M_c and

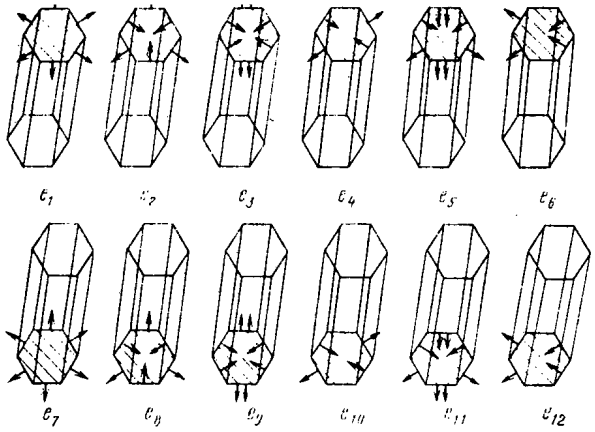

Fig. 1. Set of basis vectors.

introducing the scalar product $(\mathbf{r}_1, \mathbf{r}_2) = \sum_{j=1}^{12} (\mathbf{r}_j^{(1)}, \mathbf{r}_j^{(2)})$, where $(\mathbf{r}_j^{(1)}, \mathbf{r}_j^{(2)})$ is the usual scalar product in two-dimensional space, group-representation theory may be used to find the basis vectors of space M.

The symmetry group of a hexahedral rod is the group of motions of a hexagon D_6 of twelfth order. The representation of this group acting on the elements of the given space will be called a mechanical representation. Then, the irreducible subspaces of M_c will be transformed with respect to irreducible representations of the mechanical representation.

Determining the number of appearances of the irreducible representations of group D_6 in the mechanical representation and the corresponding basis vectors, a set of basis vectors for deviation space is obtained (Fig. 1). The coordinates relative to these vectors are called symmetric.

The potential energy of the rod is expressed in the form of a positive-definite quadratic form of the symmetric coordinates. On rotation and displacement of the rod as a whole, the potential energy is unchanged, since the relative distances are unchanged. This significantly limits the possible values of the coefficients of this form. Averaging over the elements of group D_6 and taking account of the orthogonality of the matrix elements, it is found that the quadratic form breaks down into the sum of quadratic forms, each of which depends only on the symmetric coordinates associated with only one irreducible representation of group D_6. The number of quadratic forms with perfectly identical coefficients into which the specified form breaks down is determined by the dimensionality of the representation. Passing to real vectors, it is found that

$$u = k_1 (q_1^2 + q_2^2 + q_3^2 + q_4^2) + k_2 (q_7^2 + q_8^2 + q_9^2 + q_{10}^2) + f_1 (q_5^2 + q_6^2) + f_2 (q_{11}^2 + q_{12}^2) + f_3 (q_5 q_{11} + q_6 q_{12}), \qquad (2)$$

where f_1, f_2, f_3 are functions expressed in terms of k_{11}, k_{12}, k_{22}, and k_1, k_2; q_i (i = 1, ..., 12) are new coordinates.

The nominal position of the fuel-assembly is characterized by two parameters i, j: respectively the number of the series and the number of the fuel-assembly in the series, counting clockwise from the Y axis (Fig. 2). The fuel-assembly faces take the number m = 1, ..., 6 for the vertex level and m = 7, ..., 12 for the center of the core.

The straight lines connecting the centers of adjacent fuel assemblies in the initial unshifted position are directed at an angle of 60° to one another. In each of these directions, the hexahedron may come in contact with the adjacent fuel-assembly. Since it is supposed that the contact forces act perpendicular to the faces which are parallel to the straight lines connecting the centers in the nominal lattice, the orientation of these faces is unchanged (they are not rotated).

Then the compatibility condition for the deformation in the fuel-assembly system will be that the gap between the centers of the hexahedra with respect to each of these directions must be larger than or equal to the sum of half the dimensions under the key of the contacting hexahedrons minus the flexure of the two adjacent faces under the action of the contact forces, i.e., the projection of the relative displacement of the centers of the hexahedra in the

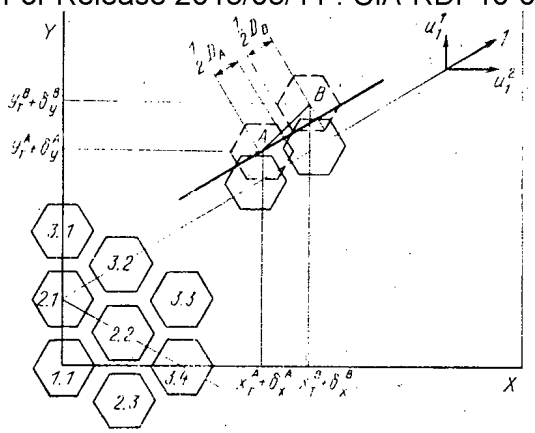

Fig. 2. Calculation scheme for core.

direction of the lines of their centers in the nominal lattice must be larger than or equal to half the sum of the dimensions under the key of the fuel-assembly minus the flexure of the two adjacent faces

$$(\delta_x^A - \delta_x^B)\, u_i^1 + (\delta_y^A - \delta_y^B)\, u_i^2 + \delta_i^A + \delta_{(i+3)_{\mathrm{mod}\,6}}^B + D + (x_T^A - x_T^B)\, u_i^1 + (y_T^A - y_T^B)\, u_i^2, \qquad (3)$$

where δ_x^i, δ_y^i denote the displacement of the center of the hexahedra due to flexural forces from the position of free flexure along the axes X and Y; x_T^i, y_T^i are the coordinates of free flexure of the i-th hexahedron (i = A, B); δA_i is the flexure of the i-th face of the hexahedron A as a result of the action of contact forces (the direction from hexahedron A is chosen as the positive direction δ_i); u_i^1, u_i^2 are the directional cosines of the straight line between centers; D is the half sum of the dimensions under the key of the hexahedra A and B, taking account of the swelling and radiational creep of the casing; $\delta^B_{(i+3)\mathrm{mod}\,6}$ is the flexure of the face of hexahedron B adjacent to the m-th face of hexhedron A. An equation of the form in Eq. (3) is written for each face of the two levels and takes the form of a deformation compatibility equation. Writing the deformation compatibility equations in symmetric coordinates entails expressing the flexure of the faces in new coordinates.

For each rod, the vector with the flexure of the 12 faces of the hexahedron as its elements may be obtained by multiplying the vector of new coordinates by the unitary orthonormalized matrix A

$$\delta = Aq; \quad A = \begin{pmatrix} a & 0 \\ 0 & a \end{pmatrix}$$

$$a = \frac{1}{2\sqrt{3}} \begin{pmatrix} \sqrt{2} & \sqrt{2} & 2 & 0 & -2 & 0 \\ \sqrt{2} & -\sqrt{2} & -1 & \sqrt{3} & -1 & \sqrt{3} \\ \sqrt{2} & \sqrt{2} & -1 & -\sqrt{3} & 1 & -\sqrt{3} \\ \sqrt{2} & -\sqrt{2} & 2 & 0 & 2 & 0 \\ \sqrt{2} & \sqrt{2} & -1 & \sqrt{3} & 1 & \sqrt{3} \\ \sqrt{2} & -\sqrt{2} & -1 & -\sqrt{3} & -1 & \sqrt{3} \end{pmatrix}$$

Substituting the value of δ into compatibility Eq. (3), it follows for internal fuel-assemblies of sector 60° that:

a)

$$\begin{aligned} &-\sqrt{3}\,[(k_{11}^{i,j}k_1^{i,j}q_6^{i,j} + k_{12}^{i,j}k_2^{i,j}q_{12}^{i,j} - \\ &- k_{11}^{i+1,j}k_1^{i+1,j}q_6^{i+1,j} - k_{12}^{i+1,j}k_2^{i+1,j}q_{12}^{i+1,j})\, u_1^1 + \\ &+ (k_{11}^{i,j}k_1^{i,j}q_5^{i,j} + k_{12}^{i,j}k_2^{i,j}q_{11}^{i,j} - k_{11}^{i+1,j}k_1^{i+1,j}q_5^{i+1,j} - \\ &- k_{12}^{i+1,j}k_2^{i+1,j}q_{11}^{i+1,j})\, u_1^2] + \sum_{l=1}^{6} a_{1l}q_l^{i,j} + \\ &+ \sum_{l=1}^{6} a_{4l}q_l^{i+1,j} + b_1^{i,j} \leqslant 0; \end{aligned} \qquad (4)$$

$$b_1^{i,j}=\frac{1}{2}(E_1^{i,j}+E_1^{i+1,j})+(x_{T1}^{i,j}-x_{T1}^{i+1,j})u_1^1+(y_{T1}^{i,j}-y_{T1}^{i+1,j})u_1^2;$$

b) the equations for the remaining faces are written analogously.

In general form, the compatibility equation is

$$B\mathbf{q}\leqslant\mathbf{b}.$$

Thus, the following nonlinear-programming problem is obtained: to minimize $1/2q^TCq$ under the condition $Bq \leqq b$, where C is a symmetric positive-definite matrix, so that the target function is strictly convex. The Lagrangian double problem consists [6] in maximization of $\theta(\lambda)$ when $\lambda \geqq 0$, where

$$\theta(\lambda)=\inf\left\{\frac{1}{2}\mathbf{q}^TC\mathbf{q}+\lambda^T(B\mathbf{q}-\mathbf{b}):\mathbf{q}\in E_n\right\}. \tag{5}$$

At fixed λ, the function $1/2q^T\ Cq + \lambda^T\ (Bq - b)$ is strictly convex, and reaches a minimum at a point satisfying the equation

$$C\mathbf{q}+B^T\lambda=0. \tag{6}$$

Thus, the double function may be written in the following form: to minimize $(1/2)q^T\cdot Cq + \lambda^T\ (Bq - b)$ under the condition $Cq + B^T\ \lambda = 0;\ \lambda \geqq 0$.

Since C is a positive-definite matrix, there exist an inverse matric C^{-1} and a unique solution of Eq. (6)

$$\mathbf{q}=-C^{-1}B^T\lambda.$$

Substituting this expression into Eq. (5) gives

$$\theta(\lambda)=\frac{1}{2}\lambda^TD\lambda-\lambda^T\mathbf{b},$$

where

$$D=-BC^{-1}B^T.$$

Then the double problem is written in the following form: to maximize $(1/2)\lambda^T\ D\lambda - \lambda^Tb$ under the condition $\lambda \geqq 0$. It is solved by the gradient method by the scheme given below.

With specified λ, $\nabla\theta(\lambda)$ is calculated:

$$\nabla\theta(\lambda)=D\lambda-\mathbf{b}=g.$$

The definition of $\hat{g}$ is

$$\hat{g}_i=\begin{cases} g_i, & \text{if} \quad \lambda_i>0 \text{ or } g_i\geqslant 0;\\ 0, & \text{if} \quad \lambda_i=0 \text{ and } g_i<0.\end{cases}$$

Next, λ is specified. If $\hat{g} = 0$, the vector λ is the optimal solution. Otherwise, $\hat{g}$ is an acceptable direction of search. Optimizing θ from the point λ_k along the direction $\hat{g}$ so that the condition of nonnegativity holds, the new point λ_{k+1} is reached. Then the process is repeated, i.e., in each step the problem of maximizing $\theta(\lambda_k+u\hat{g}_k)$ under the condition $\lambda_k + u\hat{g}_k \geqq 0$ is solved.

Let u_k be the optimal solution of this problem,

$$u_k\leqslant-\frac{\hat{g}_k^T\hat{g}_k}{\hat{g}_k^TDg_k}.$$

Then it is assumed that

$$\lambda_{k+1}=\lambda_k+u\hat{g}_k$$

and the vector g_{k+1} is determined. If $g_{k+1} = 0$, the vector λ_k is an optimal solution of the given problem.

To determine the matrix D, the coordinates are expressed in terms of Lagrangian coefficients

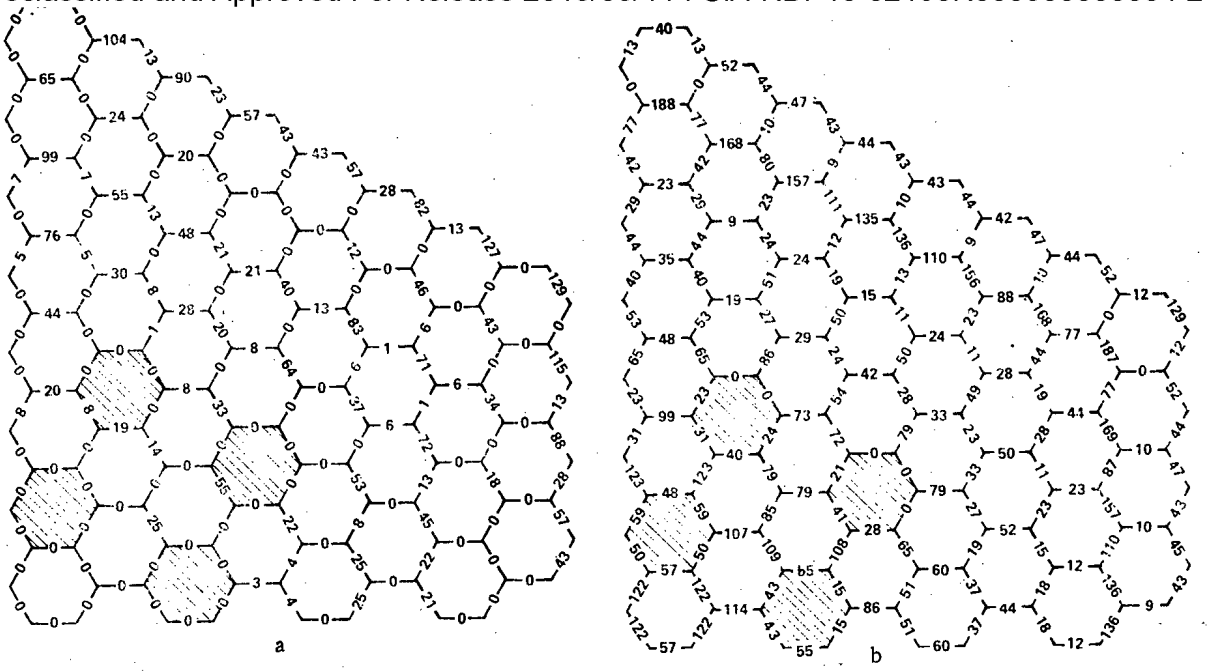

Fig. 3. Contact forces (kgf; 1 kgf = 9.807 N) at the fuel-assembly faces of a reactor of type BN-350 after 500 h operation without reloading, at the level of the planes (a) and at the level of the central core (b).

$$q_n = -\frac{1}{2k_1}\sum_{m=1}^{6}\lambda_m a_{mn};$$

$$q_{n+6} = -\frac{1}{2k_2}\sum_{m=1}^{6}\lambda_{m+6}a_{mn},\quad n = 1,\ \ldots,\ 4;$$

$$q_n = F_n\sum_{l=1}^{6}\lambda_l u_l^s + \Psi_n\sum_{l=1}^{6}\lambda_{l+6}u_l^s - \sum_{m=1}^{6}\chi_n;$$

$$n = 5,\ 6,\ 11,\ 12;$$

$$F_n = \sqrt{3}\,(f_3k_{1j}k_j - 2f_jk_{1l}k_l)/(f_3^2 - 4f_1f_2);$$

$$\Psi_n = \sqrt{3}\,(f_3k_{j2}k_j - 2f_jk_{l2}k_l)/(f_3^2 - 4f_1f_2);$$

$$\chi_n = a_{mp}\,(f_3\lambda_{i1} - 2f_j\lambda_i);$$

$$j = 2,\ l = 1,\ i = m,\ i_1 = m + 6 \text{ for } n = 5, 6;$$

$$j = 1,\ l = 2,\ i = m + 6,\ i_1 = m \text{ for } n = 11, 12;$$

$$s = 2,\ p = 5 \text{ for } n = 5, 11;$$

$$s = 1,\ p = 6 \text{ for } n = 6, 12.$$

Substituting the results in Eq. (4) gives the system

$$-\sum_{l=1}^{6}(u_l^1u_1^1 + u_l^2u_1^2)\,(\lambda_l^{i,j}k_{11}^{i,j} - \lambda_l^{i+1,j}k_{11}^{i+1,j} +$$

$$+\lambda_{l+6}^{i,j}k_{12}^{i,j} - \lambda_{l+6}^{i+1,j}k_{12}^{i+1,j}) -$$

$$-\left(\frac{1}{2k_1^{i,j}} + \frac{1}{2k_1^{i+1,j}}\right)\lambda_1^{i,j} + b_1^{i,j} = g_1^{i,j};$$

$$-\sum_{l=1}^{6}(u_l^1u_1^1 + u_l^2u_1^2)\times$$

$$\times(\lambda_l^{i,j}k_{12}^{i,j} - \lambda_l^{i+1,j}k_{12}^{i+1,j} + \lambda_{l+6}^{i,j}k_{22}^{i,j} - \lambda_{l+6}^{i+1,j}k_{22}^{i+1,j}) -$$

$$-\left(\frac{1}{2k_2^{i,j}} + \frac{1}{2k_2^{i+1,j}}\right)\lambda_7^{i,j} + b_7^{i,j} = g_7^{i,j},$$

which is a developed form of the system $\nabla^{\theta}(\lambda) = D\lambda - b = g$. It is obvious that the coefficients λ may be understood as contact forces.

In each row of the resulting matrix D there are no more than 24 nonzero elements. For the BN-600 reactor, its order is approximately 4000. The given algorithm is realized in the form of a program written in Fortran for the ES-1060 computer, the scope of which satisfies the constraints imposed.

The calculation time for a single variant of the equilibrium state of the zone, with an accuracy of ~1 N for the interaction force beteeen the fuel assemblies, is no more than 30 sec. The results of calculating the interaction force between fuel assemblies in the middle part of the core of a reactor of type BN-350 including elements of the safety and control system are shown in Fig. 3. The interaction forces (at the faces) after 5000 h of reactor operation at nominal power without reloading are shown. The elements of the safety and control system are shaded in Fig. 3. It is evident that the distribution of contact forces at the fuel-assembly faces is inhomogeneous, and depends on the position and orientation of fuel assemblies in the core.

LITERATURE CITED

1. R. Menssen, "DDD-A. Three-dimensional program for the analysis of bowed reactor cores," in: Transactions of the Fourth SMIRT International Conference, San Francisco (1977).
2. A. Bernard, "Calculation of equilibrium configurations of a hexagonal array of deformed subassemblies," in: Transactions of Fifth International SMIRT Conference, Berlin (1979).
3. Yu. N. Rabotnov, Mechanics of a Deformed Solid [in Russian], Nauka, Moscow (1979).
4. Yu. I. Likhachev and Yu. N. Vashlyaev, Method of Calculating the Interaction between Fuel Assemblies of the Core of Fast Reactors in Use, Preprint FÉI-933 [in Russian], Physics and Energy Institute, Obninsk (1979).
5. Yu. I. Likhachev, Yu. N. Vashlyaev, and I. N. Kravchenko, Method of Calculating the Interaction Forces and Deformation of Fuel Assemblies in the Core of a Fast Reactor, Taking Account of the Influence of Elements of the Safety and Control System and the Shutdown Cooling of the Reactor, Preprint FÉI-1087 [in Russian], Physics and Energy Institute, Obninsk (1980).
6. M. Bazara and K. Shetti, Nonlinear Programming, Theory and Algorithms [Russian translation], Mir, Moscow (1982).

PULSATIONAL CHARACTERISTICS OF THE NATURAL-CIRCULATION LOOP OF A LARGE-SCALE MODEL OF A LIGHT-BOILING BOILING-WATER REACTOR

A. S. Babykin, B. F. Balunov,
T. S. Zhivitskaya, E. L. Smirnov,
V. I. Tisheninova, and N. G. Chernykh

UDC 621.039.553.34

In this paper the results of an experimental study of a natural-circulation (NC) loop, whose geometrical and hydraulic characteristics are presented in [1], are described. The range of state parameters encompassed in the experiments is also indicated in [1].

The distinguishing feature of a light-boiling NC loop is the substantial change in the coolant density in it in the thrust section accompanying an insignificant change in the output steam content x_c^{out}. This phenomenon is linked to the nonlinearity of the dependence $\rho = f(i)$, which has a zone of high values $|d\rho/di|$ at $i \approx i'$. Significant increments to the values of the heat content of the coolant in the simulator of the core (c) $\Delta i_c = \bar{c}_p(\Delta t_{under})_c^{in} + rx_c^{out} - (di'/dp)\Delta p_c$ [where c_p is the isobaric heat capacity of the coolant; $(\Delta t_{under})_c^{in} = t_{sat} - t_{in}^c$ is the underheating of the coolant up to the saturation temperature at the inlet to the simulator of the core; r is the latent heat of vaporization; Δp_c is the pressure drop in the simulator of the active zone; $x_c^{out} = 1/r\ (i_c^{out} - i')$ is the balancing steam content of the coolant at the outlet from the core simulator] lead to the fact that small relative changes in the coolant flow rate or the intensity of the core (with $t_c^{in} = \text{const}$) are associated with changes by several factors in the coolant density in the thrust section. The height of this section is equal to

Translated from Atomnaya Énergiya, Vol. 58, No. 4, pp. 237-241, April, 1985. Original article submitted January 17, 1984; revision submitted June 11, 1984.

0038-531X/85/5804-0265$09.50

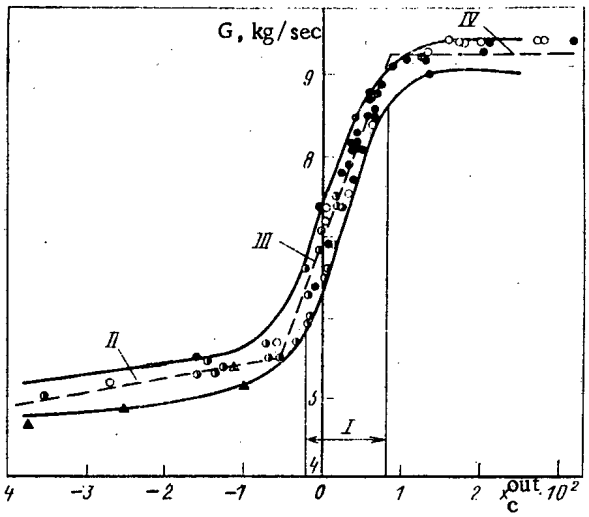

Fig. 1. The dependence $G = f(x_c^{out})$ with p = 1.7-2.3 MPa. Here and in Fig. 2: ●) N_c = 1760 kW; ○) N_c = 1580-1630 kW; ◑) N_c = 1430-1560 kW; ▲) N_c = 1110-1340 kW; I) zone of pulsations of the coolant flow rate; II, III, IV) lines averaging the experimental data; ——) boundaries of the spread in the experimental data.

7.2 m, or 70% of the total height of the NC loop. Thus, the thrust pressure in the NC loop is primarily determined by the steam content in the thrust section. The actual transit time of the two-phase coolant through the thrust section is equal to 6-12 sec. As pointed out in [2], the indicated factors can lead to the appearance of general loop pulsations in the flow rate of the coolant in the NC loop.

The calculation of the hydrodynamic stability of the circulation loops is based, in particular, on the stationary characteristics of the loop [for an NC loop, for example, $G = f(x_c^{out})$ for constant values of the pressure p_c^{out}, intensity N_c or temperature t_c^{in}, and water level in the model]. These characteristics of the NC loop under study are presented in [1]. This paper is concerned with the solution of the following problems: to determine the boundaries of instability of the operation of the NC loop under study accompanying a change in the state parameters and the introduction of several structural changes and to check the effectiveness of the methods used to increase the stability of the NC loop.

The pulsations in the flow rate of the coolant, accompanied by pulsations in the pressure in the model and of the coolant temperature at the outlet from the core simulator, were observed in the zone where the natural circulation of water changes into the natural circulation of the two-phase flow (see Figs. 1 and 2). This transition is characterized by high values of $B = dG/Gdi_c^{out}$. For a known stationary flow rate characteristic of the loop, we used the following dimensionless parameter as the static feedback gain:

$$A = \frac{\delta G_{out}}{\delta G_{in}} = \frac{dG}{di_c^{out}} \frac{\Delta i_c}{G}.$$

The validity of this identity can be easily demonstrated, since for N_c = const a perturbation of the flow rate $\delta G_{in}/G_{in}$ leads to a perturbation of the modulus of the output heat content $\delta i_c^{out}/\Delta i_c = \delta G_{in}/G_{in}$.

The presence of a heat exchanger, the coolant transit time through which exceeds approximately by a factor of three the period of the pulsations of the flow rate, practically eliminates the pulsations in the coolant temperature at the inlet to the core simulator. For this reason, the loop can be viewed as a quasiopen loop at the inlet. To simplify the calculations we shall approximate the experimental dependence $G = f(x_c^{out})$ presented in Fig. 1 by the dashed line II–IV. We note that for natural circulation of a single-phase coolant (the line II) the value $B \approx 2 \cdot 10^{-3}$ kg/kJ, and for the transitional region (the line III) $B \approx 26 \cdot 10^{-3}$ kg/kJ,* i.e., for the same values of G the gain in the second case is approxi-

*In determining B we shall use the value $G = G_{sp}$ at the point of intersection of the lines II and III. In the first approximation this value of G corresponds to the minimum flow rate of the coolant in the pulsation state.

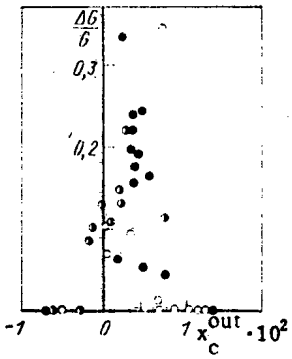

Fig. 2. The dependence $\Delta G/G = f(x_c^{out})$.

mately 10 times higher than that in the first case. From what was said above it also follows that pulsations (or their maximum amplitude) with x_c^{out} corresponding to the center of the line III are most likely to appear. The latter fact is confirmed by experiment (see Figs. 1 and 2).

An increase in the power leads to a growth of Δi_c, but decreases the probablility of finding the entire range δi_c^{out} in the zone of large values $B = B_{max}$ (with $\delta G/G$ = idem). In addition, an increase in power is accompanied by an increase in the flow rate of nonboiling coolant G_{sp} (line II) with, for all practical purposes, constant flow rate G_{tp} on the line III and by a decrease in the value of B_{max}. The monotonic increase in the amplitude of the pulsations with increasing power of the NC loop is therefore not obvious. The latter was registered in experiments (see Fig. 2). The depencence $\Delta G/G = f(N_c)$ cannot be clearly discerned in the graph.

The amplitudes of the pressure pulsations were equal to $\delta p = \pm(1\text{-}2)\cdot 10^{-2}$ MPa, the amplitudes of the pulsations of the total pressure drop on the core simulator $\delta(\Delta p_c) = \pm(0.4\text{-}2.6)$ kPa, and the amplitudes of the pulsations in the temperature of the coolant $\delta t_c^{out} = \pm(0.2\text{-}0.5)$°C, i.e., $\delta t_c^{out} = \partial t_{sat}/\partial p(\delta p)$.

The value of the parameter A with constant power can be decreased by injecting dry inert gas with a low relative flow rate $\beta_g \approx G_g\rho_w/G\rho_g$ into the lower part of the thrust section (Figs. 3 and 4). In this case, the maximum values of the parameter A decrease both as a result of the increase in G_{sp} [with G_{tp} remaining practically unchanged (line IV)] and as a result of a decrease in $\Delta i_c = N_c/G$. In experiments with injection of cold air ($t \approx 20$°C) at the inlet to the thrust section, the amplitude of the pulsations was reduced to an admisable level ($\Delta G/G < 0.07$) in the entire range of x_c^{out} studied for $\beta_g > 0.01$ (N_c = 1000 kW). At the same time, the value of B for the transitional region decreased by a factor of 1.5.

It follows from Fig. 3 that for the zone with the nonboiling coolant the tangent of the slope angle of the line II is larger than that of line I. This phenomenon is attributable to the increase in the volume of gas bubbles in the thrust section as a result of their heating up and the evaporation of moisture into them from the surrounding water. Calculations as well as separate experiments showed that the intensity of the heat and mass transfer process studied is high and the thrust pressure of the NC loop can be determined with

$$\bar{\beta}_{t.s} = \beta_{mix} = \frac{G_g\rho_w}{G\rho_g^{mix}} \frac{1 - p^{inj}_{H_2O}/\bar{p}_{t.s}}{1 - p^{t.s}_{H_2O}/\bar{p}_{t.s}}.$$

where $\bar{\beta}_{t.s}$ is the average volume flow rate of the gas content over the height of the thrust section in the nonboiling operational states of the NC loop; ρ_g^{mix} is the density of the gas in the thrust section, determined at the temperature of the mixture t_{mix}; $\bar{p}_{t.s}$ is the average pressure of the coolant at the height of the thrust section; $p^{inj}_{H_2O}$ is the water vapor pressure in the gas injected from the outside; and $p^{t.s}_{H_2O}$ is the equilibrium pressure of the water vapor in the thrust section, determined for t_{mix}.

For the low values of $G_g/G \approx 2.3\cdot 10^{-4}$ observed in the experiments, the evaporation of water in the gas bubbles causes t_{mix} to drop below the initial temperature of the water t_w by less than 1°C. Thus, for $x_c^{out} \approx -0.5\%$ in the experiment, as a result of the process under study the volume of the gas bubbles increased by a factor of ten, and this in what is responsible for the high efficiency of the proposed method for eliminating pulsations in the flow rate of the coolant.

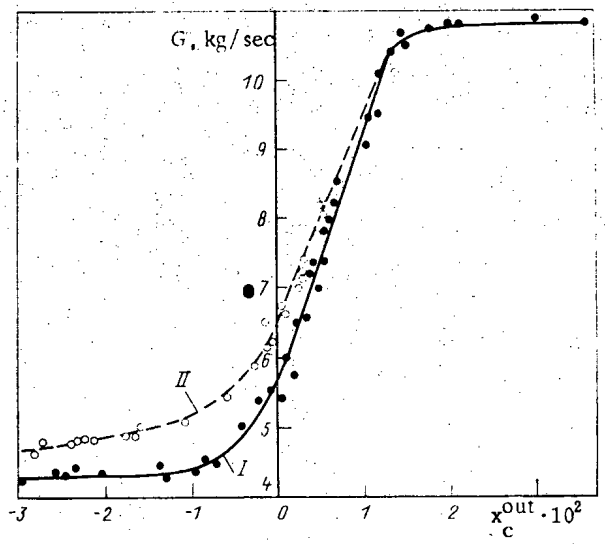

Fig. 3. The dependence $G = f(x_c^{out})$ with p = 1.8-2.3 MPa, and N_c = 1000 kW. Here and in Fig. 4: •) without injection of air; o) with injection of cold air into the lower part of the thrust section ($G_{air} \approx 1.1 \cdot 10^{-3}$ kg/sec); I, II) lines generalizing the experimental data.

The approximately 40-fold increase in the value of the overall reduced drag of the NC loop ξ^{NC}_{red}, with the ratio of the total drags of the single- and two-phase parts of the loop remaining unchanged, caused an expansion of the zone x_c^{out}, characterizing the region with pulsations in the flow rate:

$$-0.2\,\% < x_c^{out} < 0.8\,\% \text{ for } \xi^{NC}_{red} = 21.1,\ \xi^{tp}_{red} = 4.3;$$
$$-0.5\,\% < x_c^{out} < 1.8\,\% \text{ for } \xi^{NC}_{red} = 700 - 900,$$
$$\xi^{tp}_{red} = 170^*.$$

The displacement of the lower boundary is probably associated with the longer, for the second case, delay time for the change in the thrust pressure (the dynamic feedback gain), since the time of arrival of the boiling water ($x_c^{out} = 0$) in the two-phase part of the NC loop was equal to 15.3 sec and 37 sec, respectively. The displacement of the upper boundary is largely associated with the trapping of steam in the descending section of the NC loop, which decreases the value of x_{tp} and G_{tp} (the coordinates of intersection of the lines III and IV). Thus, this "parasitic" phenomenon has a positive effect on the stability of the NC loop.

A significant destabilization of the coolant flow rate in the NC loop occurs when the water level in the descending section drops to the bottom cutoff of the overflow openings and lower ($h_{des} \leq 0$) (Fig. 5). In the last case, a "rupture" of the NC loop occurs formally, though when steam is being generated the weight of the column of water in the descending section of the loop is still greater than the weight of the steam–water mixture in the ascending section; circulation along the loop remains, but it is accompanied by free flow of the coolant (the so-called "waterfall state"). In this case, in the presence of the disturbance the drop in the flow rate of the coolant, accompanied by a growth in the steam content in the ascending section, causes part of the water to be ejected not into the stagnant zone above the NC loop (as in the case $h_{des} > 0$), but rather into the descending branch of the loop, which additionally increases the amplitude of the oscillations in the flow rate. In

*In calculating the total reduced drag of the two-phase part of the NC loop (ξ^{tp}_{red}), we included 12% of the length of the core simulator (from the calculation Δi_c = 210 kJ/kg, x_c^{out} = 0.5%), the upper end and one spacer grating, the entire thrust section, and the overflow openings (the latter is linked to the specific experimental loop, whose thrust section has a small diameter, and therefore in this case a large fraction of the gas bubbles is carried away through the overflow openings [1]).

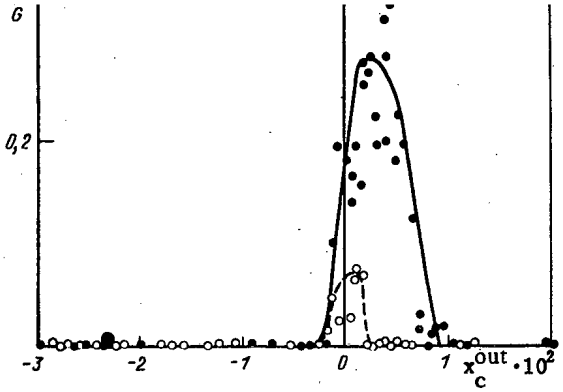

Fig. 4. The dependence $\Delta G/G = f(x_c^{out})$.

the experiments performed, for $h_{des} < -0.3$ m, the minimum value of the flow rate over the period of the pulsations $G_{min} = 0$ and $\Delta G/G = 1.0$. We point out that in our previous work [3], on a somewhat different NC loop (with $p \geq 2.5$ MPa, $x_c^{out} = 0.07$-0.1), the lowering of the water level in the descending section to $h_{des} = -2$ m ($h_{NC} = |h_{des}|/h_{NC} = 2/3$, where h_{NC} is the height of the NC loop) gave rise to a linear decrease in the flow rate in the loop and was not accompanied by pulsations in the flow rate. The periods of the pulsations in the flow rate (T_p) were equal to 5-15 sec, which differed by not more than ±15% from the computed transit time (T_{comp}) of the equilibrium homogeneous coolant through the two-phase part of the NC loop.

Increasing the water level in the model, i.e., lowering the height of the pressure compensator (PC) below 0.5 m decreased the amplitude of the pulsations in the flow rate and the amplitude of the pressure pulsations [from $(1\text{-}2)\cdot10^{-2}$ MPa to 0.03 MPa]. This fact was reported in [4], where this phenomenon was attributed to the increase in the "rigidity" of the pressure compensator, or amplification of the negative feedback (increase in the flow rate—decrease in the steam content in the ascending branch of the NC loop—increase in the volume of the PC—drop in the pressure—increase in the steam content in the NC loop, i.e., decrease in the change in the thrust pressure accompanying a change in the flow rate of the coolant over the period of the pulsation). The practical equality $T_p = T_{comp}$ confirms the important contribution of the increase in the rigidity of the PC to the stabilization of the flow rate of NC. With a constant volume of the PC (V_{PC}) the increase in the volume of the boiling coolant in the ascending section of the NC loop ($Vboil_{asc}$) increases the rigidity of the PC, while the presence of boiling coolant outside the NC loop (with volume $V^{boil}{}_{out}$) lowers the rigidity. For this reason, some cooling of the water over the NC loop and a transition to gas—steam pressure compensation is preferable. Most experiments were performed with $V_{PC} \approx 0.2\text{-}0.35$ m^3, $Vboil_{asc} = 0.12$ m^3, $Vboil_{out} = 0.14\text{-}0.28$ m^3.

It is pointed out in [4] that the flow rate of the coolant is stabilized by choking the single-phase part of the loop. In the experiments performed by the authors, when the total drag of the NC loop was increased 40-fold, choking of its single-phase part by insertion of rings with diameters of 34, 30, and 28 mm narrowed the range of limiting values $(X_c^{out})_{lim}$ with which pulsations in the flow rate of the coolant were observed and decreased the maximum amplitudes of the pulsations (Fig. 6).

Increasing the minimum limiting value of x_c^{out}, however, does not increase the "limiting" flow rate of the coolant, i.e., it does not compensate the negative effect associated with the increase in the drag of the NC loop. We point out also that even greater choking (rings with a diameter of 20 mm) did not further decrease the range $(x_c^{out})_{lim}$ and the values $(\Delta G/G)_{max}$. The latter is probably attributable to the increase in the delay time of the thrust pressure, which begins to prevail over the positive effect of the choking of the loop.

In the experiments performed with a drag in the ascending section of the NC loop close to the realistic value, choking, i.e., increase in $\xi_{red}^{sp}/\xi_{red}^{NC}$ from 0.794 to 0.88, as follows from Fig. 7, decreased somewhat the maximum amplitudes of the pulsations (from 0.34 to 0.20), but, for all practical purposes, did not narrow the range of values $-0.2\% < |x_c^{out}|_{lim} < 0.75\%$. The latter is probably attributable to trapping of steam in the descending section for $w_{des} > |w_{des}|_{lim}$ and, as a result, virtual coincidence of the value of G_{tp} in both cases is observed (with the value of G_{sp} decreasing approximately by a factor of 30% as a result of choking of the loop).

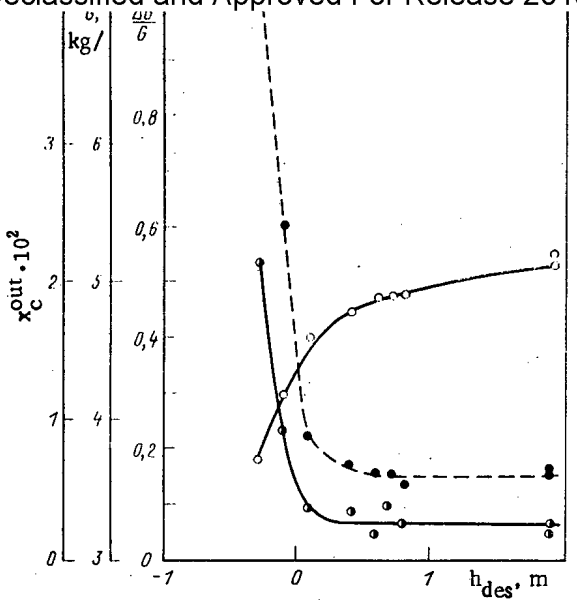

Fig. 5

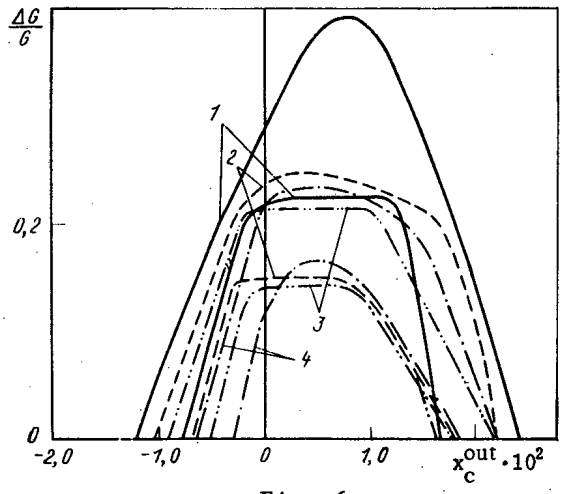

Fig. 6

Fig. 5. Variation of the circulation-pulsational characteristics of natural circulation accompanying a drop in the coolant level in the descending section of the loop for p = 2 MPa, N_c = 690 kW, t_c^{in} = 187°C: o) flow rate G; •) pulsations of the flow rate ΔG/G; ◑) the steam-content x_c^{out}.

Fig. 6. Boundaries of the spread in the experimental data on the dependences ΔG/G = $f(x_c^{out})$ with a different degree of choking of the single-phase part of the NC loop with increased drag of the thrust section: 1) diameter of rings d_r = 34 mm; 2) d_r = 30 mm; 3) d_r = 28 mm; 4) d_r = 20 mm.

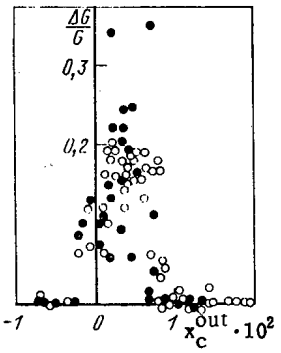

Fig. 7

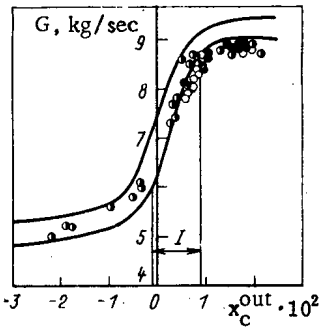

Fig. 8

Fig. 7. The dependence ΔG/G = $f(x_c^{out})$ with different degree of choking of the single-phase part of the NC loop: •) d_r = 77 mm; o) d_r = 59 mm.

Fig. 8. The dependence G = $f(_c^{out})$. Here and in Fig. 9: ◑) p = 3.3-3.8 MPa, N_c = 1530 kW; •) p = 3.3-3.8 MPa, N_c = 1730 kW; o) p = 4.3-5.0 MPa, N_c = 1730 kW. I) Zone of pulsations of the flow rate of the coolant; ——) boundaries of the spread in the experimental data with p = 1.7-2.3 MPa (see Fig. 1).

Increasing the pressure in the model from 2 MPa to 3.7 and 4.7 MPa procduced only a small change in the upper boundary value x_c^{out} (Figs. 8 and 9), characterizing the zone of pulsations in the flow rate of the coolant, from 0.75 to 0.90% and lowered the maximum values of the amplitude of the pulsations ΔG/G from 0.34 to 0.25-0.20. At the same time, the value of $(G_{tp} - G_{sp})/G_{sp}r(x_{tp} - x_{sp})_c^{out}$ decreased by 25-30%.

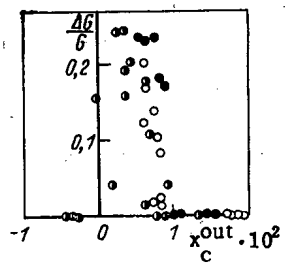

Fig. 9. The dependence $\Delta G/G = f(x_c^{out})$.

Thus, using a large-scale model of a low-boiling boiling-water reactor, with natural heights and reduced drags of separate elements of the NC loop, we performed an experimental study which confirmed that under the conditions studied ($p \leq 5.0$ MPa; $-2\% < x_c^{out} < 4\%$) the pulsations in the flow rate of the coolant occurs only in the transitional zone from natural circulation of the single-phase medium to natural circulation of the two-phase coolant [the latter is characterized by a plateau-like peak in the dependence $G = f(x_c^{out})$]. Data were obtained on the effect of different factors on the further narrowing of the studied range of variation of the boundary values x_c^{out} and the decrease in the amplitude of the pulsations. The most effective method for avoiding pulsations in the flow rate of the coolant in the entire studied range of variations of the state parameters is to inject dry inert gas with a low relative flow rate $\beta_g \geq 0.01\ T_g/293$ into the bottom cross section of the thrust section.

LITERATURE CITED

1. N. S. Alferov, A. P. Babykin, B. F. Balunov, V. A. Vakhrushev, V. S. Kuul', and E. L. Smirnov, "Circulation characteristics of the natural circulation loop of a large-scale model of a low-boiling reactor," At. Energ., 58, No. 3, 159-162 (1985).
2. F. M. Mitenkov and B. I. Motorov, Mechanisms of Unstable Processes in Thermal and Nuclear Power Production [in Russian], Atomizdat, Moscow (1981).
3. V. F. Balunov, R. A. Rybin, E. L. Smirnov, et al., "Study of the characteristics of natural circulation of a pressurized boiling reactor accompanying a drop in the water level in the reactor," Vopr. At. Nauki Tekh., Ser. Fiz. Tekh. Yad. Reaktorov, No. 3(16), 26-36 (1981).
4. F. M. Mitenkov, L. N. Kut'in, B. I. Motorov, and O. B. Samoilov, "Hydrodynamic stability of natural circulation in YaÉU with boiling of the coolant," At. Energ., 52, No. 4, 227-230 (1982).

CONSTRUCTION OF A MODEL OF THE PROCESS OF ACCUMULATION OF RADIONUCLIDES OF CORROSION PRODUCTS ON THE EQUIPMENT IN NUCLEAR POWER PLANTS WITH BOILING-WATER REACTORS

S. A. Tevlin

UDC 621.039.58'68

With modern methods for preparing water the main impurities that form deposits on the fuel elements are the products of corrosion of the structural materials of the reactor loop. Studies performed on nuclear power plants with water-cooled reactors show that the intensity of the exposure dose of radiation from the equipment in the part of the loop outside the reactor after the reactor is 80-95% shut down is due to the γ decay of the activated corrosion products (CP) [1].

One way to lower the dosage loads on the personnel at the nuclear power plant and to increase plant efficiency is to develop measures for decreasing the amount of radioactive deposits forming on the equipment. According to data obtained by French specialists, when the dosage is reduced by 100 rem per year (1 rem = 0.01 Sievert), the savings accruing from the decrease in the number of maintenance personnel is equal to 2-20 million francs [2]. Based on data obtained by American economists, one man-rem translated into ~$5000.00, and in Canada it is regarded that expenditures of up to $16,000 are compensated if they lower the dosage load by 1 rem per year [3]. These economic estimates provide the motivation for constantly improving the methods for studying the mass transfer of radionuclides along the reactor loop in nuclear power plants and calculating their accumulation on the equipment.

At the present time the accumulation of radionuclides on the equipment is calculated by constructing complicated systems of differential equations. The main drawbacks of these systems are the presence of polynomial empirical coefficients in them and the large amount of computer time required. The empirical coefficients permit solving the system and obtaining a good description of the processes occurring under those conditions for which these coefficients were determined (the "status-quo" state [1]). They do not, however, enable a satisfactory forecast of the events accompanying a change in the operational conditions of the equipment and especially accompanying a change over to other types of setups. This problem can be solved by constructing physical models of the process of accumulation of radionuclides on the equipment at nuclear power plants and by constructing the analytical apparatus for describing them. Such models permit analyzing the effect of separate states and thermophysical factors, determining the basic factors, and foreseeing in timely fashion the water state and structural measures required to lower the rate of growth and to decrease the amount of radionuclides deposited on the equipment in the nuclear power plant.

The generation of radionuclides of CP and their penetration into the coolant are determined by three processes: corrosion of the structural materials in the core, which is constantly located in a neutron field during reactor operation, and transfer of the radioactive CP into the coolant; corrosion of the structural materials in the part of the loop outside the reactor, transfer of the CP into the coolant, activation of the CP in the neutron field of the reactor within the transit time of the coolant through the core; formation of deposits of inactive CP on the heat-conducting surfaces (fuel elements) of the core, their activation in the neutron field, and the reverse transfer by partial erosion of radionuclides of the CP into the coolant.

The first two processes can be easily incorporated into the analytical apparatus due to the satisfactory approximation based on extensive experimental material, encompassing both corrosion and transfer of the CP into the water, for different conditions close to the operational conditions of the reactor loops in water-cooled power plants. At the same time, the approximation dependences have primarly only one argument – time [4]. The process of formation of deposits on the fuel elements includes a large number of thermophysical, hydrodynamic, water-state, and other factors and does not at the present time have a generally accepted

Translated from Atomnaya Énergiya, Vol. 58, No. 4, pp. 242-246, April, 1985. Original article submitted February 27, 1984.

 0038-531X/85/5804-0272$09.50

analytical description. A model of the process of formation of deposits on the heat-conducting surface accompanying boiling of the coolant was developed at the Moscow Energy Institute [5]:

$$A = \frac{C_{\bar{a}}}{\beta (K_c - 1)} [1 - e^{-B\beta (K_c - 1)\tau}], \quad (1)$$

where A is the specific quantity of the deposits of the CP, mg/m²; β is the coefficient of erosion of the deposits, m²/kg; K_c is the multiplicity of the circulation in the wall layer; B is the intensity of vaporization, kg/m²·sec; $C_{\bar{a}}$ is the part of the total concentration of impurity that actually participates in the formation of the deposits, mg/kg; and τ is the time, sec.

According to this model, the rate of change of the specific quantity of deposits in time

$$dA/d\tau = BC_{\bar{a}} - BC_{\bar{a}} [1 - e^{-B\beta (K_c - 1)\tau}] \quad (2)$$

depends on the thermophysical conditions of steam generation (B, K_c), the characteristics of the water state ($C_{\bar{a}}$), and a combination of the properties of the impurity in the solid phase, the material of the surface, and the hydrodynamics of the wall layer (β). The product $BC_{\bar{a}}$ in expression (2) determines the rate at which the impurity flows into the layer of deposits: initially at τ = 0, when there are no deposits, $dA/d\tau = BC_{\bar{a}}$, i.e., deposits are accumulated. The expression $BC [1 - e^{-B\beta(K_c - 1)\tau}]$ describes the dynamics of the reverese flow of impurities from the layer of deposits into the coolant (erosion) as a function of time. Erosion increases from zero initially to the value $BC_{\bar{a}}$ (at τ = ∞), equal to the inflow of the impurity. During this period, dynamic equilibrium between the inflowing and outflowing impurities forms and the amount of the deposits in the layer and the thickness of the layer stop increasing.

A comparison of the calculations based on this model with the experimental data on the formation of iron oxide deposits gives entirely satisfactory agreement both with regard to the general quantity of deposits and the kinetics of their growth in time (it was assumed in the calculations, in accordance with the experimental data, that for $C_{Fe_{tot}} \leq 0.2$ mg/kg $C_{\bar{a}} = C_{tot}$, $\beta = 1.5 \cdot 10^{-6}$ m²/kg for a steam-generating surface consisting of austenitic stainless steel and $\beta = 1.0 \cdot 10^{-5}$ m²/kg for a zirconium alloy). A model of the deposition process, in which the flow of impurities into and out of the layer is balanced in an explicit form, permits formulating a differential equation for the balance of the CP impurities as a whole for the reactor loop of the boiling-water reactor:

$$M \frac{dC}{d\tau} = D_{f.w} C_{f.w} + (S_{core} + S_{ex}) W_C + BC_{\bar{a}} S_{f.e} [1 - e^{-B\beta (K_c - 1)\tau}] - D_b C - D_s [\omega + (1 - \omega) K_d] C - BC_{\bar{a}} S_{f.e} - (S_{core} + S_{ex}) A_0 C. \quad (3)$$

Here M is the total mass of the coolant in the reactor loop, kg; C and $C_{f.w}$ are the concentration of the impurity under study in the coolant and in the feed water, respectively, mg/kg; $D_{f.w}$, D_s, and D_b are the flow rates of the feed water, steam, and blow-through, respectively, kg/sec; S_{core}, S_{ex}, and $S_{f.e}$ are the surface areas of the structural materials in the core, the extrareactor part of the loop, and the fuel elements, respectively, m²; W_C is the rate of outflow of the CP of the element under study, mg/(m²·sec); ω is the moisture content of the live steam; K_d is the coefficient of distribution of the impurity under study between the liquid and the steam phases under a given pressure; A_0 is the coefficient of deposition of the impurity under study on isothermal surfaces (with nonuniform deposition of the impurity on isothermal surfaces $S_{tot} A_0 = \sum_1^n S_i A_i$, where S_i is the part of the total area S_{tot} for which the coefficient of deposition A_i is known). For constant $D_{f.w}$, $C_{f.w}$, W_C, $C_{\bar{a}}$, D_b, D_s, Eq. (3) has the following analytical solution:

$$C = C_0 e^{-G\tau} + [D_{f.w} C_{f.w} - (S_{core} + S_{ex}) W_C] (1 - e^{-G\tau})/GM + BC_{\bar{a}} S_{f.e} [e^{-G\tau} - e^{-B\beta (K_c - 1)\tau}]/M [G - B\beta (K_c - 1)], \quad (4)$$

where $G = \{D_b + D_s [\omega + (1 - \omega) K_d] + (S_{core} + S_{ex}) A_0\}/M$; and C_0 is the initial (τ = 0) concentration of the impurity under study in the coolant. Since the quantity G, entering into the exponent of the main exponential, is much larger than zero, the concentration of the impurity C increases rapidly with τ up to a value close to the stationary value:

$$C_{stat} = [D_{f.w} C_{f.w} + (S_{core} + S_{ex}) W_C]/GM - BC_{\bar{a}} S_{f.e} e^{-B\beta (K_c - 1)\tau}/M [G - B\beta (K_c - 1)].$$

The concentration of the impurity in the coolant changes further with time due to its deposition on the fuel elements until dynamic equilibrium is established in the deposited layer. In the limit $\tau \to \infty$ the impurity concentration in the coolant is given by

$$C^{\infty}_{stat} = [D_{f.w} C_{f.w} + (S_{core} + S_{ex}) W_C]/GM. \quad (5)$$

The time required to achieve dynamic equilibrium in the deposited layer is usually calculated to be hundreds of hours (it can be equal to thousands of hours and longer only under supercritical pressure). This is a small fraction of the total operational lifetime of the installation (tens of thousands of hours). Most of the time the installation therefore operates with the content of the impurity under study in the coolant equal to C^{∞}_{stat}. As follows from expression (5), the impurity concentration is increased by impurities in the feed water and the corrosion of the structural materials in the reactor loop, whereas the impurity concentration is decreased by the blow-through, as a result of the impurity being carried away with the steam and deposition of the impurity on isothermal surfaces. Since the amount of impurity carried away with the steam is small, the value of C^{∞}_{stat} for fixed $C_{f.w}$ and W_C is established as a function of D_b and the intensity of the deposits, determined by the value of A_0. It should be emphasized that the magnitude of the blow-through D_b is controllable, while the value of A_0 is not.

From here it follows that the efficiency of the blow-through process depends on the ratios of these quantities. If $D_b \geq (S_{core} + S_{ex})A_0$, then blow-through is effective and an increase in its intensity can appreciably affect the impurity concentration in the coolant (but not proportionally to the increase in the intensity of the blow-through); if, on the other hand, $D_b << (S_{core} + S_{ex})A_0$, then the blow-through is ineffective and a change in its intensity in either direction does not sufficiently affect the impurity content in the coolant.

For this reason, the development of measures for increasing blow-through must precede the technical-economic evaluation of the effectiveness of these measures.

Using expression (4) to calculate the concentration fo the impurity studied in the coolant at any moment in time, it is possible to compare the differential equation for calculating the concentration of radionuclides of this impurity in the coolant:

$$M\frac{dC^*}{d\tau} = \frac{\sigma_a \Phi f_1 f_2}{\lambda}(1-e^{-\lambda\tau}) W_C S_{core} + Y_1 C D_{core} + Y_2 B C_a S_{f.e}[1-e^{-B\beta(K_c^{-1})\tau}] - \\ -\lambda MC^* - D_b C^* - (S_{core} + S_{ex}) C^* A_0 - D_s [\omega + (1-\omega) K_d] C^*, \quad (6)$$

where C^* is the concentration of the radionuclide of the impurity studied, mg/kg; Y_1 and Y_2 are the activation terms; D_c is the flow rate of the coolant through the core of the reactor, kg/sec; σ_a is the microscopic activation cross section, cm^2; f_1 is the relative fraction of the element of interest in the structural material; f_2 is the relative fraction of the parent isotope in the natural mixture of the isotopes of the element of interest; Φ is the neutron flux density, irradiating the structural material, $cm^{-2} \cdot sec^{-1}$; and λ is the radioactive decay constant, sec^{-1}. Here we ignored the possible flow of radionuclides from the feed water, and we also assumed that radionuclides only settle on isothermal surfaces (erosion does not occur), while only nonradioactive elements form deposits on the surfaces of the fuel elements.

The first three terms in the expression (6) describe the three above-mentioned processes, responsible for the flow of the radionuclides of the impurity of interest into the coolant (corrosion of the structural materials in the core; activation of the impurity during transit through the core; and activation of deposits on the fuel elements). The remaining terms in expression (6) describe the loss of radionuclides of the impurity of interest by radioactive decay and due to blow-through, deposition on isothermal surfaces, and removal with the steam, respectively.

The activation terms Y_1 and Y_2 can be determined analytically. The activation of the impurity of interest during its transit together with the coolant through the core is easily described quantitatively by the expression

$$Y_1 = \bar{\Phi}\sigma_a f_2 \tau_{act}. \quad (7)$$

Here $\bar{\Phi}$ is the average density of the flux of activating neutrons along the core, $cm^{-2} \cdot sec^{-1}$; τ_{act} is the average residence time of the impurity in the core, sec; $\tau_{act} = \tau_{core}$, where τ_{core} is the single-passage time of the coolant through the core, sec.

Since $M = D_{core}\tau_{loop}$,

$$D_{core} = M/\tau_{loop}, \tag{8}$$

where τ_{loop} is the single-passage time of the coolant through the circulation loop as a whole, sec. Both quantities τ_{core} and τ_{loop} are in general calculated based on the same scheme

$$\tau = \sum_{1}^{n} \frac{L_i}{v_i},$$

where L_i is the length of the section of the loop (in meters), in which the coolant moves with a velocity v_i (in m/sec).

Thus, the second term in Eq. (6), describing the generation of radionuclides in the coolant as the coolant flows through the core, is expressed with the substitution of (8) as follows:

$$CM\bar{\Phi}\sigma_a f_2 \tau_{core}/\tau_{loop}. \tag{9}$$

The activation term Y_2, determining the activation of the impurity in the deposits on the fuel elements, can be obtained analogously. With a constant quantity of deposits (after dynamic equilibrium is established in them), neglecting the radioactive decay in the deposited layer we obtain

$$Y_2 = \bar{\Phi}\sigma_a f_2 \tau_l, \tag{10}$$

where τ_l is the average lifetime of the impurity in the deposits (from the moment the impurity enters the layer up to the moment that it returns into the coolant), sec. Applying the mean-value theorem, from expression (1) we obtain

$$\tau_l = 1/B\beta(K_c - 1).$$

Thus, expression (10) for the activation term Y_2 finally assumes the form

$$Y_2 = \bar{\Phi}\sigma_a f_2/B\beta(K_c - 1). \tag{11}$$

Correspondingly, the complete expression for the third term in Eq. (6), describing the generation of radionuclides in the layer deposited on the fuel elements, has the form

$$C_a S_{f.e}[1 - e^{-B\beta(K_c-1)\tau}]\,\bar{\Phi}\sigma_a f_2/\beta(K_c - 1).$$

The differential equation (6) has an analytic solution for time-independent W_C, D_{core}, D_b, $\bar{\Phi}$, D_s, C_a, v_i. For $C = C^{\infty}_{stat}$,

$$\begin{aligned} C^* = C_0^* e^{-Q\tau} + (Y_1 D_{core} C^{\infty}_{stat} + \sigma_a \Phi f_1 f_2 W_C S_{core}/\lambda + \\ + Y_2 S_{f.e} B C_a)(1 - e^{-Q\tau})/QM + \sigma_a \Phi f_1 f_2 W_C S_{core} \times \\ \times (e^{-Q\tau} - e^{-\lambda\tau})/GM\lambda + BC_a \sigma_a f_2 \bar{\Phi}\tau_l S_{f.e} \times \\ \times [e^{-Q\tau} - e^{-B\beta(K_c-1)\tau}]/M[Q - B\beta(K_c - 1)], \end{aligned} \tag{12}$$

where $Q = \{\lambda M + D_b + D_s[\omega + (1 - \omega)K_d] + (S_{core} + S_{ex})A_0\}/M$. The quantity C_0^* determines the initial concentration of radionuclides of the impurity of interest in the coolant, i.e., after a given concentration is achieved (in this case, $C = C^{\infty}_{stat}$).

As follows from expression (12), the concentration of radionuclides in the coolant increases with time from the initial level C_0^* to the level

$$C^{*\infty}_{stat} = (Y_1 D_{core} C^{\infty}_{stat} + \sigma_a \Phi f_1 f_2 W_C S_{core}/\lambda\ Y_2 S_{f.e} B C_a)/QM. \tag{13}$$

During the initial period of operation, a relatively rapid growth of C^*, determined by the exponent in the main exponential in Q and the high rate of corrosion and correspondingly the large yield of corrosion products, occurs. Subsequently, the rate of growth of C^* will be determined by the exponent of the other exponentials ($e^{-B\beta(K_c-1)\tau}$ and $e^{-\lambda\tau}$) and will decrease as the stationary level is approached. The rate of decrease in the rate of growth of C^* depends on the individual physical properties of the radionuclide, as well as the thermophysical and hydrodynamic conditions of boiling. Prolonged processes, occurring during the prolonged operation of the installation, are primarily affected by the value of $C^{*\infty}_{stat}$. In calculating $C^{*\infty}$ based on expression (13), all quantities except A_0 are usually known. The value of A_0 for each specific installation can be obtained from expression (4) with the known (from the operational data) value of C at any given moment in time or from expression (5) with the known (from the operational data) value of C^{∞}_{stat} for the impurity of interest.

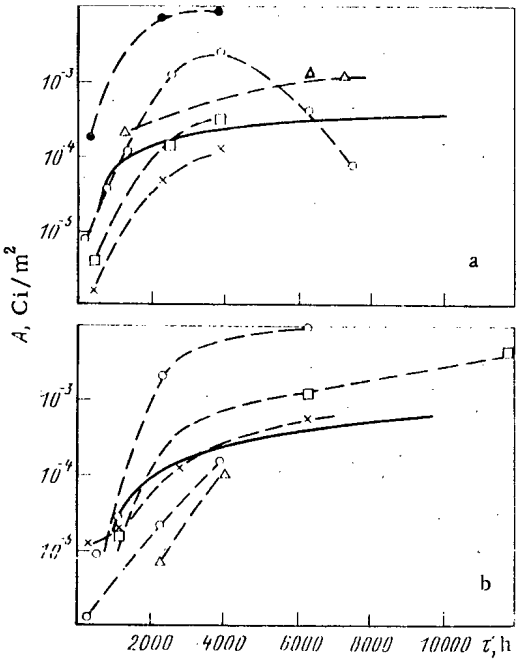

Fig. 1. Average computed and actual local activity of deposits of corrosion products on the equipment of the extrareactor part of the first loop according to ^{59}Fe (a) [1, 6], ^{60}Co (b) [6, 7]: ——) the computed curve of the mean activity versus time according to the first loop; o, ×, □, Δ, •) curves constructed from the experimentally measured activity in different sections of the first loop.

The value found for $G^{*\infty}_{stat}$ can be used to calculate the accumulation of radionuclides of the impurity of interest on the equipment of the reactor loop of a nuclear power plant. The differential equation describing this process has the form

$$\frac{dn^*}{d\tau} = S_{ex} A_0 \frac{N_A}{\mu} C^{*\infty}_{stat} - \lambda n^*.$$

If it is assumed that $n^* = 0$ at $\tau = 0$, then the expression

$$n^* = S_{ex} A_0 N_A C^{*\infty}_{stat} (1 - e^{-\lambda\tau})/\lambda\mu$$

will be the solution of this equation.

Here n^* is the amount of the radionuclides of the impurity of interest; N_A is Avogadro's number; and μ is a mole of the impurity element of interest.

The specific activity of the equipment, averaged over all surfaces, can be represented by the expression (in Bq)

$$A^{sur}_{spec} = A_0 N_A C^{*\infty}_{stat} (1 - e^{-\lambda\tau})/\mu. \qquad (14)$$

The results of the calculations of the specific activity are shown in Figs. 1 and 2. The calculations were performed for the first loop of the RBMK-1000 reactor with the following values of the determining quantities: the concentration of iron in the feed water was 10 μg/kg, the enthalpy of the coolant at the inlet into the core was 1184 kJ/kg, the average thermal power of the heat-generating plant was 0.66 MW, the coefficient of erosion of the deposits from the fuel elements was 10^{-5} m^2/kg, and the working time period was 1 year.

Figure 1a compares the computed specific activity of ^{59}Fe on the equipment of the first loop as a function of time with the experimental data for different sections of the loop; Fig. 1b shows the same for ^{60}Co. It follows from the figure that the computed curves give a qualitatively and quantitatively completely satisfactory description of the experimental data.

It is evident from Fig. 2a that the specific activity of the equipment in the first loop is directly proportional to the iron content in the feed water, which is confirmed by data

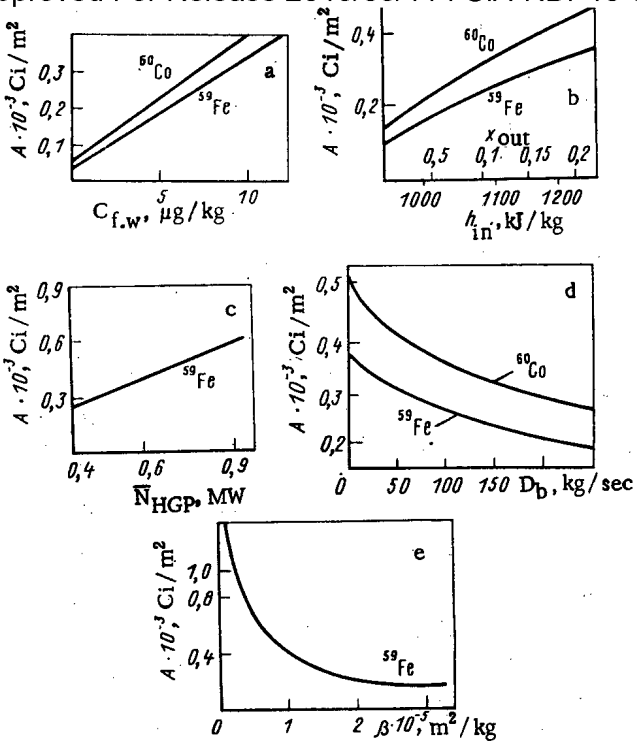

Fig. 2. Computed dependence of the specific activity of the equipment in the first loop of the RBMK-1000 reactor on the iron concentration in the feed water (a), the enthalpy of the coolant at the inlet to the core (b), the average thermal power of the heat-generating plant (HGP) (c), the blow-through of the first loop with τ_0 = 1 yr (d), and the coefficient of erosion of the deposits from the fuel elements (e).

from other studies. An analogous dependence is also observed for other elements in the corrosion products. This suggests that the specific activity is directly proportional to the content of the corrosion products in the feed water. Therefore, the transition from RBMK-1000 to more powerful installations, for example, to RMBK-1500, where the inflow of corrosion products into the feed water can be greater, requires the development of measures for additional removal of corrosion products from the feed water [8]. This requirement increases with the power of the reactor installation, since the specific activity increases with the enthalpy of the coolant at the inlet to the core or the mass steam-content at the outlet from it (see Fig. 2b). As the average thermal load on the heat-generating plant increases, the specific activity also increases (see Fig. 2c), which, in its turn, requires that the content of corrosion products in the feed water be decreased with the transition to more powerful installations in order to preserve the rate of growth of activity and its magnitude at least at the previous level. The blow-through, as expected, is less effective and has a different effect for different radionuclides. As is evident from Fig. 2d, a fourfold increase in the blow-through for RBMK-1000 decreases the specific activity by only a factor of 1.5. Thus, it is impossible to compensate the growth in the activity due to other effects (increasing surface area of the structural materials, mass steam-content at the outlet from the core, average thermal load on the heat-generating plant) by increasing the flow rate of the coolant in the blow-through. At the same time, an increase in the coolant flow rate for the blow-through gives rise to an increase in the thermal losses, the dimensions of the buildings, the metal content of the filters, the consumption of sorbents, and the volume of liquid wastes buried in repositories.

Figure 2e shows the dependence of the specific activity on the coefficient of erosion of the corrosion products from the deposits on the surface of the fuel elements. This component makes the main contribution to the total quantity of radionuclides of the corrosion products in the coolant and, correspondingly, in the equipment in the first loop. It follows from Fig. 2e that the specific activity of the equipment is very sensitive to the value of β. It seems that this dependence conceals definite reserves for lowering the activity of the equipment. For example, the water–chemical measures, preventing accumulation of deposits

on the fuel elements or at least facilitating their constant removal from them, will decrease the residence time of the corrosion products in the neutron field and in the final analysis will decrease the specific activity of the equipment in the first loop.

LITERATURE CITED

1. Yu. A. Egorov, Foundations of Radiation Safety at Nuclear Electrical Power Plants [in Russian], Énergoizdat, Moscow (1982).
2. A. Lhuillery, "Influence of operating problem on nuclear plant design," Trans. Am. Nucl. Soc., 20, 424 (1975).
3. H. Dickson, "Controlling occupational radiation exposure at operating nuclear power stations," Nucl. Safety, 18, No. 4, 492-501 (1977).
4. V. V. Gerasimov, Corrosion of Reactor Materials [in Russian], Atomizdat, Moscow (1980), p. 251.
5. S. A. Tevlin, "Study of the process of formation of and methods for removing active deposits from nuclear power plant loops," Teploenergetika, No. 10, 8-13 (1980).
6. N. V. Butin, Yu. A. Egorov, A. P. Eperin, et al., "Activity of corrosion products in the coolant and radiation environment in the first block of the Leningrad nuclear power plant, in: Radiation Safety and Shielding of Nuclear Power Plants [in Russian], No. 3, Atomizdat, Moscow (1977), pp. 5-17.
7. Yu. A. Egorov, A. A. Noskov, V. P. Sklyarov, et al., "Study and application of the TRAKT-1 model for calculation of the activity of corrosion products in the operating loop of a nuclear power plant with a channel reactor," in: Radiation Safety and Shielding of Nuclear Power Plants [in Russian], No. 5, Atomizdat, Moscow (1981), pp. 10-22.
8. T. Kh. Margulova, V. M. Zorin, V. F. Tyapkov, et al., "Water cycle in a nuclear power plant with RMBK-1500," Teploenergetika, No. 12, 4-7 (1983).

EFFECT OF THE SOLUTION TEMPERATURE ON THE EXTRACTION COLUMN HYDRODYNAMICS

S. M. Karpacheva and O. K. Maimur

UDC 621.039.327

In uranium extraction and refining at the hydrometallurgical stage as well as in radiochemical production, extraction is ordinarily performed at the usual, i.e., room, temperature of ~20°C, while reextraction is usually performed with heating. This is explained by the fact that the coefficient of uranium distribution between the most widely used extracting agent, a solution of tributyl phosphate (TBP) in a solvent, and the aqueous phase increases with temperature. It might prove advisable in certain cases to carry out the extraction process at an elevated temperature, especially as the phase separation rate usually also increases, i.e., the volume of the settling zone diminishes. Under these circumstances, a change in the extractor hydrodynamics with temperature variation can also exert an influence. The optimum process conditions can evidently be determined by considering all these factors.

Effect of the Temperature on Contact between Mutually Saturated Solutions. There are virtually no publications devoted to the effect of temperature on the hydrodynamic parameters of column extractors (the correlations (1)-(3) given in [1] for determining these parameters have been derived for a temperature of 20°C). Therefore, we found it useful for the time being to investigate this problem in a narrow temperature range (15-30°C). The investigation was performed by using a pulsation column with KRIMZ packing [2] and a mutually saturated system: an aqueous solution containing 0.3-0.4 mole/liter HNO_3 and 25% TBP in synthine. The column has a diameter of 0.2 m, the height of the packing section is equal to 2.0 m, and the spacing between plates is 0.1 m. The effective cross section of the packing amounts to 21% for 10 × 18 mm openings. The temperature was kept contant in each experiment by suitable thermostatic control of the solution supplied.

We investigated the physicochemical characteristics of the solutions, the drop size d_d was determined by photographing, and we subsequently counted the drops on the positive [3].

Translated from Atomnaya Énergiya, Vol. 58, No. 4, pp. 246-249, April, 1985. Original article submitted April 19, 1984.

 0038-531X/85/5804-0278$09.50

TABLE 1. Physical Characteristics of the Solutions

T, °C	ρ_c, g/cm³	ρ_{di}, g/cm³	$\Delta\rho$, g/cm³	μ_c, cP	μ_{di}, cP	σ, dyn/cm
15	1,010	0,832	0,180	1,15	2,8	9,58
20	1,008	0,828	0,180	1,04	2,5	10,25
25	1,0065	0,824	0,182	0,95	2,25	10,8
30	1,005	0,820	0,185	0,85	2,0	11,2

The retention of the disperse phase was measured by using the sampling method, while the limiting load was determined visually [4].

It is known that, for a column of this type, the hydrodynamic calculations are performed on the basis of the parameter d_d [1], which facilitates calculation of the other quantities: the characteristic velocity V_0, the disperse phase retention Ω, and the flooding load ΣW_f:

$$d_d = (0.135 - 0.17) F \left(\frac{\sigma}{\rho_c}\right)^{0.6} \left(\frac{\mu_{di}}{\mu_c}\right)^{0.107} I^{-1}; \quad (1)$$

$$V_0 = 22 \left(\frac{\rho_c}{\mu_c}\right)^{0.33} \left(\frac{\Delta\rho}{\rho_c}\right)^{0.66} d_d; \quad (2)$$

$$\Sigma W_f = 0.3 V_0 n^{-0.18}; \quad (3)$$

$$\Omega = \left(\frac{\mu_c^4 g}{\Delta\rho^2 \sigma^3}\right)^{0.059} \left(\frac{\mu_c}{\mu_{di}}\right)^{0.4} \frac{\Sigma W}{V_0}, \quad (4)$$

where ρ_c and ρ_{di} are the densities of the continuous and the disperse phases, respectively (g/cm³), μ_c and μ_{di} are the viscosities of the above phases, respectively (P), σ is the interphase tension (dyn/cm) (1 dyn = 10^{-5} N), F is the effective cross section of the packing based on the sum of slots and the blade slope (%), and d_d is the surface–volume dimension of drops. Expression (4) holds in the range of free motion of drops for Ω = 15%.

Table 1 provides the physical characteristics of the solutions used in the investigations. Substituting the data from Table 1 in Eq. (1), we find that, as the temperature rises from 15 to 30°C, the drop size should increase somewhat due to a rise in the interphase surface tension, with the density of the continuous phase remaining virtually unchanged (a change in the viscosity ratio by a few percentage points does not affect noticeably the drop size). The characteristic velocity V_0 (2) should rise not only because of the increase in d_d, but also largely due to a reduction in μ_c, which, in turn, would reduce the disperse phase retention and increase the flooding load of the column extractor.

Drop Size. Figure 1 provides a comparison between the d_d values obtained experimentally for different temperatures and vibration intensities (with a load of 10 m³/(m²·h)) and those calculated by means of expression (1). There is evidently sufficiently good agreement between these data. The diagram confirms the tendency for the drop size to increase with heating from 15 to 30°C. The characteristic velocity was not determined experimentally because of the complexity of such measurements, and the value of V_0 was calculated by means of expression (2).

Disperse Phase Retention. As is known, the value of Ω first increases with the load according to a sloping straight line, which is followed, after passage through a certain critical point, by a sharp increase in the buildup of the disperse phase, which ends with flooding. Equation (4) describes the initial, straight segment.

Measurements show that Ω decreases in all cases with an increase in temperature (Fig. 2), while the overall tendency of Ω to increase with the load and the vibration intensity persists (Fig. 3). For I = 900 mm/min and loads of up to 25 m³/(m²·h) (see Fig. 2b), the temperature dependence of Ω is rectilinear, and the experimental results agree with calculations based on (4). If the intensity or the load increases, the linear relationship between Ω and T is distorted (see Fig. 2a), and a discrepancy between the experimental and theoretical values of Ω arises.

A nomogram of Ω in relation to the intensity and the load ΣW makes it possible to find the difference $\Delta\Omega$ at 15 and 30°C for equal values of I and ΣW and determine the operating condition variants for securing equal values of Ω at T = 15 and 30°C. For instance, for

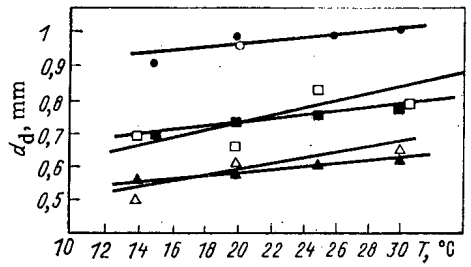

Fig. 1

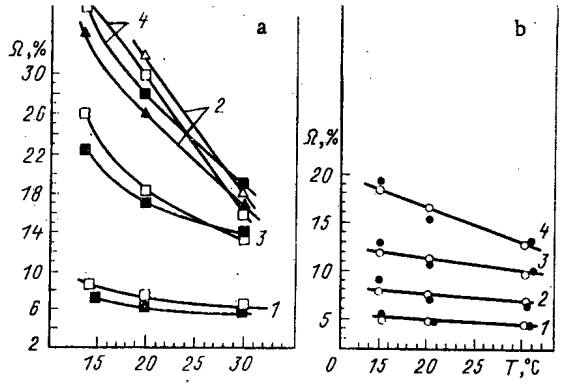

Fig. 2

Fig. 1. Dependence of d_d on temperature. Here, as in Figs. 2 and 3: o, □, Δ) experiment; •, ■, ▲) calculation; o, •) I = 900 mm/min; □, ■) I = 1200 mm/min; Δ, ▲) I = 1500 mm/min.

Fig. 2. Dependence of Ω on the temperature. a) I = 1200-1500 mm/min; b) I = 900 mm/min; 1) ΣW = 10; 2) ΣW = 15; 3) ΣW = 20; 4) ΣW = 25 $m^3/(m^2 \cdot h)$.

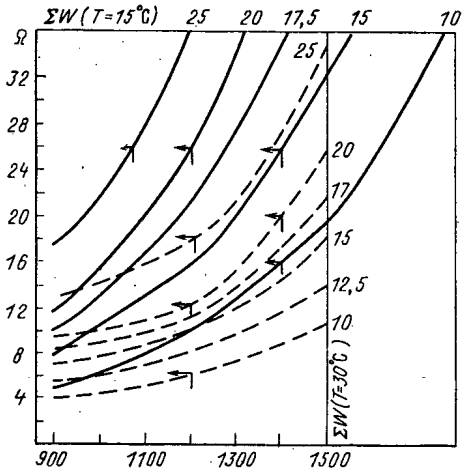

Fig. 3. Nomogram for determining Ω as a function of I and ΣW: ——) T = 15°C; ---) T = 30°C.

I = 1200 mm/min, Ω = 19% is achieved for loads of 12 and 15 $m^3/(m^2 \cdot h)$, respectively, and Ω = 20% is obtained for 18 and 27 $m^3/(m^2 \cdot h)$, i.e., it is possible to increase the load by a factor of 1.5 for equal values of Ω.

For the region characterized by the parameters I = 900-1300 mm/min, ΣW = 10-20 $m^3/(m^2 \cdot h)$ and T = 15-30°C, we have derived an equation for calculating Ω with the ranging of variables at two different levels [5] within the variation ranges ΔI = 200 mm/min, ΔW = 5 $m^3/(m^2 \cdot h)$, and ΔT = 8°C, using I_0 = 1100 mm/min as the scheme center. With an allowance for the interaction of all factors, the regression equation is given by

$$\Omega = 31 - 37.6 \cdot 10^{-3} I - 5.36W - 1.187T + 6.92 \cdot 10^{-3} IW + 0.1814WT + 1.37 \cdot 10^{-3} IT - 0.213 \cdot 10^{-3} IWT \qquad (5)$$

which allows us to calculate Ω with an error of less than 10% with all the factors varying in the investigated region.

The flooding load ΣW (Fig. 4) increases by 20-25% as the temperature rises from 15 to 30°C, while it coincides with its theoretical value based on Eq. (3) for I = 900 mm/min and is somewhat different for I = 1200-1500 mm/min, since ΣW varies more sharply under intensive conditions.

Thus, we have established a direct relationship between the hydrodynamic conditions of column operation and temperature variation, even in the narrow range of 15-30°C. It was found that changes in the operating conditions in relation to the temperature can be deter-

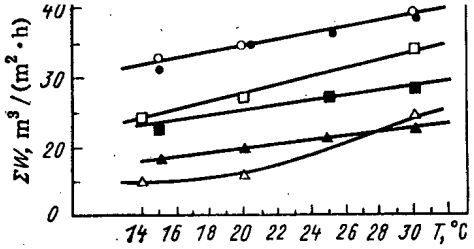

Fig. 4. Temperature dependence of ΣW.

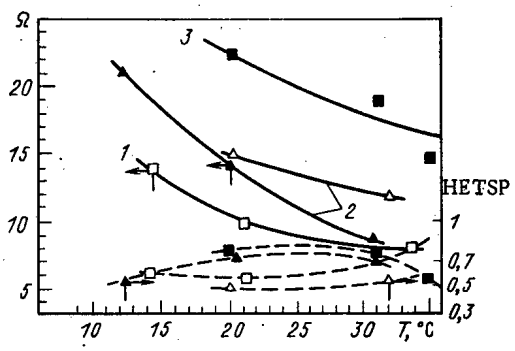

Fig. 5. Temperature dependences of Ω in mass transfer (——) and of the column's operating efficiency (---): ▫, △) extraction; ▪, ▲) reextraction; ▫, ▪) I = 1200 mm/min; △, ▲) I = 1500 mm/min; 1) ΣW = 20; 2) ΣW = 15; 3) ΣW = 30 $m^3/(m^2 \cdot h)$. HETSP = height of equivalent theoretical separation phase.

mined approximately by means of Eqs. (1)-(4) on the basis of the physical characteristics of solutions. An increase in the temperature causes an increase in d_d and ΣW and a reduction in Ω. changes in the process parameters with a temperature rise to a value above 30°C and for different solution compositions require further investigations.

Efficiency. The temperature effect on the mass transfer efficiency is complex, while it depends on the values of d_d and Ω (i.e., the change in the surface area) and also on the mass transfer rate. We have checked the effect of temperature changes on the hydrodynamics and the efficiency of column operation in uranium VI extraction (using a system consisting of 0.3-0.4 mole/liter HNO_3 + 30 g/liter uranium VI–25% TBP in synthine) and in reextracting uranium VI with a solution of HNO_3 0.05 mole/liter from the same TBP solution with 30 g/liter uranium.

The variations of d_d and Ω in both extraction and reextraction conform to roughly the same laws as the variations found earlier in hydrodynamic tests, i.e., d_d increases while Ω decreases with a rising temperature for constant values of I and ΣW (Fig. 5). Thus, in the temperature range of 14-34°C for I = 1200 mm/min and ΣW = 20 $m^3/(m^2 \cdot h)$, retention is reduced by almost one half, from 14 to 8% in extraction, and from 14.5 to 7% in reextraction, which correspondingly alters the surface area of mass transfer. If the mass transfer rate remains unchanged, the value of HETSP in extraction should increase according to [1] by almost 70%, while it actually increases by only 25% (from 0.6 to 0.75 m). This may be caused by acceleration of the chemical stage of the extraction process due to the temperature rise (according to data from [7], the activation energy of the extraction reaction is E = 9.5-11 kcal/mole) and also by a possible increase in vibrations and a diminution of the laminar layer near the drop surface. This observation is very important for determining the optimum set of operating conditions, since the process in this case permits an increase of 50% (from 20 to 30 $m^3/(m^2 \cdot h)$) in the working load even with a small increase in temperature for virtually unchanged values of Ω and the extraction efficiency.

In calculating the process, it must be considered that, with temperature variation, the extraction equilibrium is in many cases shifted so that a larger number of stages is necessary for completing the process, i.e., a greater total height of the column may be necessary at higher temperatures, even for equal height of equivalent theoretical separation phase values.

The above data indicate that the effect of temperature on the characteristics of the extraction processes in a column must be taken into account in determining the optimum process conditions, performing hydrodynamic tests, comparing equipment and packing of various types, etc.

LITERATURE CITED

1. S. M. Karpacheva and E. I. Zakharov, Fundamentals of the Theory and Calculation of Pulsating Column Reactor Vessels [in Russian], Atomizdat, Moscow (1980), pp. 69, 82, and 100.
2. S. M. Karpacheva, L. S. Raginskii, E. I. Zakharov, et al., "Packing for extraction column," Inventor's Certificate No. 175489, Byull. Izobret., No. 20, 9-10 (1965).
3. L. M. Batuner and M. E. Pozin, Mathematical Methods in Chemical Technology [in Russian], Khimiya, Leningrad (1968), p. 634.
4. S. M. Karpacheva, L. P. Khorkhorina, O. K. Maimur, and Z. D. Pankratova, Khim. Prom., No. 8, 614 (1978).
5. R. Treibal, Liquid Extraction [Russian translation], Khimiya, Moscow (1966), p. 883.
6. A. Yu. Zakgeim, Introduction to Simulation of Chemical Technology Processes [in Russian], Khimiya, Moscow (1973), p. 172.
7. M. F. Pushlenkov and N. P. Shchepetil'nikov, Radiokhimiya, No. 11, 19 (1969).

SOLIDIFICATION OF INTERMEDIATE-LEVEL LIQUID WASTES WITH THE USE OF INORGANIC BINDERS

A. S. Polyakov, M. I. Zhikharev, K. P. Zakharova, O. M. Khimchenko, T. T. Karpova, G. F. Surzhikov, V. L. Pankratov, V. P. Shelud'ko, and L. N. Shimarova

UDC 621.039.7...14

In most countries with a developed nuclear power industry, both organic (bitumen, thermoplastic polymers) and inorganic binders are used to solidify the liquid wastes from nuclear power plants. In our country methods are being developed for solidying wastes with the use of thermoplastic binders and different types of inorganic binders: Portland cement, metallurgical slags, and Portland blast-furnace cement.

Previous work on cementing [1, 2] concerned primarily the solidification of low-level wastes. Since for such wastes in our country the method of pouring the cement solution into trenches with solid wastes has been adopted, the required fluidity is achieved by a high water–binder ratio (about 0.7). At the same time, the salt content in the mixture does not exceed 4-5 mass%, which substantially increases the volume of the wastes on solidification. The possibility of increasing the waste content in the final product by selecting the appropriate composition of the binder and the conditions for carrying out the process without degrading the properties of the product formed is now under study.

In this paper we present the results of studies using simulators of wastes from nuclear power plants with RBMK (high-boiling channel reactor) and VVÉR (water-cooled–water-moderated power reactor) and AST-500 (Table 1). For the binders we used Portland cement, special cements, metallurgical slags, and Portland blast-furnace cement (Table 2). The main criterion for comparing samples was the mechanical strength of the solidified wastes. For this, we prepared two types of samples: standard 4 × 4 × 16 cm blocks and 2-cm cubes. The first experiments with the Portland blast-furnace cement demonstrated that it can be used for solidifying radioactive wastes. For the example of wastes from a nuclear power plant with RBMK (Table 3), it is evident that with an equal salt content in the solidified product its strength increased as the slag content of the Portland blast-furnace cement is increased from 20 to 80 mass%. At the same time, the water–binder ratio was low (about 0.2).

An increase in the content of RBMK wastes in the final product from 12.5 to 25-26 mass% appreciably lowers the strength, but even with a high waste content the strength of the solidfied product for all ratios of the components in the binder exceeds 100 kgf/cm^2. Experiments with wastes from nuclear power plants with VVÉR and AST-500 showed that the strength of

Translated from Atomnaya Énergiya, Vol. 58, No. 4, pp. 249-252, April, 1985. Original article submitted July 11, 1984.

 0038-531X/85/5804-0282$09.50

TABLE 1. Chemical Composition of Wastes from a Nuclear Power Plant and AST-500

Chemical composition of wastes, mass%	RBMK	VVÉR	AST-500
$NaNO_3$	54,5	45	63,9
$Na_2C_2O_4$	8,1	10	8,1
NaOH, KOH	8,3	12	9,0
Na_3PO_4	7,1	—	—
NaCl	1,1	—	—
Sulfonole	3,6	10	11,6
Mn_2O_3	1,2	—	—
Fe_2O_3	2,9	—	—
Filter-perlite	4,5	—	—
Ion exch., AN-31	8,7	—	—
$Na_2B_4O_7$	—	12,5	—
Na_2CO_3	—	10	7,3

TABLE 2. Chemical Composition of Inorganic Binders, mass%

Binder	SiO_2	Al_2O_3	Fe_2O_3	FeO	MnO_2	CaO	MgO	SO_3	S	TiO_2	$Na_2O + K_2O$	BaO
Clinker-1	21,7	5,9	4,1	—	—	63,8	1,5	0,1	—	—	0,4	—
Clinker-2	22,1	4,7	4,2	—	—	67,0	1,2	0,1	—	—	0,2	—
Slag-1	36,2	12,6	—	0,4	0,9	39,0	8,4	—	0,5	—	1,0	—
Slag-2	35,6	10,8	—	0,3	0,1	42,0	7,5	—	1,8	—	0,9	—
Slag-3	38,5	9,1	—	0,2	1,3	45,6	3,5	—	1,1	0,2	1,0	—
Slag-4	39,1	8,8	0,7	0,6	0,1	37,8	11,3	—	0,5	1,0	1,0	—
Barium-containing Portland cement	22,5	5,2	4,5	0,4	—	52,2	1,5	1,5	—	—	0,4	9,9
Bariated alumina cement	2,2	35,9	0,3	—	—	1,3	—	0,2	—	—	—	60,2
Expanding Portland cement	18,6	17,3	6,2	—	—	45,4	—	4,8	—	—	Not analyzed	—
High-alumina cement	0,6	75,0	0,2	—	—	24,1	—	Traces	—	—	—	—
Talyum	0,7	74,8	0,3	—	—	23,8	—	—	—	—	—	—

the solidified products even based on the Portland blast-furnace cement with a high slag content – 80 mass% of slag-1 and 20 mass% of clinker – is lower than the strength of the analogous product with RBMK wastes (Table 4). For these wastes the strength drops appreciably even with an insignificant increase in the degree of filling (from 11.4 to 15.0 mass%). The chemical composition of the wastes from nuclear power plants with VVÉR and AST-500 differs from that of the wastes from power plants with RBMK by a higher content of sulfinole and the presence of sodium carbonate, and the wastes from power plants with VVÉR also contain sodium tetraborate.

For the VVÉR wastes, the products with the best mechanical strength were obtained with Portland blast-furnace cement containing 70 mass% of slag-4 and 30 mass% of clinker-2 (Table 5). In this case, their strength remains unchanged when the degree of filling is increased up to 7.1 mass%. In the interval 10.3-18.7 mass% the strength decreases, but it is still high. It increases with time and after 28 days reaches ~260 kgf/cm^2 (with a content of dry remainder up to 7.1 mass% and 170-200 kgf/cm^2 with 10 mass%).

In order to study in greater detail the effect of the composition of the matrix material on the strength of the product formed on solidification, we performed experiments with different binders, including special cements (Table 6). For the filler we used a model composition of AST-500 wastes (for comparison, the strength of concretes obtained with the use of the corresponding binders is also shown in the same table). The results showed that the Portland blast-furnace cement is least sensitive to the presence of salts. Satisfactory results were also obtained with the barium-containing Portland cement.

We studied the effect of separate components of the wastes on the strength of the product formed for three types of binders: Portland cement, slag-1, and Portland blast-furnace cement (80 mass% slag-1 and 20 mass% clinker-1). The permissible amount of components whose presence is discernible was determined: surfactants (sulfinole, OP-10, household soap), oil, and sodium hydroxide. It was established that with a water–binder ratio of about 0.3 the

TABLE 3. Dependence of the Strength of Solidified Wastes from a Nuclear Power Plant with RBMK on the Clinker and Slag Ratio in the Binder

Composition of binder, mass fraction			$C_{d.w}$, mass%	W/B	σ_{comp} after 28 days, kgf/cm^2
clinker	slag	gypsum			
80	20	5	12,4	0,21	236
50	50	5	12,5	0,20	312
20	80	5	12,5	0,20	408
80	20	5	26,1	0,15	128
50	50	5	25,2	0,19	216
20	80	5	25,2	0,19	228

Here and in the tables below, $C_{d.w}$ is the content of dry remainder of the wastes in the solidified product, W/B is the water–binder ratio, and σ_{comp} is the compression strength.

TABLE 4. Strength of Solidified Wastes from Nuclear Power Plants with VVÉR and AST-500

Solutions with salt content of 300 g/liter	$C_{d.w}$, mass%	S/B*	σ_{comp} after 5 days, kgf/cm^2
Power plants with VVÉR	11,4	0,4	84
	13,3	0,5	58
	15,0	0,6	30
AST-500	11,4	0,4	84
	13,3	0,5	58
	15,0	0,6	38

*S/B – solvent–binder ratio.

TABLE 5. Mechanical Strength of Samples Based on Slag-4 and Clinker-2

Composition of mixture, mass fraction			$C_{d.w}$, mass%	W/B	σ_{comp}, kgf/cm^2		
binder	dry remainder of wastes	water			7 days	14 days	28 days
100	5	30	3,7	0,3	106	175	267
100	10	30	7,1	0,3	107	182	262
100	15	30	10,3	0,3	101	152	175
100	20	30	13,3	0,3	76	117	200
100	25	30	16,2	0,3	93	130	168
100	30	30	18,7	0,3	66	120	170

strength is not appreciably lowered if the content of sulfinole in the final product does not exceed 10 mass%; the compression strength of such materials reaches 200 kgf/cm^2. Household soaps in amounts of 8-10 mass % substantially reduce the strength (up to 50 kgf/cm^2). The limiting content of OP-10 in the solid product, above which the strength decreases, is equal to 5 mass%. Oil has the same negative effect on the strength of the solid products.

Since wastes from nuclear power plants and AST are usually caustic, it is of interest to study the effect of sodium hydroxide on the strength of the product. The results (Table 7) showed that increasing its content above 7 mass% lowers the mechanical strength if Portland cement is the binder, while for metallurgical slag and the Portland blast-furnace cement the strength increases as the sodium hydroxide content increases in the interval of concentrations studied (up to 10 mass%). The positive effect of NaOH with the use of the Portland blast-furnace cement as the binder was demonstrated in a series of experiments, in which we added sodium hydroxide to the wastes from nuclear power plants with VVÉR (Table 8). The NaOH content in all cases was equal to about 14 mass% of the amount of dry wastes remaining. The positive effect of NaOH is manifested all the more strongly the higher the content of the dry waste remainder in the solidified product.

TABLE 6. Mechanical Strength of Products Based on Different Binders and AST-500 Wastes

Form of binder	$C_{d.w.}$, mass%	W/B	σ_{comp} of sample after 28 days, kgf/cm²	σ_{comp} of concretes, kgf/cm²
Portland cement-400	9,7	0,40	50	400
Barium-containing Portland cement	21,2	0,30	123	474
Bariated alumina cement	20,6	0,35	28	612
Expanding Portland cement	20,6	0,35	77	367
High-alumina cement	20,0	0,40	167 (cracks)	717
Talyum	20,6	0,35	281 (cracks)	783
Portland blast-furnace cement (80 mass% slag-1 and 20 mass% clinker-1)	21,2	0,30	197	515

TABLE 7. Effect of the Content of Sodium Hydroxide on the Strength of the Solidified Product

Form of binder	W/B	NaOH content in the mixture, mass%	σ_{comp}, kgf/cm²
Slag-1	0,33	1	200
	0,31	5,1	300
	0,35	10,1	425
Portland blast-furnace cement	0,33	7	345
	0,33	10	362
Portland cement-400	0,33	5	420
	0,33	7	405
	0,33	10	235

TABLE 8. Effect of the Amount of Alkali in the Wastes on the Strength of the Solidified Product Based on Portland Blast-Furnace Cement (80 mass% slag-1 and 20 mass% clinker-1)

Mixture comp., mass fraction				$C_{d.w.}$, mass%	W/B	σ_{comp} after 28 days, kgf/cm²
binder	dry remainder of the wastes	NaOH	H_2O			
100	15,00	—	30	10,34	0,3	48
100	13,13	1,87	30	10,34	0,3	127
100	20,00	—	30	13,33	0,3	Sample is destroyed
100	17,50	2,50	30	13,33	0,3	145
100	27,75	—	30	17,59	0,3	Sample is destroyed
100	24,28	3,47	30	17,59	0,3	165

The studies performed showed that by selecting the appropriate binder and conditions for carrying out the process, products with a high salt content and mechanical strength exceeding 100 kgf/cm² can be obtained. In all cases, the mixtures were characterized by a low water–binder ratio. For a water–binder ratio of 0.3-0.4 products containing up to 20 mass% of the dry waste remainder can be obtained. The strength of the products after solidification fluctuates in the interval 1.8-2 g/cm³. This permits obtaining a solid product 1 m³ of which will contain up to 400 kg of dry remainder of radioactive wastes.

Simultaneously with the laboratory studies, we performed engineering studies, which confirmed the possibility of obtaining homogeneous mixtures with the indicated values of the water–binder ratio. For this, we built a test setup, on which we carried out the mixing directly in 20-liter drum, which was stored. We placed the drum on a movable frame with a

tion. The drum was rotated around its axis by two pairs of rollers (guide and support). The rate of rotation of the guide rollers varied from 0 to 176 rpm.

We tested the technological mixing regime for Portland cement-400 and a solution containing 300 g/liter of sodium nitrate; the solvent–binder ratio varied from 0.4 to 0.33. It turned out that one of the basic factors affecting the quality of the mixing of the components in the drum is the simultaneity of injection of solvent and binder when the drum is being filled. Good mixing is achieved with a rotational rate of 90 rpm. With a solvent–binder ratio of 0.4 the degree of filling of the drum can reach 85 vol.%, and with a ratio of 0.33-0.35 it is undesirable to fill the drum to a level exceeding 80 vol.%.

LITERATURE CITED

1. Yu. M. Bazhenov, F. S. Dukhovich, V. V. Kulichenko, et al., in: Scientific-Technical Conference of Specialists from Member-Countries of Comecon on the Problem of Research in Reprocessing and Storing of Radioactive Wastes, German Democratic Republic, Dresden, 18-22 September 1967, Moscow (1968), pp. 228-253.
2. I. A. Sobolev, L. M. Khomchik, and Yu. A. Maksimov, ibid., pp. 306-315.

T-3M TOKAMAK MATERIALS TESTING STAND

A. A. Abagyan, A. A. Alferov, V. F. Babal'yants, D. G. Baratov, V. N. Dem'yanenko, S. B. Leonov, S. P. Maksimov, S. V. Mirnov, V. N. Mikhailov, V. V. Myalton, V. S. Semenov, M. M. Fiks, and V. P. Fokin

UDC 621.039.646

The progress made in fusion research on the basis of a tokamak has made it possible to build the first experimental fusion reactors. An example is the international tokamak-reactor INTOR, the first design phase of which was recently completed [1]. Tokamaks of the new generation, TFTR in the U.S.A. (1982) and JET in Great Britain (1983), which have come into service, are to be used to demonstrate an energy release from the plasma that would exceed the energy input for heating the plasma.

At this stage the research is shifting increasingly to the area of engineering problems, viz., materials testing and fusion technology. In particular, it is necessary to study the behavior of materials for the first wall, diaphragms, and diverter plates of a reactor during prolonged interaction with deuterium–hydrogen peripheral plasma with a temperature of 10-100 eV. The importance of such research is confirmed by the reverse influence of processes in the plasma–wall region on the general characteristics of the plasma [2].

The pertinent conditions of the interaction can be simulated partially in medium-scale tokamaks now in operation because the heat transfer along the magnetic field to the wall or diaphram (this is precisely how plasma–wall contact occurs in tokamaks) is a strong function of the electron temperature T_e. Accordingly, T_e near the boundary varies little (10-100 eV) when the energy release at the wall varies over a wide range. At the same time, the energy of ions that are accelerated in the region of the Langmuir potential drop and bombard the wall should vary over not very wide limits. The maximum value of their energy should not exceed $3T_e$. This circumstance is exploited to simulate the plasma–wall interaction under reactor conditions in existing tokamaks.

Studies of the plasma–wall interaction as well as attendant problems (the properties of peripheral plasma, the erosion resistance of first-wall materials and protection of the first wall, cleansing of the first wall and the mechanisms of the entry of impurities, etc.) require a certain specialization of tokamaks and provision of appropriate diagnostics for them. The JSX tokamak [3], which went into service in 1971 in the United States, is one such specialized tokamak-testing stand. TEXTOR [4], a large-scale stand, has been functioning in the German Federal Republic since 1982. The design of these tokamaks permits rapid re-

Translated from Atomnaya Énergiya, Vol. 58, No. 4, pp. 252-256, April, 1985. Original article submitted July 16, 1984.

 0038-531X/85/5804-0286$09.50

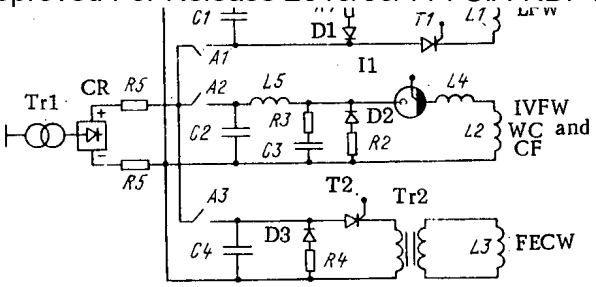

Fig. 1. Schematic of power supply of magnet systems: L1-L5 are the inductances of the LFW (L1), IFVW (L2), WC and CF (L4), FECW (L3), and the ballast inductance (L5); C1-C4 are capacitor banks; T1 and T2 are thyristor switches; I1 is an ignition spark gap; D1-D3 are diodes; R1-R5 are resistors; A1-A3 are contactor-breakers; Tr1 is a power transformer; Tr2 is a matching transformer; CR is a 5-kV charging rectifier.

TABLE 1. Parameters of Plasma of Second Stage of the T-3M Stand in Ohmic Heating Regime

B_T, T	I_p, kA	$\bar{n}_e$, cm^{-3}	τ_E, msec	τ_{Ei}, msec	$T_e(0)$, eV	$T_i(0)$, eV
2	180	$3{,}1\cdot10^{13}$	16	25	600	500
3	270	$4{,}7\cdot10^{13}$	24	45	850	700
4	360	$6{,}4\cdot10^{13}$	32	60	1050	900

placement of elements of the first wall that are to be tested. The reconstruction of the T-3 tokamak conformed to the same requirements [5]. The first phase of the resulting T3-M (materials-testing) engineering stand-tokamak of the USSR Ministry of Energy has been in operation at Shatur since the end of 1980 [6].

The T-3M stand, built on the basis of the T-3A winding designed at the D. V. Efremov Scientific-Research Institute of Electrophysical Apparatus [7], was simplified to the utmost in order to speed up its dismantling and assembly: the double vacuum was dispensed with, a high-vacuum bakable joint was used to allow the chamber to be taken apart for replacement of the inner liner, and an air-core inductor nd control turns permitting rapid dismantling were used.

The stand was started up in stages. The longitudinal magnetic field winding (LFW) of the T-3M stand consists of 16 copper coils, connected in pairs into eight units. The maximum magnetic field on the axis of a unit is B_T = 4 T (1 T in the first stage), the major axis of the toroidal winding is 0.97 m, and the radius of the aperture in the unit is 0.33 m. The corrugation of the magnetic field on the axis and radius of the diaphragm (0.16 m) is 0.5 and 4%, respectively.

The plasma is excited inductively by an air-core inductor of a vortex electric field, consisting of a central solenoid (45 turns) and a system of poloidal turns of the windings of the compensation and control magnetic fields (WC and CF). The turns of the WC and CF are placed on the outside of the LFW units symmetrically about the equatorial plane of the torus and perform two functions: compensation of the scattering fields $B_\perp$ of the solenoid in the plasma to a level $B_\perp/B_T \sim 1\cdot10^{-3}$ and generation of a vertical controlling field ($\sim1\cdot10^{-2}$ T).

The equilibrium of the plasma column is maintained by a stabilizing copper sheath (radius 0.25 m, thickness 0.03 m, time constant 200 msec), which has transverse and longitudinal cuts. In addition, vertical magnetic fields, generated by the WC and CF as well as by a fast equilibrium-controlling winding (FECW), are used. The discrete structure of the FECW along the torus makes it possible to produce dipole or quadrupole configurations of magnetic fields of up to $1\cdot10^{-2}$ T in the region of the plasma column.

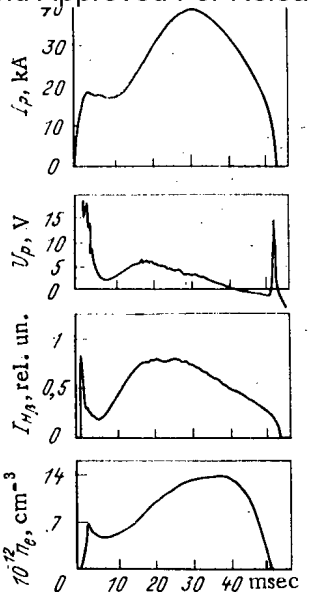

Fig. 2

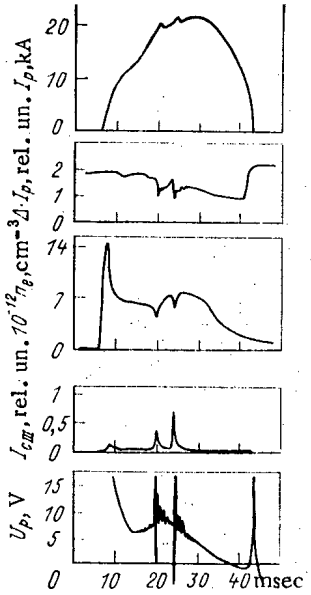

Fig. 3

Fig. 2. Oscillograms of the plasma current I_p, the bypass voltage U_p, the intensity $I_{H\beta}$ of the $H\beta$ line, and the plasma density n_e in the stable discharge regime for B_T = 0.96 T.

Fig. 3. Characteristic oscillograms in a regime with tearing instability: I_p is the plasma current, ΔI_p is the product of the displacement of the plasma column and the plasma current, n_e is the plasma density, I_{CIII} is the intensity of the CIII line, U_p is the bypass voltage, and B_T = 0.96 T.

The schematic of the power supply of the magnet systems of the T-3M stand is shown in Fig. 1 and the parameters of the system are given below:

Longitudinal magnetic-field winding:
- current, kA 2.0
- energy capacity of capacitor bank C1, MJ 3.0
- current half-period, sec 1.1
- induction at the axis, T 1.0

Windings of inductive vortex field (IVFW), WC and CF:
- energy capacity of capacitor bank C2, MJ 0.8
- current in windings, kA. 13
- L5 ballast inductance, mH. 8.1
- current half-period, msec. 80
- inductance of IFVW, mH 1.0
- maximum flux, V·sec. 0.32
- energy capacity of capacitor bank C3 for organization of initial gas breakdown, MJ 0.15
- discharging resistance R3, Ω 0.5

Fast equilibrium-control windings:
- energy capacity of capacitor bank C4, MJ 0.16
- current, kA. 11
- current half-period, msec. 18

A T-4 chamber [8], into which two bakable flange joints were introduced, formed the basis of the discharge chamber (major and minor radii 0.97 and 0.2 m, respectively). These joints and the sliding platform of the tokamak permit the discharge chamber to be divided into two half-toruses for expeditious access to the inner part of the torus.

The pumping system ensures that hydrogen can be pumped out of the chamber at an effective rate of 200 liters/sec and that an ultimate vacuum of $1.3 \cdot 10^{-5}$ Pa is attained. The preparation of the chamber for experiments includes heating and decontamination of the walls by a glow discharge. In the experiments a glow discharge was ignited at a pressure of 10 Pa and a voltage of 5 kV and was maintained with a current of 2.5 A and a voltage of 0.4 kV at a pressure of 0.66 Pa and a temperature of 250°C in the chamber. As a result of aging, the

chamber wall became saturated with hydrogen, and to eliminate the hydrogen the chamber was subjected to additional heating at a pressure of $(2.6\text{-}6.6)\cdot10^{-4}$ Pa. Such decontamination made it possible to reduce the amount of light impurities entering the discharge in the tokamak and reduce the rate of this process, to increase the plasma conductivity almost two-fold, and to increase the fraction of stable discharges.

Oscillograms characterizing the stable operating regime of the first stage of the T-3M stand are given in Fig. 2. The principal plasma-physical parameters of this regime are:

Major radius of torus, m	0.97
Radius of circular stationary diaphragm of carbon-reinforced pyroceramic, m	0.16
Number of diaphragms	3
Toroidal magnetic field at axis, T	1
Plasma current, kA	.40
Reserve of stability at the radius of the diaphragm	2.6
Bypass voltage, V	1.8-3
Density of hydrogen plasma at axis, cm^{-3}	$(0.5\text{-}1.5)\cdot10^{13}$
Electron temperature at axis, eV	250
Mean effective plasma charge	1.6-2
Duration of discharge, msec	.30-50
Plasma energy lifetime, msec	2-3
Particle lifetime, msec	.20-10
Resistance heating power, kW	100
Mean power of thermal flux through a unit surface area of the plasma column, W/cm^2	1.5-2

A regime with tearing instability, accompanied by bursts of emittance of the line of carbon – the material of the diaphragm (Fig. 3) – is typical in the case of a poorly aged chamber wall, a nonoptimal current rise time, or nonoptimal plasma density.

The comparatively low energy intensity of the discharges of the first stage of the T-3M stand hinder experiments to study wall erosion and, therefore, the materials-testing experiments were devoted to an investigation of the behavior of the disphragms and the mechanism of their erosion in regimes with tearing instability [9, 10].

The experimental complex of the T-3M stand incorporates the following component parts.

A stand for high-power thermal action on materials of diaphragms to study the nature of thermal erosion in a vacuum. A GOS-1001 neodymium-glass laser is used as the source of thermal radiation. The radiation parameters: wavelength 1.06 μm, pulse duration 1 msec, energy flux $10^2\text{-}10^4$ MW/m^2, and beam diameter on specimen $4\cdot10^{-3}$ m.

A stand of model experiments (ME), intended for testing of elements of diaphragms of different types, as well as for the development of methods and apparatus for plasma diagnostics in the wall zone of the tokamak. The stand (working volume 1 m^3, vacuum $6.6\cdot10^{-4}$ Pa, and air-pumping rate $4\cdot10^3$ liters/sec) is complemented with a UZDP plasma accelerator [11], making it possible to obtain inert-gas plasma flows with an energy of 0.3-1 keV with a beam current of up to 3 A.

Devices for the study of plasma in the wall zone on the basis of: a method of measuring proton fluxes on a carbon probe in the wall zone, with recording of the desorbed hydrogen by an ROMS-4 radio-frequency mass spectrometer; a method of analysis of the surface of the collecting probes (station for the diagnostics of the surface with the aid of an 09IOS-2 Auger-electron spectrometer and secondary-ion mass-spectrometry); a method of laser ablation and desorption to study the composition and state of the chamber surface.

An IVK-2 information-computational complex based on an SM-4 computer for automation of the experiment, processing of experimental data, and execution of calculations.

The improvement to the T-3M stand-tokamak postulates the creation of conditions for full-scale materials testing of elements of the first wall in regimes close to those in a reactor with regard to the plasma parameters and the mean power of the energy intensity at the wall. The following systems are being developed and built for this purpose:

an SIN injector of fast atoms of hydrogen isotopes (energy up to 80 keV, total power of two beams 2 MW, and duration of injection 0.1 sec);

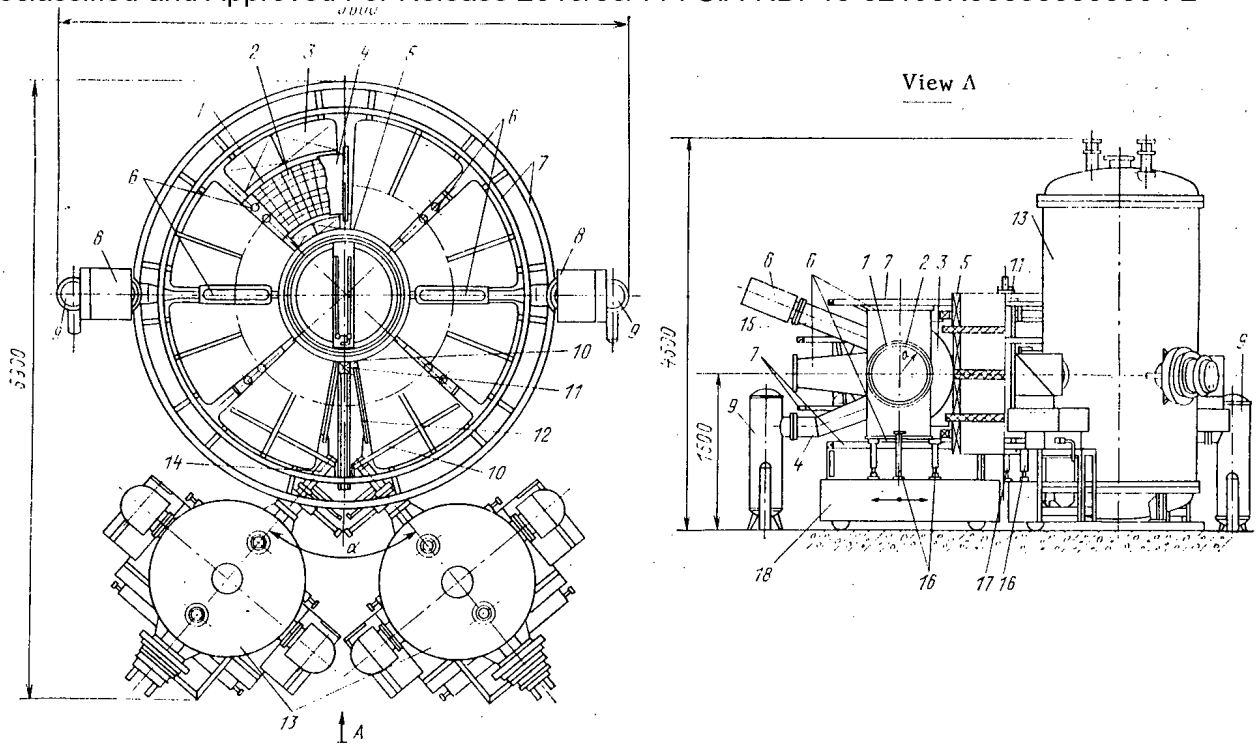

Fig. 4. General view of the T-3M stand-tokamak (second stage): 1) discharge chamber; 2) first wall; 3) unit of longitudinal field winding; 4) stabilizing jacket; 5) solenoid of vortex-field inductor; 6) diagnostic stems; 7) WC and CF; 8) magnetic discharge pump; 9) evacuation system; 10) support; 11) compensating coil; 12) injection section; 13) high-current injector of fast atoms; 14) atom guide; 15) evacuation stems; 16) adjustable supports; 17) support of compensating coil; 18) sliding platform; $\alpha = 80°$ is the angle between the injectors.

discharge chamber ($R = 1.06$ m, $a = 0.29$ m) with subsystems (a removable insert carrying the facing of the first wall, an injection section, a thin stabilizing jacket, etc.);

an electric supply system with a total power of 63 MVA, ensuring the formation of pulses of the longitudinal magnetic field (2 sec, field at axis of chamber 4 T), plasma current (up to 400 kA), vortex electric field (change in the flux in the air-core inductor 2 V·sec), and compensating and controlling magnetic fields.

Figure 4 gives a schematic view of the T-3M stand-tokamak in the second stage. The discharge chamber of 12Kh18N10T stainless steel, assembled with the aid of three joints of diameter 0.6 m of two half-toruses and an injection section, has a major radius of 1.06 m and a minor radius of 0.29 m; the wall thickness is 0.8 mm. A changeable insert of 55 circular sections, carrying the specimens to be tested and forming the toroidal surface of the first wall, can be introduced into the chamber. The minor radius of the chamber to the first wall is 0.28 m. The chamber is pumped down by a vacuum system that ensures a maximum vacuum of $1.3 \cdot 10^{-6}$ Pa and an effective pumping rate of 1000 liters/sec.

A 12-mm thick water-cooled stabilizing jacket made of ADO-6 alloy is placed between the layer of thermal insulation of the chamber and the windings of the longitudinal field. The thin jacket, with a time constant of 30 msec, permits an easing of the requirements concerning the speed of the feedbacks in the control of the equilibrium of the plasma column.

The air-core inductor of a vortex electric field, designed to produce a flux of 2 V·sec and a plasma current of 400 kA, consists of a central solenoid and three pairs of poloidal compansating turns. The solenoid coils are fastened together by means of massive glass-textolite disks which are supports for the longitudinal field units. The maximum current in the inductor is 30 kA and a capacitor bank with an energy capacity of 3.0 MJ is the power supply.

The injectors introduce fast atoms into the plasma through an atom guide and an injection section with two windows of horizontal and vertical dimensions 13 and 30 cm, respec-

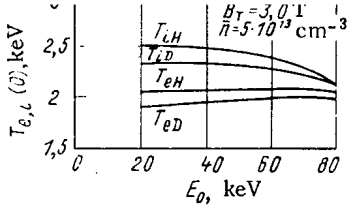

Fig. 5. Dependences of the electron and ion temperatures at the center of column of hydrogen plasma on the energy E_0 of the injected hydrogen (T_{eH}, T_{iH}) or deuterium (T_{eD}, T_{iD}) atoms.

tively. The local attenuation of the longitudinal field as a result of the arrangement of the injection sections is compensated by coils of radius 0.5 m to a level close to the value of the corrugation of the longitudinal field (0.7% at the axis and 8.5% at the outer circumference of the chamber).

High-current injectors developed at the I. V. Kurchatov Institute of Atomic Energy [12] will be used to produce beams of fast atoms. The intensity of the beams of atoms at an energy of 40 keV is 25 eq. A, which ensures that a power of 2 MW is delivered into the plasma with an injection time of 0.1 sec. Injectors with an energy of 80-100 keV are to be used in the future. In view of this a 100-kV GIN-100 pulsed-voltage generator with a 4-MJ capacitive storage element is being built to be the high-voltage power supply for the ion-optical system.

The expected plasma parameters in the second stage of T-3M for ohmic and injection heating were calculated with the following assumptions: the maximum plasma current was obtained for a stability reserve of 3; the ion temperature $T_i(0)$ on the axis is determined by the Artsimovich formula; the values of the plasma density $\bar{n}_e$, plasma energy lifetime τ_E, ion energy liftetime τ_{Ei}, and the electron temperature $T_e(0)$ were obtained from TFR scalings [13]; the effective plasma charge is assumed to be 2. The results for different longitudinal field strengths B_T are given in Table 1.

The data in the table were taken as the initial data for the calculation of the plasma parameters under the conditions of injection heating. The calculations indicated that transverse injection on the T-3M stand can be effective only at a high plasma density ($\bar{n}_e > 5 \cdot 10^{13}$ cm^{-3}) and a low injection energy ($E_0 < 40$ keV). These limitations can be overcome by a switch to longitudinal injection. Figure 5 gives the calculated dependences of the electron and ion temperatures on the energy E_0 of the beams during longitudinal injection of two beams with a total power of 2 MW. In this case the optimal injection is attained for an integrated capture coefficient of 0.99-0.93 for fast atoms in the energy range 20-80 keV, magnetic field strength 4-3 T, and plasma density 6-10^{13} cm^{-3}. This version is being considered as the main version for realization on the T-3M stand-tokamak.

LITERATURE CITED

1. B. B. Kadomtsev and V. I. Pistunovich. At. Energ., 54, No. 2, 83 (1983).
2. "Regime of enhanced energy and particle confinement in discharges heated by a neutron beam with a diverter in a doublet III," in: Proceedings of Eleventh European Conference on Controlled Fusion and Plasma Physics, Aachen (1983), Vol. 1, p. 11, Paper 0-03.
3. Impurity Study Experiment. Proposal, ORNL-TM-4884 (1975).
4. Report on the Planning of TEXTOR, KFA, Julich (1975), Nov. 15.
5. D. G. Baratov, V. N. Dem'yanenko, N. V. Evseev, et al., "The T-3M materials testing stand: program and design data" [in Russian], Papers Read at Soviet–American Scientific Meeting "Interaction of Plasma with a Tokamak Wall," Moscow (1978).
6. Novosti Termoyadernykh Issled. SSSR, No. 3(21), 1 (1981).
7. M. A. Gashev, G. K. Gustov, K. K. D'yachenko, et al., At. Energ., 17, No. 4, 287 (1964).
8. L. A. Artsimovich, V. A. Vershkov, A. V. Glukhov, et al., "Research on plasma confinement and heating in the Tokamak-4 device," in: Proceedings of Fourth International Conference on Plasma Physics and Controlled Fusion, Vol. 1, Madison, Wisc. (1971), pp. 443-449.
9. D. Baratov et al., in: Proceedings of Tenth Eurpoean Conference on Fusion and Plasma Physics, Vol. 1, Moscow (1981), J-11.

10. D. G. Baratov, G. V. Gordeeva, M. I. Guseva, et al., At. Energ., 53, No. 6, 390 (1982).
11. V. N. Dem'yanenko, I. P. Zubkov, A. I. Morozov, et al., Zh. Tekh. Fiz., 46, No. 4, 718 (1976).
12. N. N. Semashko, "Fast-atom injectors," in: Itogi Nauki i Tekhniki. Ser. Fiz. Plazmy, 1, 232-282 (1980).
13. Eguipa TFR, Nucl. Fusion, 20, No. 10, 1227 (1980).

SINGLE-CRYSTAL LITHIUM FLUORIDE DETECTORS

A. I. Nepomnyashchikh, S. N. Mironenko, G. P. Afonin, and A. I. Selyavko

UDC 539.1.074.535.377

Lithium fluoride has now been used for more than 30 years as detectors for thermoluminescence dosimetry. At the present time 70% of the detectors employed in this area [1] are made on the basis of lithium fluoride. About 30 methods and compositions are known for the fabrication of LiF-based phosphors. In most cases lithium fluoride is used in the form of pressed and polycrystalline tablets as well as in the form of items made of Teflon with LiF powder dispersed in it. All of these detectors have one inherent drawback: a considerable background signal which is determined by the large surface in contact with the surrounding atmosphere.

In single-crystal detectors this disadvantage is eliminated because of the small surface of interaction with the atmosphere, transparency over a wide region of the spectrum, and as a consequence of these properties a small value of the background signal, as well as an increase in the sensitivity of the detector. The application of such detectors, however, has been limited by the difficulty of obtaining large lithium fluoride single crystals that would have a uniform sensitivity [2, 3].

The A. P. Vinogradov Institute of Geochemistry, Siberian Branch of the Academy of Sciences of the USSR, has developed single-crystal detectors (DTG-4) on the basis of LiF:Mg, Ti and methods of growing single crystals of the desired configuration that would have a uniform sensitivity and a sensitivity spread of no more than ±15%. The diameter of these detectors is 5 mm and their thickness is 1 mm. Moreover, detectors of diameters 3, 8, and 10 mm can also be produced. We shall consider their principal characteristics.

Lower Limit of Detectable Dose. One of the principal characteristics of a thermoluminescent detector, determining its range of application, is the lower limit of detectable dose, which in turn is determined by the combination of the yield of thermally stimulated luminescence (TSL), the background signal of the detector, and the degree of correspondence between the radiation spectrum of the detector and the region of maximum sensitivity of the photodetector.

The TSL yield of different detectors of LiF:Mg, Ti is in the range 10^9-10^{10} quanta·g^{-1}·cGy^{-1}, while the optimum apparently is (0.5-1)·10^{10} quanta·g^{-1}·cGy^{-1}. The TSL yield is practically independent of the magnesium concentration within the limits 0.03-0.5%. An increase in the titanium oxide concentration leads to a considerable growth of the low-temperature peaks (Fig. 1). In LiF:Mg crystals luminescence is caused by impurity "titanium" centers formed because of traces of titanium in the raw materials.

When the TSL yield is of the order of 10^{10} quanta·g^{-1}·cGy^{-1} measuring instruments based on present-day electronics, especially when the photon-counting method is used, permit doses at a level of 10^{-3} cGy or lower to be detected with a sufficient degree of accuracy and the radiation spectrum of detectors based on LiF:Mg, Ti corresponds to the region of maximum sensitivity of photodetectors. Thus, the lower limit of the detectable dose will be limited by the level of the intrinsic background signal of the detector. For single-crystal detectors the level of the intrinsic background signal is below 10^{-3} cGy and, therefore, such detectors are capable of detecting doses of 10^{-3} cGy or less with a sufficient degree of accuracy (Fig. 2).

Translated from Atomnaya Énergiya, Vol. 58, No. 4, pp. 257-259, April, 1985. Original article submitted June 1, 1984; revision submitted September 11, 1984.

 0038-531X/85/5804-0292$09.50

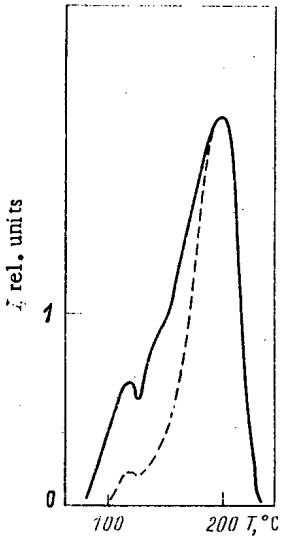

Fig. 1

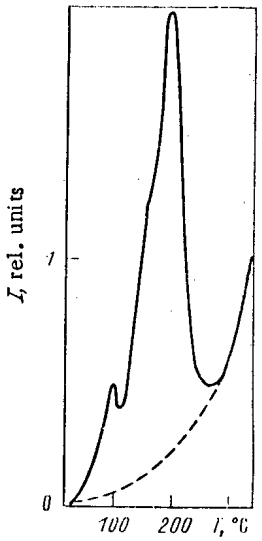

Fig. 2

Fig. 1. Thermoluminescence curves of Li:Mg (---) and LiF:Mg, Ti (——) crystals.

Fig. 2. Thermoluminescence curve of DTG-4 detectors for a radiation dose of 10^{-5} Gy; the dashed line represents the background of the heater with the detector.

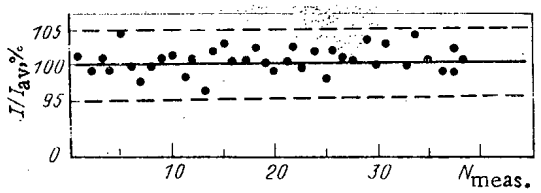

Fig. 3. Agreement of indications of detectors during repeated use at a radiation dose of 10 cGy per cycle: •) experimental points; ——) zero line; ---) confidence interval.

Repeated Use of Detectors. One of the main service characteristics of a detector is the number of times it can be used. Special regimes of additional heat treatment are necessary for practically all known lithium fluoride detectors when they are used repeatedly [4, 5].

The change in the intensity of the TSL peak at 200°C is determined by the diffusion processes of the aggregation of $Mg^{2+}V_c^-$ dipoles [6], which is the main initial component for the formation of $Mg^+V_a^+V_c^-$ centers [7] that are responsible for the TSL peak at 200°C. The rate of diffusion aggregation of Mg^{2+} V_c^- dipoles depends on the magnesium concentration. When the latter decreases, the aggregation rate decreases accordingly and at certain values of the concentration the detector sensitivity will not change during storage, and this is indeed observed in the case of DTG-4 single-crystal detectors.

Additional heat treatment is not required for the repeated use of DTF-4 detectors at radiation doses of less than 300 cGy (Fig. 3). The agreement between the results of measurements of the radiation dose on TELDE and Victoreen instruments does not exceed 3%. The detectors can be used no less than 500 times without additional heat treatment.

Unlike the case in [8], we did not detect a change in the thermoluminescence curves of unirradiated detectors after prolonged storage. Thus, the storage of LiF:Mg crystals for 10 yr and LiF:Mg, Ti crystals for several years (Fig. 4, curves b, c, d) does not lead to a change in the thermoluminescence curves. A distinctive feature of detectors that have been stored for a sufficiently long time is the absence of peak 2.

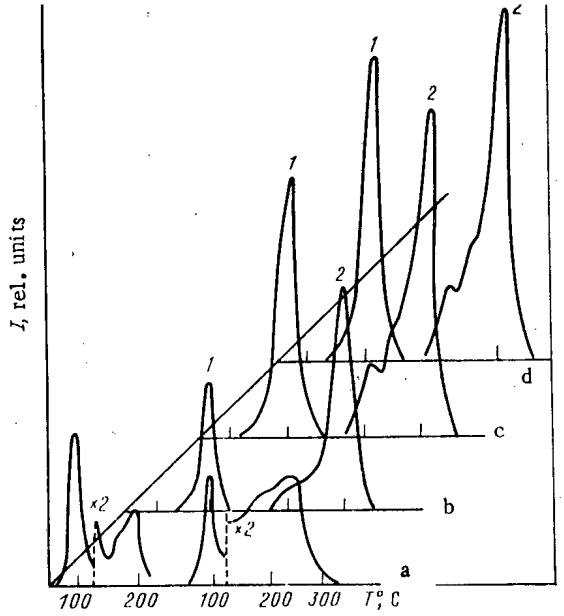

Fig. 4. Thermoluminescence curves of DTG-4 detectors: a) data for LiF:Mg from [5]; b, c, d) after storage of unirradiated LiF:Mg detectors for 11 yr (b), 8 yr (c), and 3 yr (d); 1) "fresh" detectors; 2) next luminescence.

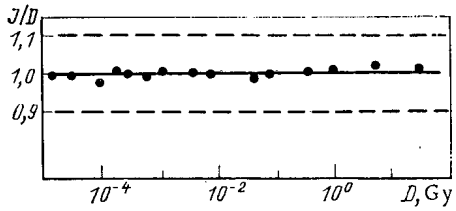

Fig. 5. Dependence of the indications of DTG-4 detectors on the dose of x radiation: •) experimental points; ——) zero line; ---) confidence interval.

Dependence of the TSL Yield on the Radiation Dose. Most papers indicate that the dependence of the light sum on the dose is not a linear function in the range of small doses (at the levels of the background signal) and large doses of radiation [9]. The region of a superlinear dependence as a rule begins at radiation doses above 300 cGy. The region of the linear dependence of the dose characteristic for large doses of radiation can be expanded substantially by sensitization of the phosphor. The TSL yield is increased at the same time. Despite this, however, sensitization does not permit the limits of measurements to be extended to the region of small radiation doses since the background luminescence increases strongly. Since in a sensitized phosphor the dose characteristic is linear for high radiation doses, it is used preferentially in clinical dosimetry in the range 10-10^4 cGy [10].

The dependence of the TSL yield of DTG-4 single-crystal detectors on the radiation dose is given in Fig. 5. After irradiation with a dose of more than 300 cGy the detector was heated to 370°C and held there for 15-16 sec. As follows from Fig. 5 the dose characteristic is linear in the range 10^{-3}-$3 \cdot 10^3$ cGy and the characteristics of the detector do not change after exposure to large radiation doses (up to $5 \cdot 10^4$ cGy), and as a result small doses can be measured without altering the sensitivity of the detector (Fig. 6).

Loss of Accumulated Light Sum during Storage of Detectors. The preservation of the light sum (dosimetric information) accumulated by a detector is determined by the characteristics of the trapping centers (activation energy E and frequency factor P_0) as well as by the ambient temperature.

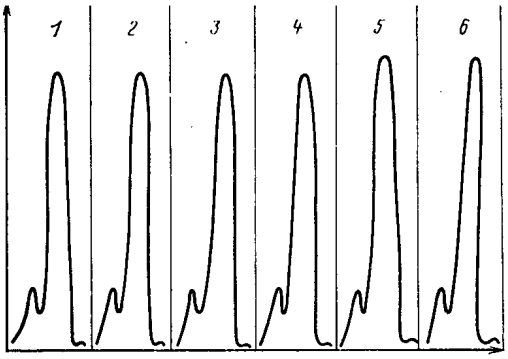

Fig. 6. Stability of indications of detectors after irradiation with doses of $1.8 \cdot 10^{-1}$ Gy (1), 6.0 Gy (2), $1.8 \cdot 10^{-1}$ Gy (3), 30 Gy (4), $1.8 \cdot 10^{-1}$ Gy (5), $1.8 \cdot 10^{-1}$ Gy (6) after irradiation with a dose of $5 \cdot 10^{2}$ Gy.

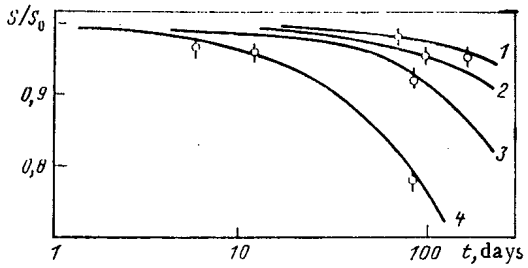

Fig. 7. Dependence of the loss of dosimetric information on the duration of detector storage at 120 (1), 35 (2), 40 (3), and 50°C (4); ——) calculation; o) experiment.

The number n of filled traps at the temperature T by the time t (for a first-order kinetics) can be described by the formula

$$n = n_0 \exp[-P_0 \exp(-E/kT)],$$

where n_0 is the number of filled traps at the initial time.

In order to ensure preservation of the accumulated light sum for a long time it is necessary that the trapping centers responsible for the main dosimetric TSL peak have a sufficiently high activation energy. Moreover, small centers should not be present or their concentration should be considerably below the concentration of the main traps, i.e., on the thermoluminescence curve the light sum accumulated in the low-temperature peaks as a percentage of the light sum of the main peak should be smaller than the allowable loss of dosimetric information.

Figure 7 presents the calculated dependence and experimental values of the loss of the accumulated light sum of a DTG-4 detector on the storage time at different temperatures. For the calculation we took the values E = 1.25 eV and $P_0 = 5 \cdot 10^{11}$ sec^{-1}. As follows from Fig. 7, the loss of dosimetric information when detectors are stored for one year at +20 or +35°C does not exceed 5%. To obtain reliable results at +50°C the storage time of the detectors must be limited to 3 months. Below we give the principal dosimetric characteristics of single-crystal detectors based on LiF:Mg, Ti:

Specific sensitivity of detector to radiation, quantum/cGY·g . . . . . not below $6.6 \cdot 10^9$
Contribution of low-temperature peaks to total light sum, % 6
Dose equivalent of intrinsic background, cGy . . . . . $1 \cdot 10^{-3}$
Convergence of sensitivity, % . . . . . ±3
Measuring range of absorbed dose, cGy . . . . . $1 \cdot 10^{-3}$-$5 \cdot 10^3$
Variation of detector sensitivity in the absorbed dose range $5 \cdot 10^{-3}$-$5 \cdot 10^3$, cGy, % . . . . . ±15
Number of times detectors used 500
Loss of accumulated light sum during storage for 1 yr, %:
at 20°C . . . . . no more than 5
at 40°C . . . . . no more than 15

The detector preserves its characteristics to within ±15% after irradiation with a dose of $5 \cdot 10^4$ cGy.

LITERATURE CITED

1. A. D. Sokolov, "State and problems of the application of thermally stimulated phosphors in personnel dosimeters," in: Abstracts of All-Union Conference "Synthesis, Properties, Studies, and Technology of Phosphors for Representation of Information" [in Russian], Stavropol' (1983), p. 61.
2. I. A. Bochvar, T. I. Gimadova, I. B. Keirim-Markus, et al., Method of X-Ray Dosimetry [in Russian], Atomizdat, Moscow (1977).
3. K. K. Shvarts, Z. A. Grant, T. K. Mezhs, and M. M. Grube, Thermoluminescent Dosimetry [in Russian], Zinatne, Riga (1968), p. 183.
4. M. M. Grube and Z. A. Grant, Izv. Akad. Nauk Latv. SSR, Ser. Fiz. Tekh. Nauk (1968), pp. 40-46.
5. J. Cameron, N. Suntaralingam, and G. Cenney, Thermoluminescent Dosimetry, University of Wisconsin, Madison, Wisc. (1968).
6. A. I. Nepomnyashchikh and E. A. Radzhabov, Dep. No. 1316-79, All-Union Institute of Scientific and Technical Information (VINITI), Moscow (1979).
7. A. I. Nepomnyashchikh and E. A. Radzhabov, Opt. Spektrosk., 48, No. 2, 273 (1980).
8. I. A. Parfianovich, E. P. Alekseeva, and G. V. Sotserdotova, "Influence of 'aging' of lithium fluoride on its dosimetric properties," in: Proceedings of Third All-Union Symposium on Luminescence Detectors and X-Ray Converters" [in Russian], Stavropol' (1980), p. 106.
9. V. Jain, Phys. Status Solidi (a), 38, No. 1, K65 (1976).
10. V. G. Krongauz and I. Kh. Shaver, Phosphors for Thermoluminescent Dosimetry [in Russian], Scientific-Research Institute of Technicoeconomic Studies of the Ministry of the Chemistry Industry of the USSR (NIITEKhIM), Moscow (1978), p. 35.

USE OF POLARIZED RADIATION FOR INCREASING THE SENSITIVITY OF MULTIELEMENT X-RAY FLUORESCENCE ANALYSIS

A. A. Ter-Saakov and M. V. Glebov

UDC 543.423.8:543.426

The use in x-ray fluorescence analysis (XFA) of the direct radiation from a tube for determining the elements in a light matrix significantly limits the sensitivity of the method, which mainly is due to the strong scattering of the continuous bremsstrahlung.

At the present time, different methods have been developed for increasing the sensitivity of XFA, among which one of the most promising from our point of view is the polarization of the primary radiation. In [1-6] methods are considered for obtaining polarized radiation. With excitation of the characteristic emission of the sample by polarized x-radiation, the Compton scattering cross-section dG can be represented in the form [4]

$$dG = \left(\frac{e^2}{mc^2}\right)^2 \sin^2 t d\Omega, \qquad (1)$$

where e and m are the charge and mass of the electron; c is the velocity of light; and t is the angle between the direction of the intensity vector of the electromagnetic field of the polarized radiation and the direction of observation. In the ideal case, when t is equal to 0° or 180°, it is possible to get rid of the scattered radiation of the sample in the apparatus spectrum.

The most widespread mechanism is considered to be scattering of the primary radiation at an angle of 90° (Thompson condition of polarization). It should be noted that this method has a considerable limitation – the low intensity yield. Another method is based on the use of a diffraction crystal as a polarizer [2, 3]. In order that the crystal should "function" as a polarizing monochromator, it is necessary to fulfill the Thompson condition and Bragg's law. The drawback of this method is the reduction of the probability of excitation in the case of multielement XFA and also difficulties connected with the technical achievement.

An experimental XFA facility has been developed using polarized radiation. The excitation system is designed with consideration of the Thompson condition of polarization. A modernized small-sized REIS-I emitter is used as the x-ray generator. Its characteristics are: a straight-through drift tube with a copper, molybdenum, or silver anode; a smmothly controlled working voltage from 0 to 45 kV; an anode current of 50-450 μA; and a maximum power in the tube of 12 W. The fluorescence from the sample is detected with a Si(Li)-semiconductor detector of the type BDÉR-2-25 with a resolution of 290 eV at the 5.9 keV line; the thickness of the inlet beryllium window is 100 μm. The recording system is the NTA-1024 spectrometric equipment, coupled with the EMG-666 minicomputer.

A series of experiments was carried out on the facility on the optimization of fluorescence excitation conditions of biological samples (choice of the tube anode material, high voltage, anode current, and polarizer material). The analytical possibilities of the x-ray fluorescence facility using the tubes are determined to a considerable extent by their spectral characteristics. The investigations conducted by us of the dosimetric and spectral characteristics of the BS-1, BS-3, and BKh-7 x-ray tubes with copper, silver, and molybdenum anodes have shown that for the analysis in samples of biogenic elements, it is most efficient to use the BKh-7 and BS-1 tubes with a copper anode. This is because in the primary spectra of the x-ray tubes with molybdenum and silver anodes, "interfering" lines of the characteristic radiation are present and the total radiation intensity of these tubes is a factor of 5-15 less than tubes with a copper anode.

The polarizer material is chosen depending on the group of the elements being analyzed, which was due to two factors. Firstly, the scattering efficiency of the polarizer material is found to have a direct dependence on the ratio of scattering to the photoelectric absorption. Secondly, the interaction of the primary radiation with the polarizer material takes

Translated from Atomnaya Énergiya, Vol. 58, No. 4, pp. 260-262, April, 1985. Original article submitted June 6, 1984.

0038-531X/85/5804-0297$09.50

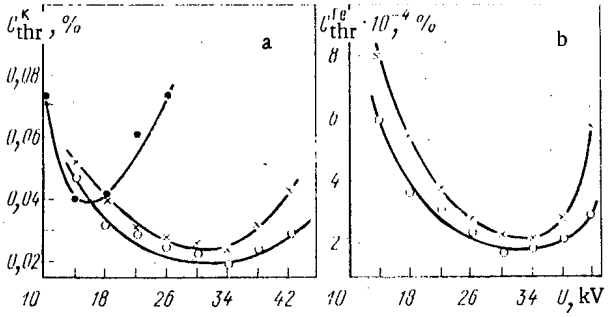

Fig. 1. Dependence of the threshold of detection of potassium (a) and iron (b) on the high voltage on the tube, for a polarizer of beryllium (•), plastic (×) and graphite (o).

place in a limited region, depending on the actual geometric dimensions of the collimation system. An estimate of the scattering efficiency of the polarizer material conducted by us by the procedure of [6] showed that for the analysis of biological samples for elements from chlorine to zinc, polarizers of graphite, boron carbide, and plastic are the most sound.

As a criterion of optimality with respect to current, high voltage, and polarizer material, the threshold of detection was chosen:

$$C_{\text{thr}} = \frac{3\sqrt{N_B}}{N_p} C, \qquad (2)$$

where N_B is the number of background pulses, N_p is the number of pulses in the photopeak, and C is the concentration in the sample of the element being analyzed.

A study of the dependence of the threshold of detection on the anode current (y) revealed that over the whole working range from 50 to 450 μA, $C_{thr} \sim 1/\sqrt{y}$; the investigations were conducted with fixed values of the voltages – 10, 20, and 30 kV.

For opimization of the high voltage in the range 10-42 kV, experiments were conducted on tubes with a copper anode and with different polarizers at a fixed anode current of 250 μA. From the results obtained, Fig. 1 shows the dependence of the threshold of detection of potassium and iron on the high voltage for different polarizer materials: the optimum value of the high voltage is found to be in the range 20-35 kV, which confirms the numerical-theoretical estimates of the polarizer material given above.

Thus, the optimization experiments for the conditions of fluorescence excitation of biological samples showed that for the analysis of biogenic elements it is most efficient to use an x-ray tube with a copper anode with operating conditions of the generator at a voltage of 20-35 kV and anode current of 200-300 μA and to use graphite or plastic as the polarizer material.

Experiments were conducted in order to develop the potentialities of XFA for biological samples. Cl, K, Ca, Mn, Fe, Zn, Br, and Sr were identified in vegetable samples; Si, K, Ca, Ti, V, Fe, Sr, and Zr in soil samples; and K, Ca, Mn, Fe, Zn, and Cr in soil extracts. Typical spectra of a vegetation sample as the result of fluorescence excitation with polarized and direct radiation are shown in Fig. 2. In order to estimate the threshold of detection, standards were prepared, based on standard materials of cereal grass mixture (SMBT-01), wheat grain (SBMP-01), and potato tubers (SBMK-01).

Experiments to determine the dependence of the threshold of detection on the atomic number of the element being analyzed were conducted in conditions close to optimum. In the case of excitation with polarized radiation, x-ray tubes with a copper anode (24 kV, 250 μA) were used with a plastic polarizer; the measurements were made in a "saturated" layer. In the case of excitation with direct radiation, tubes with a silver anode were used (18 kV, 50 μA); the measurements were made in a "thin" layer. The time of collection of the spectrum was 1000 sec. Some results of these experiments are shown in Fig. 3.

The investigations showed that in the case of x-ray fluorescence analysis of samples with light matrices, the use of a source of excitation of polarized radiation from x-ray tubes significantly increases the sensitivity of the determination of the elments.

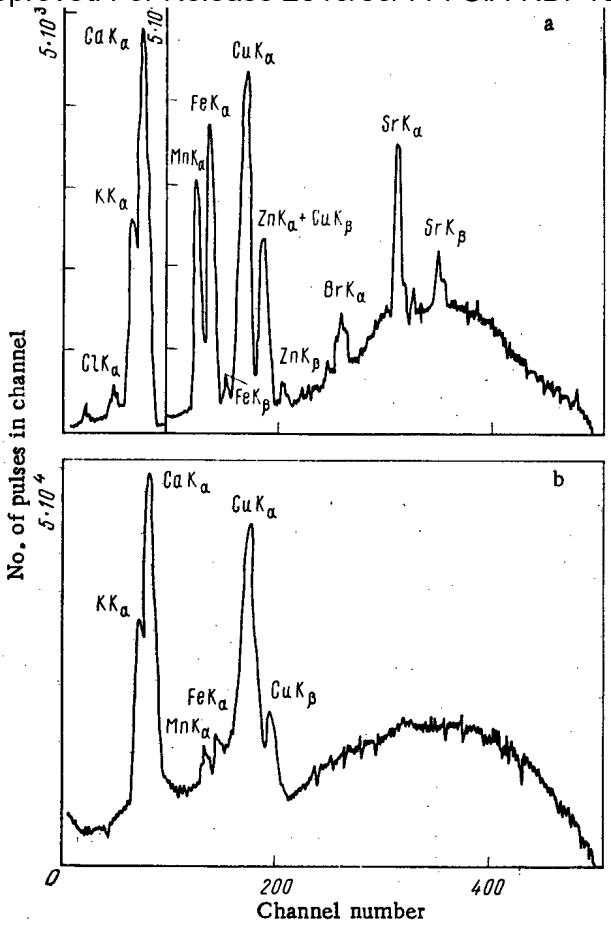

Fig. 2. Spectrum of a vegetation sample as a result of excitation with polarized (a) and direct x-radiation (b).

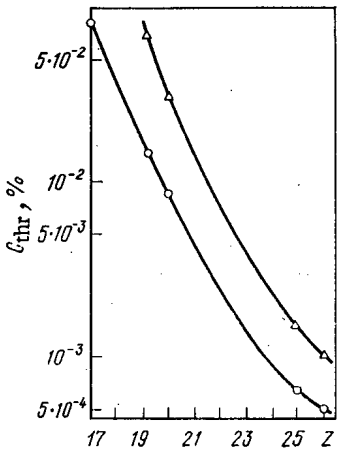

Fig. 3. Dependence of the threshold of detection on the atomic number of the element being analyzed in the case of polarized (o) and direct radiation (Δ).

LITERATURE CITED

1. R. Vol'dset, Applied X-Ray Spectrometry [in Russian], Atomizdat, Moscow (1977).
2. P. Ong and I. Randall, X-Ray Spectrometry, 7, No. 4, 241 (1978).
3. H. Aiginger, P. Wobranschek, and C. Branner, "Measurement, detection, and control of environmental pollutants," in: Proceedings of a Symposium, Vienna (1976), p. 644.
4. T. Dzubay, B. Iarratt, and I. Iaklevic, Nucl. Instrum. Methods, 115, No. 1, 297 (1974).

5. T. Dzubay, USA Patent No. 3,844,822/19/4.
6. R. Ryon, in: 27th Conference on Applications of X-Ray Analysis, Denver, Colorado (1978), p. 15.

THE KERMA-CONSTANT AND KERMA-EQUIVALENT OF A RADIONUCLIDE SOURCE

V. P. Mashkovich

UDC 539.166.2

The introduction of the International System of Units (SI) in our country on January 1, 1980, as the obligatory system [1-3] gave rise to a discussion [4-9] about the choice of derivative physical quantities and their SI units, which should replace the γ-ray constants of radionuclides [10-16] and γ-ray equivalents of radionuclide sources [15, 16] used extensively in non-system units in the field of ionizing radiations to characterize photon radiation. The need of such a substitution is due to the fact that during the period of the introduction of SI, which should be completed by January 1, 1990, in the field of ionizing radiations, the exposure dose and its derivative quantities are subject to elimination [17]. Consequently, the γ-ray constant and the nonstandard quantity, the γ-ray equivalent, which are defined in terms of the exposure dose rate, are also subject to elimination.

The discussion was brought to an end by the elaboration of methodological instructions [17], in which the rare constant of the air kerma† of a radionuclide (kerma-constant) and the kerma-equivalent of a source are introduced in place of the γ-ray constant and the γ-ray equivalent. These quantities are determined from the air kerma rate. The convenience of using the kerma in the solution of practical problems stems from the fact that the SI unit for the kerma has a simple whole-number relation to the non-system unit (1 rd = 10^{-2} Gy); the kerma is appreciable to the determination of fields of both photons and neutrons in any range of values of radiation doses and energies and does not introduce multivalued parameters into the calculations.

The kerma-constant of a radionuclide [17] is $\Gamma_\delta = \dot{K}_\delta r^2/A$, where $\dot{K}_\delta$ is the rate of the air kerma produced by photons of an energy greater than the prescribed threshold value δ from a point isotropically emitting source of the given radionuclide in a vacuum at a distance r from the source, and A is the activity of the source. The unit of the kerma-constant is the gray-meter squared per second-becquerel, Gy·m²/sec·Bq. The unit aGy·m²/sec·Bq is recommended as the preferred unit.

The physical meaning of the kerma-constant is the rate of the air kerma produced by photons of an energy higher than the prescribed threshold value δ at a distance r = 1 m from a point isotropically emitting source of the given radionuclide with an activity A = 1 Bq, placed in a vacuum. The value of the kerma-constant is numerically equal to the air kerma produced by photons from a point isotropic radionuclide source in one decay at a distance r = 1 m from the source in a vacuum. It is recommended that δ = 30 keV be taken in calculations since photons of lower energy are usually of no practical importance as a consequence of intense absorption.

Calculation of the kerma-constant Γ_δ [aGy·m²/sec·Bq] for a radionuclide emitting photons of m different energy groups, with the energy of the i-th group E_{0i} [MeV], quantum yield n_i [photon per decay], and mass energy transfer coefficient $\mu_{tr,i}$ [m²/kg], must be made from the formula

$$\Gamma_\delta = \frac{\sum_{i=1}^{m} E_{0i} n_i \mu_{tr,i} 1.602 \cdot 10^{-13} \cdot 10^{18}}{4\pi \quad 1} = 12750 \sum_{i=1}^{m} E_{0i} n_i \mu_{tr,i} = \sum_{i=1}^{m} \Gamma^*_{\delta_i} n_i = \sum_{i=1}^{m} \Gamma_{\delta_i}, \quad (1)$$

where $1.602 \cdot 10^{-13}$ is the factor for the conversion of a megaelectron volt to joules, 10^{18} is the factor for the conversion of a gray to attograys, 1 J/kg·Gy is the energy equivalent

†The word "air" indicates the substance for which the kerma is determined.

Translated from Atomnaya Énergiya, Vol. 58, No. 4, pp. 262-265, April, 1985. Original article submitted April 19, 1984; revision submitted October 2, 1984.

 0038-531X/85/5804-0300$09.50

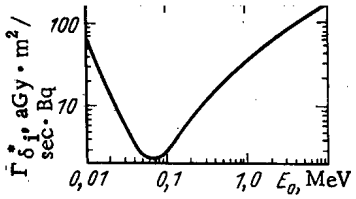

Fig. 1. Dependence of normalized differential kerma-constant $\Gamma_{\delta i}^*$ on the photon energy E_0.

of a gray, Γ_{δ_i} is the differential kerma-constant (calculated for the i-th monoenergetic group of photons), and $\Gamma_{\delta_i}^*$ is the normalized differential kerma-constant (calculated for a yield of 1 photon per decay, i.e., for $n_i = 1$) (Fig. 1).

If in (1) we replace $\mu_{tr,i}$ for air by the mass energy absorption coefficient $\mu_{en,i}$ in air, then when the condition of electron equilibrium is fulfilled the constant will be calculated from formula (1) in the same units but on the basis of the absorbed dose rate in air. It is known that $\mu_{en} = \mu_{tr}(1 - g)$, where g is the fraction of the energy of secondary charged particles that is transferred to bremsstrahlung in the given material (Fig. 2). As follows from Fig. 2, for most radionuclides, whose radiation has an energy $E_0 < 3$ MeV, the fraction $g < 0.01$ for air and, therefore, the value of the air kerma can exceed the value of the absorbed dose in air by no more than approximately 1%. This means that with an error of approximately 1%, which is smaller than the error of determination of the coefficients of photon interaction with the material (±2% [19]), we can assume the kerma-constant to be equal to the absorbed dose rate in air, calculated for the same conditions under which the kerma-constant is calculated. We note that the above is correct only for light-atom media (air, water); for heavy substances the value of g can be considerably higher (see Fig. 2).

It can be easily shown that the kerma-constant Γ_δ [aGy·m²/sec·Bq] is 6.55 times greater than the γ-ray constant Γ [R·cm²/h·mCi], calculated in non-system units from the exposure dose rate, if we assume that g = 0, which is valid for the problems considered in this paper.

The calculated values of the kerma-constants of the radionuclides used most extensively are given in Table 1. The calculations took annihilation radiation and K-radiation into account. The kerma-constants of radionuclides with allowance for the γ-radiation of the daughter products are given for the equilibrium state. The error of the values of the kerma-constant presented here is 3-11%.

The kerma-equivalent K_e of a source [17] is $K_e = \dot{K}r^2$, where $\dot{K}$ is the air kerma rate of photon radiation, with a photon energy higher than the prescribed threshold δ of an isotropically emitting point source placed in a vacuum, at a distance r from the source. The unit of the kerma-equivalent is gray-meter squared per second (Gy·m²/sec). The units nGy·m²/sec, μGy·m²/sec, mGy·m²/sec, and Gy·m²/sec are recommended as preferred units.

The physical meaning of kerma-equivalent is the rate of the air kerma produced by photons of an energy higher than the prescribed threshold value δ from the given isotropic point radionuclide source in a vacuum, at a distance r = 1 m from the source. This value is necessary and appropriate for comparison of the γ-radiation of sources on the basis of the ionization effect in air.

From the definition it is clear that the kerma-equivalent K_e [aGy·m²/sec] is related to the activity A [Bq] through the kerma-constant Γ_δ [aGy·m²/sec·Bq] by

$$K_e = A\Gamma_\delta. \tag{2}$$

We relate the kerma-equivalent K_e [nGy·m²/sec] to the γ-ray equivalent m, expressed in milligram-equivalents of radium (mg-eq. Ra). Since the γ-ray equivalent m is related to the γ-ray constant Γ [R·cm²/h·mCi] and the activity A_0 [mCi] of the radionuclide by $m = A_0\Gamma/8.4$ [8.4 R·cm²/h·mCi is the γ-ray constant of radium in equilibrium with the principal daughter products of decay after a platinum filter of thickness 0.5 mm], when Eq. (2) is taken into account we can write $K_e/m = (A\Gamma_\delta 10^{-9}):(A_0\Gamma/8.4) = (A/A_0)(\Gamma_\delta/\Gamma)10^{-9}\cdot 8.4 = 3.7\cdot 10^7\cdot 6.55\cdot 10^{-9}\cdot 8.4 = 2.04$. Therefore, we have approximately

$$K_e = 2.04\ m. \tag{3}$$

TABLE 1. Values of the γ-Ray Constants and Kerma-Constants of the Most Widely Used Radionuclide*[1] for δ = 30 keV

Radionuclide	Half-life	Γ, R·cm²/h·mCi		Γ_δ, aGy·m²/sec·Bq*[4]
		[15] *[2]	[14] *[3]	
$^{22}_{11}Na$	2,603 yr	11,85	11,8 (5)	77,6 (33)
$^{24}_{11}Na$	15,029 h	18,13	18,1 (8)	119 (5)
$^{54}_{25}Mn$	312,16 days	4,616	4,61 (27)	30,3 (18)
$^{59}_{26}Fe$	44,52 days	6,177	6,2 (3)	41 (2)
$^{57}_{27}Co$	271,5 days	0,553	0,56 (3)	3,7 (2)
$^{60}_{27}Co$	5,273 yr	12,85	12,8 (6)	84,2 (39)
$^{65}_{30}Zn$	243,9 days	3,056	3,07 (18)	20,2 (12)
$^{73}_{33}As$	80,30 days	0,0372	0,0373 (30)	0,245 (20)
$^{74}_{33}As$	17,77 days	4,349	4,3 (2)	28 (1)
$^{75}_{34}Se$	119,8 days	2,029	1,99 (16)	13,1 (10)
$^{85}_{36}Kr$	10,73 yr	0,0129	0,013 (1)	0,086 (6)
$^{91}_{39}Y$	58,51 days	0,0312*[5]	0,019 (2)	0,12 (1)
$^{95}_{40}Zr + ^{95m}_{41}Nb$	64,02 days	4,125	4,12 (18)	27,1 (12)
$^{95}_{40}Nb$	35,01 days	4,269	4,22 (27)	27,8 (18)
$^{103}_{44}Ru + ^{103m}_{45}Rh$	39,36 days	2,829	2,8 (2)	18 (1)
$^{106}_{44}Ru + ^{106}_{45}Rh$	367 days	1,150	1,16 (5)	7,63 (33)
$^{110m}_{47}Ag + ^{110}_{47}Ag$	249,9 days	15,39	15,0 (10)	98,7 (66)
$^{113}_{50}Sn + ^{113m}_{49}In$	115,1 days	1,451	1,48 (9)	9,74 (59)
$^{124}_{51}Sb$	60,20 days	9,617	9,6 (4)	63 (3)
$^{131}_{53}I$	8,054 days	2,156	2,16 (10)	14,2 (6)
$^{131m}_{54}Xe$	11,97 days	0,423	0,45 (3)	3,0 (2)
$^{134}_{55}Cs$	2,062 yr	8,724	8,72 (32)	57,4 (21)
$^{137}_{55}Cs + ^{137m}_{56}Ba$	30,18 yr	3,242	3,24 (16)	21,3 (10)
$^{140}_{56}Ba$	12,789 yr	1,095	1,13 (5)	7,44 (33)
$^{140}_{57}La$	40,24 h	11,48	11,6 (5)	76,3 (33)
$^{141}_{58}Ce$	32,50 days	0,433	0,43 (2)	2,8 (1)
$^{144}_{58}Ce + ^{144}_{59}Pr$	284,4 days	0,265	0,27 (2)	1,8 (1)
$^{144}_{59}Pr$	17,28 min	0,141	0,14 (1)	0,92 (6)
$^{152}_{63}Eu$	13,60 yr	6,284	6,5 (5)	43 (3)
$^{170}_{69}Tm$	128,6 days	0,0266	0,0274 (11)	0,180 (7)
$^{192}_{77}Ir$	74,08 days	4,605	4,72 (13)	31,0 (8)
$^{198}_{79}Au$	2,695 days	2,305	2,33 (14)	15,3 (9)
$^{203}_{80}Hg$	46,73 days	1,292	1,29 (8)	8,49 (53)
$^{210}_{84}Po$	138,3763 days	$5,35 \cdot 10^{-5}$	$5,5\ (3)\ 10^{-5}$	$3,6\ (2)\ 10^{-4}$
$^{226}_{88}Ra$*[6]	1600 yr	9,031	—	59,4
$^{226}_{88}Ra$*[7]	1600 yr	8,4	—	55,3

*[1] In parentheses is the error of the given value in the last significant figure (last significant figures) for a confidence coefficient of 0.68. For example, 4.61(27) means 4.61 ± 0.27 with a confidence coefficient of 0.68.

*[2] The values of [15] were cited from the reference book [13] with correction: photons of energy up to 30 keV have not been taken into account and the value of the energy equivalent W of the roentgen has been taken to be 87.3 erg/g·R [in [13] W = 87.7 erg/g·R].

*[3] The calculations were performed for photons of energy higher than 30 keV and W was assumed to be 87.7 erg/g·R.

*[4] The kerma-constant was calculated by multiplying the γ-ray constant from [14] by 6.55 with a correction for W = 87.3 erg/g·R.

*[5] The value corresponds to out-dated data about the decay scheme.

*[6] $^{226}_{88}Ra$ in equilibrium with the principal daughter products of decay to RaD without a filter.

*[7] $^{226}_{88}Ra$ in equilibrium with the principal daughter products of decay to RaD with an initial platinum filter of thickness of 0.5 mm.

Since K_e and m are different physical quantities, the last equality should be understood arbitrarily as meaning that K_e corresponds to 2.04 m.

In conclusion, taking the above into account we shall write formulas for the calculation of different dose characteristics of a radiation field, using the kerma-constant and kerma-equivalent.

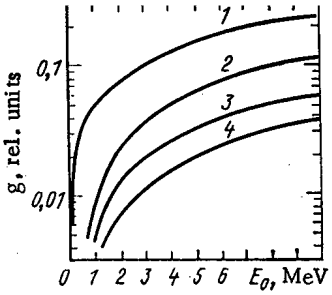

Fig. 2. Dependence of g on the photon energy for different media (plotted from the data of [17] and [18]): 1) lead (Z = 82); 2) iron (Z = 26); 3) aluminum (Z = 13); 4) air (Z_{eff} = 7.54).

For an isotropic point radionuclide source of activity A [Bq] with kerma-equivalent K_e [nGy·m²/sec] and kerma-constant Γ_δ [aGy·m²/sec·Bq] the dose characteristics of the field at a distance r [m] from the source can be calculated from the following formulas:

$\dot{K} = A\Gamma_\delta/r^2$ for the air kerma rate, in attograys per second;

$\dot{K} = K_e/r^2$ for the air kerma rate, in nanograys per second;

$\dot{D} \approx \dot{K}$ for the adsorbed dose rate in air;

$\dot{H} = 1.09\ \dot{D} \approx 1.09\ \dot{K}$ for the equivalent dose rate.

The last two formulas for $\dot{D}$ and $\dot{H}$ are valid if the condition of electron equilibrium is fulfilled. In these formulas the sign ≈ means that the equality is valid for g = 0; the value 1.09 corresponds to the ratio of μ_{en} for biological tissue (water) and air, which is equal to 1.09 ± 0.03 [20] over the wide range of energies from 0.04 to 15 MeV.

The dose field of an isotropic volume source is calculated as the superposition of the fields of isotropic point sources with allowance for self-absorption, possible attenuation of radiation in the environment of the source, and multiple scattering, using the well-known methods [16].

LITERATURE CITED

1. All-Union State Standard (GOST) 8.417-81 (COMECON Standard (ST SÉV) 1052-78). State System for the Supervision of Units of Measurement (GSI). Units of Physical Quantities [in Russian], Standartov, Moscow (1981).
2. COMECON Standard (ST SÉV) 1052-78. Metrology. Units of Physical Quantities [in Russian], COMECON and Standartov, Moscow (1980).
3. Methodological Instructions. Introduction and Applications of COMECON Standard (ST SÉV) 1052-78. "Metrology. Units of Physical Quantities," RD 50-160-79 [in Russian], Standartov, Moscow (1979).
4. É. M. Tsenter, At. Energ., 31, No. 1, 74 (1971).
5. Yu. I. Bregadze, B. M. Isaev, and P. F. Maslyaev, Izmer. Tekh., No. 8, 65 (1979).
6. N. G. Gusev and V. P. Mashkovich, At. Energ., 49, No. 5, 330 (1980).
7. B. M. Isaev and É. M. Tsenter, Izmer. Tekh., No. 9, 60 (1980).
8. V. V. Bochkarev, I. B. Keirim-Markus, and U. Ya. Margulis, At. Energ., 55, No. 1, 53 (1983).
9. Yu. I. Bregadze, B. M. Isaev, and P. F. Maslyaev, Izmer. Tekh., No. 8, 59 (1984).
10. N. G. Gusev, Handbook of Radioactive Radiations and Protection [in Russian], Medgiz, Moscow (1956).
11. N. G. Gusev, V. P. Mashkovich, and G. V. Obvintsev, Gamma-Radiation of Radioactive Isotopes and Fission Products [in Russian], Fizmatgiz, Moscow (1958).
12. N. G. Gusev, V. P. Mashkovich, and B. V. Verbitskii, Radioactive Isotopes as Gamma Emitters [in Russian], Atomizdat, Moscow (1964).
13. N. G. Gusev and P. P. Dmitriev, Quantum Radiation of Radioactive Isotopes [in Russian], Atomizdat, Moscow (1977).
14. Yu. V. Khol'nov, V. P. Chehev, Sh. V. Kamynov, et al., Characteristics of the Radiation of Radioactive Nuclides Applied in the National Economy. Estimated Data [in Russian], Atomizdat, Moscow (1980).

15. V. P. Mashkovich, Protection from Ionizing Radiation [in Russian], Énergoatomizdat, Moscow (1982).
16. Yu. G. Gusev, V. P. Mashkovich, and A. P. Suvorov, Protection from Ionizing Radiation. Vol. I. Physical Foundations of Radiation Protection [in Russian], Atomizdat, Moscow (1980).
17. Methodological Instructions. Introduction and Application of All-Union State Standard (GOST) 8.417-81 "State System for the Supervision of Units of Measurement (GSI). Units of Physical Quantities" in the Field of Ionizing Radiations. RD 50-454-84 [in Russian], Standartov, Moscow (1984).
18. J. Hubbel, Photon Cross Sections, Attenuation Coefficients, and Energy Absorption Coefficients from 10 keV to 100 GeV. National Standard Reference Data Series, NBS, No. 29, U.S. Government Printing Office, Washington, D.C., 20402 (1969).
19. J. Hubbell, Radiat. Res., 70, 58 (1977).
20. H. Penkuhn, ESIS Newsletter, No. 38-39, July-October (1981), p. 5.

ANALYSIS OF THE SENSITIVITY OF A MODEL OF TERRESTRIAL FOOD CHAINS

V. Ganushik, A. Mitro,
T. Sabova, and O. Musatova

UDC 614.876

In any section of the nuclear fuel cycle, it is possible for radionuclides to enter the environment. In an estimate of the radioecological consequences of this process, mathematical modeling occupies an important place. The common feature of these models is the computation of the transport of radionuclides into the atmosphere and the hydrosphere and also through food chains [1].

The purpose of the present paper is to estimate, by means of a sensitivity analysis, the importance of the individual parameters of the model for terrestrial food chains, which was recommended by the Permanent Commission of CMEA for the Peaceful Utilization of Atomic Energy [2]. This method creates the basis for the calculation of the numerical values of the buildup factors of radionuclides in the chain deposited from the atmosphere – the content in food products (see [1]).

Method of Sensitivity Analysis

By the analysis of sensitivity, using analytical or statistical approximation, usually is understood the study of the interaction between the information introduced into the model and the answer obtained. In the present paper, the authors have used a numerical nonstatistical approximation, increasing or decreasing the value of the input parameter by a few percent of the nominal value and keeping the other parameters constant [3]. The numerical value obtained for the coefficient of sensitivity is a measure of the sensitivity of the result to changes of value of the input parameters. The calculations were performed in the Institute of Radioecology and the Utilization of Nuclear Technology, Czechoslovakia.

It is easy to show that with a change of value of the input parameter by p %, the coefficient of sensitivity S_1 is expressed by the relation

$$S_1 = \frac{50}{p} \frac{Y_2 - Y_1}{Y_0},$$

where Y_0 is the value of the output parameter (in this case, the equivalent dose) for a nominal value of the input parameter; Y_1 (Y_2) is the value of the output parameter for an increase (decrease) of the nominal value of the input parameter by p %.

The coefficient of sensitivity (CS) can acquire a positive or a negative value. With a zero value, this parameter does not enter into the expression for the equivalent dose. With a negative CS, an increase of the value of the input parameter involves a decrease of the

Institute of Radioecology and Utilization of Nuclear Technology, Czechoslovakia. Translated from Atomnaya Énergiya, Vol. 58, No. 4, pp. 265-268, April, 1985. Original article submitted July 30, 1984.

 0038-531X/85/5804-0304$09.50

TABLE 1. Average Values of CS, Calculated for Direct Contamination and for a Change of the Nominal Value of the Parameter by 30%

Average CS value	Parameter
10^{-5} — 10^{-4}	(29), (31)
10^{-4} — 10^{-3}	(22), (27), (28)
10^{-3} — 10^{-2}	(14), (16), (17), (21), (23), (24), (26), (33), (35), (36), (46), (48), (49), (53), (55), (56), (64), (67), (68)
10^{-2} — 10^{-1}	(15), (25), (31), (34), (47), (54), (60)
0,1 — 0,2	(18), (20), (37), (50), (57)
0,25 — 0,3	(4), (5), (13), (65), (72)
0,342	(32), (45), (52)
0,361	(3), (69)
0,446	(19), (51), (58), (59)
1	(6), (73)

Note. Here and in Table 2 for brevity, for parameters with low CS values, the range is given in which is found the CS value of the corresponding parameter.

value of the output parameter. With a positive CS, an increase of the value of the input parameter leads to an increase of the value of the output parameter.

If the CS is used as an indication of changes of the output parameter with changes of the input parameter for a given set of radionuclides, it is more convenient to use the absolute value of the CS, $S = |S_1|$.

Application of the Method

The ORB-11 model [2] was suggested for describing the transportation of radioactive substances through food chains. In terrestrial food chains, the direct contamination of crops and grasses by the deposition of radionuclides on the stem parts and the indirect contamination in consequence of the absorption of radionuclides from the soil should be different. For this seven principal food products are considered: wheat, fruits, cucumbers, cabbage, potato, milk, and meat.

In forming the set of radionuclides, the authors were influenced by the requirement to collect for each radionuclide the necessary number of nominal values of the parameters. ^{3}H and ^{14}C were not analyzed, as the model being studied is unsuitable for them. Thus, a set was formed including 22 radionuclides: ^{51}Cr, ^{54}Mn, ^{55}Fe, ^{59}Fe, ^{58}Co, ^{60}Co, ^{63}Ni, ^{65}Zn, ^{95}Zr, ^{95}Nb, ^{103}Ru, ^{106}Ru, ^{110}Ag, ^{131}I, ^{134}Cs, ^{137}Cs, ^{141}Ce, ^{144}Ce, ^{144}Pr, ^{147}Nd, ^{147}Pm, and ^{238}Pu.

The content of each of the 22 radionuclides in air was assumed equal to 1 Bq/m^3, the velocity of dry settling 10^{-2} m/sec. The nominal values of 73 parameters were chosen in accordance with the recommendations of ORB-11 [2]. The list and index numbers of the parameters studied are given below.

Because of the lack of data, the authors for all parameters used a uniform separation of the values and an identical variability interval, i.e., an increase or decrease of the parameter by 30% of the nominal value was assumed. For the purpose of distinguishing linear and nonlinear parameters, the values of CS were computed also for a change by 90%. The linearity is characterized by an identical value of CS for these changes, and the nonlinearity by nonidentical values of CS.

Method of Calculation

The CS was computed for each input parameter, radionuclide, contamination route, and given change of input parameter, by formula (1). The average value of the CS, standard deviation and coefficient of variation were calculated for the set of radionuclides formed. The calculations were performed on the ADT 4300 computer. For simplicity, the parameters are denoted in the text and in Tables 1 and 2 by figures. The following symbols are used:

coefficients of transfer: soil—plant (2), fodder—milk (3), fodder—meat (4);

TABLE 2. Average CS value, calculated for Indirect Contamination and for a Change of the Nominal Value of the Parameter by 30%

Average CS value	Parameter
10^{-5}—10^{-3}	(27), (29), (30)
10^{-3}—10^{-2}	(10), (14), (16), (21), (22), (23), (26), (28), (64), (66), (67), (68)
10^{-2}—10^{-1}	(8), (11), (12), (13), (15), (17), (18), (24), (25), (31), (33), (35), (39), (41), (53), (55), (60)
0,1—0,2	(5), (20), (34), (36), (37), (40), (42), (43), (54), (56), (57), (61), (65), (72)
0,219	(7)
0,242	(44), (58), (59)
0,247	(3), (69)
0,286	(32), (38), (44), (59)
0,326	(9)
1	(2), (6), (73)
1,098	(62), (63)

effective time of removal of radionuclide from organism (5);

effective equivalent dose (6);

time interval between spring plowing and gathering of the harvest of wheat (7), fruits (8), cucumbers (9), cabbage (10), potato (11), perennial grasses (12);

time of growth of productive parts of the wheat (13), fruits (14), cucumbers (15), cabbage (16), potato (17), perennial (18), and pasture grasses (19);

duration of consumption of the products and fodders of a single crop of wheat (20), fruits (21), cucumbers (22), cabbage (23), potato (24), and perennial grasses (25);

time of initial delay from the instant of collection of the crop to the start of consumption of wheat (26), fruits (27), cucumbers (28), cabbage (29), potato (30), perennial grasses (31);

productivity of cultures of wheat (32), fruits (33), cucumbers (34), cabbage (35), potato (36), perennial grasses (37);

fraction of radionuclide fallen with precipitation, which is deposited on the surface of the soil for wheat (38), fruits (39), cucumbers (40), cabbage (41), potato (42), perennial (43) and pasture grasses (44);

coefficient of primary retention in the productive parts of wheat (46), fruits (46), cucumbers (47), cabbage (48), potato (49), perennial (50) and pasture grasses (51);

area of land per single person: wheat (52), fruits (53), cucumbers (54), cabbage (55), potato (56), perennial (57) and pasture grasses (58);

average density of grass cover of pastureland (raw weight) (59);

constant "field" losses in grass, in consequence of spoiling by cattle (60);

constant "metabolic" removal of nuclides from the root layer of soil (61);

depth of ploughing (62) and density of soil (63);

duration of life of dairy cow (64) and of beef oxen (65);

time interval between two milkings of cows (66);

time interval between milking and consumption of the milk (67);

time interval from the instant of slaughter of the animal to consumption of the meat (68);

average milk yield of cows (69);

consumption by humans of milk (70) and meat (71);

mass of beef oxen at instant of slaughter (72);

rate of dry deposition of radionuclides from air (73).

Results

Direct Contamination. The high values of the standard deviation and the coefficient of variation confirm that for the majority of the 53 parameters of this path of contamination, the CS are specific for each nuclide. The latter is not related to the effective equivalent dose (6) and the rate of dry deposition (73). Both these parameters are characterized also by the highest CS values, independently of the value of the change.

Among the parameters of direct contamination, only parameters (5), (13), (14), (15), (16), (17), (18), (20), (21), (22), (23), (24), (25), (26), (27), (28), (29), (30), (31), (60), (64), (65), (66), (67), and (68) do not exhibit a linear dependence of the output on the input value. Of these parameters, only parameter (31) is characterized by an increase of sensitivity with a reduction of the value of the percentage change. The average values of the CS, based on a 30% change of the nominal values of the parameters, are given in Table 1.

Indirect Contamination. In the 62 parameters characterizing this path of contamination, only the transfer coefficient soil–plant (2), the effective dose (6), rate of dry deposition of the radionuclide (73), depth of ploughing (62), and soil density (63) possess CS values nonspecific for a given radionuclide. These parameters are characterized also by the highest CS values. It is true, the CS value depends on the value of the percentage change only for parameters (2), (6), and (73).

A nonlinear dependence of the output on the input is observed for parameters (5), (7)-(18), (20)-(31), and (60)-(68). At the same time, only for parameters (24) and (67) is an increase of the percentage change accompanied by a decrease of the CS. The average CS, based on a 30% change of the nominal values of the parameter, are given in Table 2.

Discussion of Results

The use of sensitivity analysis allowed the relative importance of the parameters to be determined for the set of radionuclides being studied and the model of contamination used. The data obtained can be used for a stochastic approach to the modeling of the transportation of radioactive substances through the food chains, and to the planning of radioecological investigations.

The sensitivity obtained for the parameters is specially important in that high values of the CS are nonspecific for radionuclides and for the majority of them they are independent of the percentage change. Contamination, which is the input parameter of separate paths of exposure, has no effect on the average CS values, within the limits of the exposure path.

The method used has several drawbacks. In the first place, it includes ignorance of the variability of the input parameters and their nonlinearity. In the more general case, the correlation and simultaneous change of all parameters should be taken into consideration. These questions will become the subject of future investigations.

Our knowledge about the variability of the parameters of the ORB-11 model is deficient. It is known that the transfer coefficients differ with a large variability (this is not related to the variability of all parameters). Nonlinearity of the parameters also can make difficult the interpretation of the results obtained by us. In general, the CS depends on the percentage change, which is not identically representative for all parameters. The choice of the percentage change can lead to an overestimation of sensitivity for some, and to an underestimate for other parameters.

For the purpose of determining for what parameters the CS changes sharply with increase of the percentage change, its calculation was repeated for a change of the nominal value of the parameter by ±99.99%. In the case of direct contamination, the value of the CS of parameters (13)-(19) is increased, but not exceeding however the values of the parameters (6) and (73). The CS of the other parameters remains constant or varies only insignificantly.

A change of the nominal value of the parameter by 99.99% is accompanied for the depth of ploughing (62) and the soil density (63) by a sharp increase of the CS up to 4899.25, which significantly exceeds the value of the CS for parameters (2) and (6). The CS for parameters

(62) and (63), as a function of the percentage change, at the point p = 100% possesses a point singularity (+∞). This explains the sharp increase of the value of parameters (62) and (63) for p = 99.99%. Among the remaining parameters of indirect contamination, one should recall also parameters (13)-(19), for which CS = 19.08. The CS for the remaining parameters is unchanged or changes insignificantly.

It must be mentioned that for the parameters with a sharp change of CS, a high variability of their values is not expected. In realistic cases, when the quantity of the individual radionuclides ejected is known, the calculation of the suspended CS is more appropriate.

In conclusion, the authors have great pleasure in thanking D. Khorvat and M. Shtubnya for valuable advice and comments.

LITERATURE CITED

1. Methods of Calculation of the Distribution of Radioactive Substances from Nuclear Power Stations and the Irradiation of the Surrounding Population, Interatoménergo, Second Project of NTD on the theme 38.220.56-81 [in Russian], Moscow (1983).
2. Model for Determining Dosage Loadings, Taking Account of the Migration of Radionuclides and Their Entry into Food Chains, Series ORB-11 [in Russian], CMEA, Moscow (1980).
3. R. Zach, Sensitivity Analysis of the Terrestrial Food Chain Model FOOD III, Pinawa, Manitoba (1980).

STOPPING POWER OF MATTER IN SELF-SIMILAR REPRESENTATION

S. A. Gerasimov

UDC 539.12.04

The Thomas–Fermi statistical atomic model has an important self-similarity characteristic: The atomic number Z appears in any physical relationship only in the form of the combinations [1]

$$rZ^{1/3},\ EZ^{-4/3},\ pZ^{-2/3}, \tag{1}$$

where r is the length, E is the particle energy, and p is the momentum. This means that the Thomas–Fermi model has universal application in a wide range of problems: The calculation results pertain directly to all atoms, and transition from one chemical element to another is achieved by simple scale transformation.

Using combinations (1), we can show that the differential ionization cross section σ with respect to the energy ΔE transmitted to the atom by a heavy charged particle appears in the corresponding relationships in the form of the combination $Z^3\, d\sigma/d\,\Delta E$. This, in turn, means that the ionization stopping cross section $\varepsilon(T) = dT/n_0\, dx$ must correspond to the $Z^{1/3}\varepsilon(T)$ combination. Here, n_0 is the number of atoms of the material per cubic centimeter, T is the kinetic energy of a particle with the charge $Z_1 e$, and e is the electron charge. The $TZ^{-4/3}$ term determining the kinetic energy of particles is replaced by the dimensionless variable

$$t=\frac{b}{e^2Z^{4/3}}\frac{m}{m_1}T, \tag{2}$$

where $b = 1/2(3\pi/4)^{2/3}\hbar^2/me^2$; and m and m_1 are the electron mass and the mass of the oncoming particle, respectively. We also consider that for simple particles (protons, nuclei), the energy loss must be proportinal to the square of the charge Z_1^2. Under these conditions, the self-similar relationship between the stopping cross section and the velocity ($t \sim v^2$) of a particle is given by

$$\frac{1}{n_0}\frac{Z^{1/3}}{Z_1^2}\frac{dT}{dx}=F(t), \tag{3}$$

where F is a certain function.

Without performing complex calculations, and using only experimental data on the energy loss by protons in matter [2], we shall prove the validity of the self-similar representation [3] and determine its scope of applicability. From among all the experimental data available, we choose elements with relatively large atomic numbers Z ($20 \leq Z < 80$), for which the energy dependence of the stopping cross section has been investigated fairly thoroughly. The first of these conditions is connected with the fact that the Thomas–Fermi statistical model holds only for atoms with large Z values.

The relationship [3] derived on the basis of experimental data is shown in Fig. 1. This in itself proves the validity of representation (3), at least for the range $t > 0.1$. Let us examine more closely the range $t < 0.1$, where the deviation from self-similarity is considerable. We note that the deviation amplitude is equal to ~2, and we consider the fluctuations in the behavior of dT/dx with changes in the atomic number of the moderating medium [4]. These fluctuations are most strongly pronounced in the low-energy range and, thus, for small values of t. However, the fluctuation amplitude is approximately the same as the deviation amplitude. The cause of fluctuations in the behavior of dT/dx is evidently connected with the periodicity of the atomic properties with respect to Z, which, naturally, are not taken into account within the framework of the Thomas–Fermi model. Therefore, application of the statistical model in the $t < 0.1$ range is advisable only in providing estimates.

The described representation differs from those already known [5], and it can be used as a physical basis for approximating experimental data. For this, however, it is necessary

Translated from Atomnaya Énergiya, Vol. 58, No. 4, p. 269, April, 1985. Original article submitted October 4, 1983.

0038-531X/85/5804-0309$09.50

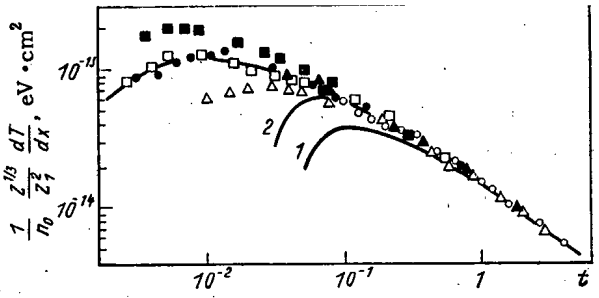

Fig. 1. Self-similar energy dependence of the stopping cross section for a charged particle. 1, 2) Calculation based on the Bethe–Bloch equation [3] for Z = 20 and Z = 79, respectively; o) Ca; Δ) Cu; •) Kr; ▲) Ag; ■) Xe; □) Au.

to use all the available experimental data, rather than a narrow selection of elements, as was done here.

In conclusion, the author extends his deep gratitude to V. F. Volkov for the useful dicussion.

LITERATURE CITED

1. D. A. Kirzhnits, Yu. E. Lozovik, and G. V. Shpatakovskaya, "Statistical model of matter," Usp. Fiz. Nauk, 117, No. 1, 3-47 (1975).
2. G. N. Potetyunko, "Experimental data on the energy loss and the range of hydrogen ions in materials," Izv. Vyssh. Uchebn. Zaved., Fiz., No. 9, 123-124 (1979) (Reg. No. 2058-79 Dep.).
3. S. V. Starodubtsev and A. M. Romanov, Passage of Charged Particles through Matter [in Russian], Izd. Akad. Nauk Uzbek SSR, Tashkent (1962).
4. Yu. V. Gott, Interaction between Particles and Matter in Plasma Investigations [in Russian], Atomizdat, Moscow (1978).
5. Yu. V. Gott and Yu. N. Yavlinskii, Interaction between Slow Particles and Matter in Plasma Diagnostics [in Russian], Atomizdat, Moscow (1973).

METHOD OF CALCULATING THE STOPPING CROSS SECTION OF NUCLEAR PARTICLES IN MATTER

V. F. Volkov and S. A. Gerasimov

UDC 539.12.04

The passage of fast neutrons, α particles, or atomic nuclei through matter is accompanied by their energy loss caused mainly by ionization moderation. One of the most efficient methods describing the atomic ionization of a heavy charged particle is the binary collision approximation [1, 2], which has been developed in [3-5] for calculating the stopping power of matter. In contrast to the well-known simple methods [6], the binary collision model describes correctly the ionization energy loss in both the low and the high energy ranges of the oncoming particles. The ionization moderation of a charged particle in matter is characterized quantitatively by the parameter dT/dx, which represents the mean energy loss per unit path. In the binary collision model, this quantity is determined by the expression

$$\frac{1}{n_0}\frac{dT}{dx}=\sum_i N_i \int_{\Delta E_t} \Delta E_t \int_0^\infty f(v_2)\,\sigma_{i\Delta E}(v_1, v_2)\,dv_2\,d\Delta E, \qquad (1)$$

where n_0 is the number of atoms of the material per cubic centimeter, $f(v_2)$ is the distribution function of atomic electrons with respect to velocities v_2, defined by the square of the modulus of the electron's wave function in the momentum representation, $\sigma_{i\Delta E}$ is the differen-

Translated from Atomnaya Énergiya, Vol. 58, No. 4, pp. 270-271, April, 1985. Original article submitted March 15, 1984.

 0038-531X/85/5804-0310$09.50

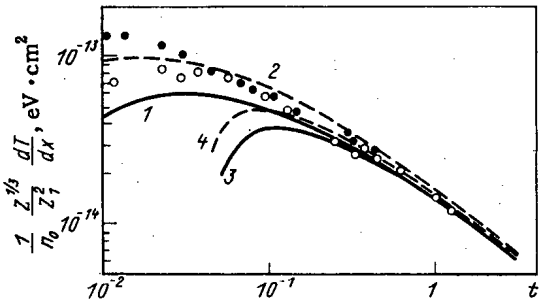

Fig. 1. Energy dependence of the ionization stopping cross section of protons. 1, 2) Our results; 3, 4) calculation based on the Bethe–Bloch equation for Ar (o) and Kr (•) atoms, respectively.

tial energy transfer ΔE_i cross section [2], v_1 is the velocity of the oncoming particle, and T is its energy. Summation in expression (1) is performed with respect to all the electron states i in the target atom.

This procedure of calculating dT/dx for atoms with a large number of electron states evidently involves many difficulties. Therefore, it is perfectly reasonable to raise the question of utilizing the statistical atomic model and its modifications in performing such calculations. We shall subsequently consider an electron gas consisting of bound electrons. We assume that the number of energy states of the electron gas is sufficiently large, so that a continuous electron energy spectrum can be substituted for the discrete energy spectrum. Assume that $f(E, v_2)$ is the function of energy and velocity distribution of electrons. If the motion of gas electrons is quasiclassical, as the statistical atomic model assumes, the energy and velocity dependence of the distribution function $f(E, v_2)$ is given by $f(E, v_2) = v_2^2 F(E - mv_2^2/2)$, where F(y) is a certain function. The function $f(E, v_2)$ must be normalized with respect to the total number of electrons Z in the atom. Therefore, with the substitution of variables $b = (3\pi/4)^{2/3}\hbar^2/2me^2$, $\varkappa = b/(e^2Z^{4/3})$, $k^2 = \varkappa mv_2^2/2$, $\varepsilon = -E\varkappa$, and $u = k^2 + \varepsilon$, we write the function $f(E, v_2)$, normalized with respect to the total number of electrons in the atom, in the following form:

$$f(E, v_2) = -\frac{1}{16}\left(\frac{3\pi}{4}\right)^{5/3}\frac{\hbar^5}{me^{10}Z^{7/3}}\frac{dg^3(u)}{du}v_2^2. \tag{2}$$

Here, m is the electron mass, e is the charge, and g(u) is a certain function of the variable u. The minus sign in (2) is due to the negative value of the derivative dg/du. It is assumed here that the distribution function (2) is defined for all $\varepsilon_m \leq \varepsilon < \infty$ and $0 \leq k < \infty$, where $\varepsilon_m = -E_m\varkappa$ and E_m is the maximum energy of atomic electrons. Beyond this region, $f(E, v_2)$ is assumed to vanish.

We use expression (1) to determine dT/dx, in which summation with respect to all electron states is replaced by integration with respect to the energy E, and we find the function of energy and velocity distribution of atomic electrons from Eq. (2):

$$\frac{1}{n_0}\frac{dT}{dx} = \int_{-\infty}^{E_m}\int_{-E}^{\infty}\int_{0}^{\infty}\Delta E\sigma_{\Delta E}(v_1, v_2) f(E, v_2)\, dv_2\, d\Delta E\, dE. \tag{3}$$

The function $\sigma_{\Delta E}(v_1, v_2)$ does not depend on the integration variable in the outer integral [2], so that, by changing the order of integration in expression (3) and calculating the inner integral with respect to E, we find

$$\frac{1}{n_0}\frac{dT}{dx} = \frac{3\pi}{32}\frac{\hbar^3}{e^6Z}\int_{-E_m}^{\infty}\int_{0}^{\infty}\Delta E\sigma_{\Delta E}(v_1, v_2)\left[g^3(k^2+\varepsilon_m) - g^3(k^2+\varkappa\Delta E)\right]v_2^3\, dv_2\, d\Delta E. \tag{4}$$

If the function g(u) has been found, the advantages of the described method of calculating dT/dx are obvious. The main difficulty now consists in determining the function g(u). There are several methods for describing it. One of them is the Thomas–Fermi model [7]. In this model, the function g(u) represents nothing but the solutions y = g(u) of the equation $u = \chi(y)/y$, where $\chi(y)$ is the universal function of the Thomas–Fermi model. However, analysis shows that this method does not yield satisfactory results in calculating dT/dx throughout the entire range of oncoming particles. This is connected with the fact

that the peripheral electrons in the Thomas–Fermi model have very small, or even zero, values of the energy ε.

Let us consider another, special method of determining the g(u) function, which is based on experimental data pertaining to the Compton x-ray profiles of free and bound atoms. This method can be used in investigating the ionization stopping of nuclear particles by crystalline solids for which the Compton profiles have been measured with a high degree of accuracy, while the energy loss description by the binary collision approximation (1) involves great difficulties.

Assume that J(q) is the Compton profile of the target element [8]. We introduce the notation $Q = qZ^{-2/3}(b/2me^2)^{1/2}$; $C(Q) = J(q)Z^{-1/3}(2me^2/b)^{1/2}$. Then, the generalized Compton profile C(Q) in the statistical atomic model is written as the integral

$$C(Q)=\frac{1}{2}\int_{Q}^{\infty} g^3(k^2+\varepsilon_m)\,kdk. \tag{5}$$

Hence

$$g^3(u)=-\frac{2}{\sqrt{u-\varepsilon_m}}\left.\frac{dC(Q)}{dQ}\right|_{Q=\sqrt{u-\varepsilon_m}} \tag{6}$$

while, for Ar and Kr atoms [9], the function g(u) can be written approximately in the following form:

$$g^3(u)=\frac{10B}{[A+B(u-\varepsilon_m)]^{7/2}}+\frac{4H+64(u-\varepsilon_m)}{[D+H(u-\varepsilon_m)+8(u-\varepsilon_m)^2]^2}, \tag{7}$$

where the coefficients A, B, D, and H, besides the traditional accuracy requirements in describing experimental data, must satisfy the condition for normalization of the Compton profile and the distribution function (2): A = 0.79; B = 70.7934; D = 0.77714; H = 17.8283. In this representation, expression (5) for the generalized Compton profile is self-similar: Simple scale transformation is used to calculate I(q) for any other atom in the first aprpoximation. This means that the g(u) function found in such a manner is applicable at least to all atoms with $18 \le Z \le 36$.

Figure 1 shows the results obtained in calculating dT/dx by means of expressions (4) and (7) for Ar and Kr target atoms as dependences of $(Z^{1/3}/n_0Z_1^2)dT/dx$ on $t = bmT/(e^2/Z^{4/3}m_1)$, which are compared with experimental data [10]. For large values of t, the results obtained by means of the described method are close to those provided by the Bethe–Bloch theory [6], while, for small and intermediate reduced energy values t, the theoretical stopping cross sections are close to their actual values. All this supports the validity of our model of ionization stopping of nuclear particles in matter. The proposed method is different from those already known and can be used for solving a number of problems in investigating the ionization stopping of heavy charged particles by matter.

LITERATURE CITED

1. E. Gerjuoy, Phys. Rev., 148, No. 1, 54 (1966).
2. F. F. Komarov and A. P. Novikov, Zh. Tekh. Fiz., 48, No. 7, 1449 (1978).
3. J. Harberger, R. Johnson, and J. Boring, Phys. Rev., 9A, No. 3, 1161 (1974).
4. M. Newton, L. Lucas, and J. Root, Chem. Phys. Lett., 34, No. 3, 552 (1975).
5. R. Johnson and A. Gooray, Phys. Rev., 16A, No. 4, 1432 (1977).
6. Yu. V. Gott, Interaction between Particles and Matter in Plasma Investigations [in Russian], Atomizdat, Moscow (1978).
7. P. Gombas, Statistical Atomic Theory and Its Application [Russian translation], IL, Moscow (1951).
8. C. Coulson and N. March, Proc. Phys. Soc., London, Sect. A, 63, No. 4, 367 (1950).
9. P. Eisenberger and W. Reed, Phys. Rev., 5A, No. 5, 2085 (1972).
10. G. N. Potetyunko, Izv. Vyssh. Uchebn. Zaved., Fiz., No. 9, 123 (1979) (Reg. No. 2058-79 Dep.).

INFORMATION SYSTEM FOR TWO RBT-10 RESEARCH REACTORS

V. A. Kachalin, A. V. Kiselev,
A. I. Kras'ko, V. G. Kusikov,
Yu. F. Sviridova, and Yu. D. Fedorov

UDC 681.3:681.142.3

The information system considered here is designed to provide simultaneous service in an adviser regime for two RBT-10 pool-type reactors. The system has facilities for automatic acquisition and processing of data about the technological parameters of reactors and some regimes of tests of experimental devices (all told about 250 sensors for temperature, pressure, level, flow rate, etc.). The information system is based on an RPT programmable terminal (manufactured by VIDEOTON, Hungary) which is a functionally improved one-processor minicomputer [1].

Leaving redundancy aside, the system is based on one RPT terminal and consists of a core and two equal subsystems, each of which serves its own reactor. The subsystems function independently of each other, thus necessitating some sort of distribution of equipment between them and organization of the computer operation in a multiprogram time-sharing mode. An exception is the situation in which one of the subsystems has received a higher-priority initiation signal (e.g., a signal of actuation of the scram system). In this case the resources of the computer are automatically assigned to one subsystem in order to record the emergency process as fully as possible.

In the system preference is given to hardware–software solutions which permit the necessary operational changes to be made in the configuration of the system without shutting down the subsystems [2].

With allowance for redundancy the information system is designed with two sets of equipment: a main set, which is sufficient for functioning throughout both subsystems simultaneously, and an auxiliary set, which contains the entire list of devices of the information system, at least one copy of each. The auxiliary set is used to simulate the operating conditions of either subsystem (e.g., during repair–restoration operations) as well as for the development of software and hardware for the information system and as an independent computing complex. Any work done on the auxiliary set, including work involving measurements of the readings of sensors served by the subsystems at that time, does not impede the functioning of the subsystems. When any device of the main set fails, it is replaced promptly by the same type of device from the auxiliary set with the aid of simple commutating gear. This ensures that the system as a whole has a high degree of readiness and is fail-safe.

Figure 1 shows the hardware of the information system. The normalizing converters allow each sensor to be connected independently to two measuring channels of the first and second sets of equipment. The permanent part of each set contains a computer and an RT peripheral interface (manufactured by VIDEOTON, Hungary), the number of whose measuring inputs has been increased by the additional connection of two 100-channel F799/1 commutators of measuring signals. Special designs have been developed for the interfaces (PI) between the RT and the F799/1, the signal panels (P 1, P 2), and the commutator for the devices. The signal panel informs the operator about the state of the subsystem by means of transparencies and acoustic signals. The device commutator makes it possible to divide three VT-340 displays (OD 1, OD 2, ED) (manufactured by VIDEOTON, Hungary), two operator's panels, and two DZM-180 alphanumeric printers (ANP 1, ANP 2) (made in Poland) between the two computers. In Fig. 1 the device commutator is shown arbitrarily in a state in which the main set of equipment of the information system is based on computer Cp 1. The printer ANP 1 is used to keep a record of the operation of both subsystems, while ANP 2 and one of the displays (ED) are connected to the auxiliary set based on Cp 2.

Each subsystem can operate in three modes: Dialog, Analysis, and Archives.

Translated from Atomnaya Énergiya, Vol. 58, No. 4, pp. 271-272, April, 1985. Original article submitted June 1, 1984.

0038-531X/85/5804-0313$09.50

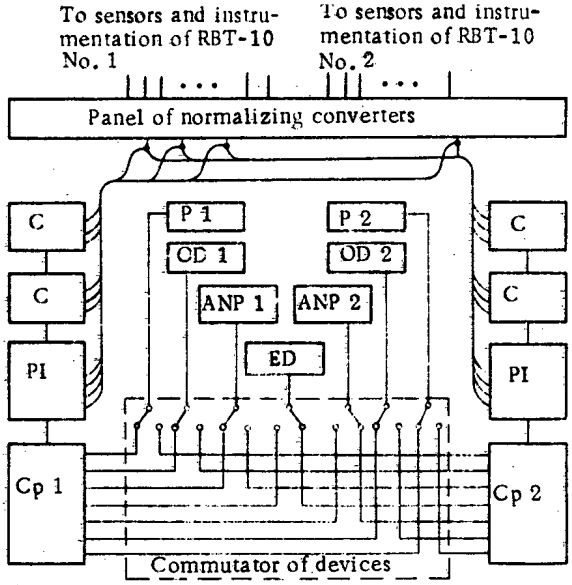

Fig. 1. Block diagram of the apparatus of the information system: OD 1 and OD 2 are the operator displays of the first and second subsystems, respectively; ED is the engineer's display; P 1 and P 2 are the signal panels of the first and second subsystems, respectively; ANP 1 and ANP 2 are the alphanumeric printers of the main and auxiliary sets, respectively; C are the measuring-signal commutators; PI is a peripheral interface.

In the Dialog mode two-way communication between the reactor operator and the subsystem is possible with the aid of displays OD 1 and OD 2. Using the list of services shown on the screen, the operator controls the operation of the subsystem: he connects or disconnects individual sensors or groups of sensors, he changes the control settings, the normalizing factors, and gains, indicates the parameters to be monitored by continuous or periodic readout on the display or printer, and so forth.

In the Analysis mode all the functions of the Dialog mode are retained and the following operations are performed:

- periodic (every 5 sec) measurement of the indications of the sensors in the subsystem;
- calculation of individual physical quantities (thermal power of the reactor, temperature drop, etc.) and readout on the operator display;
- monitoring, on the basis of the settings and the operator display readout, of the nominal and running values of the physical quantities when they deviate from the settings, including the switching on of acoustic signals and a transparency on the signal panel;
- readout on the operator display of the running values of arbitrarily selected parameters (no more than five);
- periodic (every one or three hours) printout of some calculated and measured values with notation of the calendar time;
- diagnostics of the operation of the information system.

The subsystem goes into the Archives mode automatically when the scram system is actuated in either reactor. In this case the appropriate acoustic and light signals are switched on, the readings of the sensors in the subsystem are recorded until the 8K memory is filled, and recording of the Dialog and Analysis modes in both subsystems is suspended for the entire time.

The special software of the information system plus the standard RPS operational system occupy 32K out of the total 64K capacity of the memory.

The first trial use of the information system has confirmed that the architectural concepts adopted are correct and that the system has a high degree of operational and functional reliability. The simplicity of dialog by the user coupled with prompt and clear presentation

of information make the system an accessible and effective means of monitoring the operating regimes of reactors and experimental facilities.

LITERATURE CITED

1. E. Sharkesi and I. Groth, Prib. Sistemy Upr., 8, 3 (1980).
2. V. A. Kachalin et al., Preprint NIIAR-1(613), Scientific-Research Institute for Nuclear Reactors, Dimitrovgrad (1984).

METHOD FOR REPROCESSING LIQUID RADIOACTIVE WASTES, COMBINING SELECTIVE COMPLEXING AND ULTRAFILTRATION

V. A. Kichik, G. A. Yagodin,
N. F. Kuleshov, and A. A. Svittsov

UDC 66.023.067.38.278:532.711

The methods used in practice for reprocessing liquid radioactive wastes are closely linked to the maximum desalination of aqueous solutions. Radiochemically pure water can apparently be obtained only by removing the salt component and the radionuclides contained in it.

We have proposed a fundamentally new approach to the problem of reprocessing liquid radioactive wastes, based on the idea of selective extraction of radioactive elements from the solutions. This is solved by combining the method of selective binding of the radionuclides with a macromolecular agent and the method of ultrafiltration through a semipermeable membrane: the membrane passes the radionuclide-free permeate, while the components being extracted are held back in the concentrated solution.

The method is, in principle, realizable because of the large number of chemical compounds which selectively react with inorganic ions and which satisfy the following conditions: high binding capacity and selectivity with respect to individual ions; high molecular mass (<10,000), sufficient for complete retention by the ultrafiltration membrane; sharp molecular-mass distribution of molecules; good solubility in water; and low cost and availability.

The spectrum of radionuclides in liquid radioactive wastes is quite wide (^{137}Cs, ^{134}Cs, ^{60}Co, ^{54}Mn, ^{90}Sr, ^{51}Cr, ^{131}I, and others); in addition, the absolute content of each radionuclide is determined by the source of these wastes.

The chemical properties of radionuclides differ substantially, so that the fundamental problem is to select a binding agent for each of them for selective separation from the salt component.

In selecting the binding agents, we started from the following. Transition-metal ions (cobalt, manganese, chromium, iron) have vacant d-electron orbitals and a small ionic radius, i.e., they are typical complexers. To bind them we used water-soluble polymers with amino or carboxyl groups, in particular polyethylenimine-40000 (PEI) and polyacrylic acid-100000 (PAA).

Cesium, which has a weak complexing ability, was transformed into a collidal state using the method in [1] with the help of transition-metal (usually copper) hexacyanoferrates. Iodine was bound in weakly acidic media with the help of starch, with which it forms a well-known complex in which the iodine atoms fill the channels of the amylose polysaccharide [2].

All mentioned complexes are quite stable in weakly acidic, weakly alkaline, and neutral media, which occur in real liquid radioactive wastes.

We performed the ultrafiltration with a membrane apparatus with a capacity of 1 m^3 per day for permeate under a presure of 0.15 MPa with membranes in the form of UPA-50 hollow fibers. We performed the experiments using model solutions of radionuclides, as well as non-industrial liquid radioactive wastes, entering the Moscow station for reprocessing of special discharges, using the following procedure: the pH of the starting solution was corrected to the required value; then we added the binding agent and vigorously mixed the solution, after which we subjected the solution to ultrafiltration. We analyzed the specific activity of γ-

Translated from Atomnaya Énergiya, Vol. 58, No. 4, pp. 272-273, April, 1985. Original article submitted June 7, 1984.

0038-531X/85/5804-0315$09.50

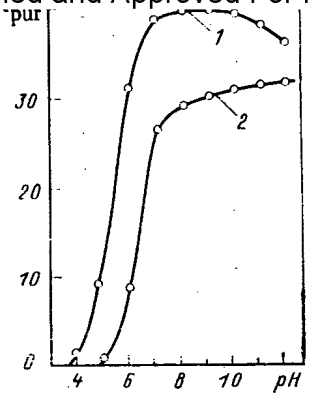

Fig. 1

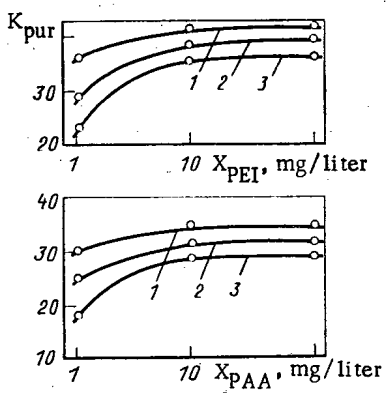

Fig. 2

Fig. 1. Dependence of K_{pur} for ^{60}Co on the pH of the starting solution. The activity of γ-emitting nuclides in the starting solution is $1.85 \cdot 10^5$ Bq/liter; the concentration of the PL is 1 mg/liter (PEI (1) and PAA (2)).

Fig. 2. Dependence of K_{pur} on the concentration of the polymer ligands with the use of different semipermeable membranes: 1) UAM-100; 2) UAM-150; 3) UAM-200.

emitting nuclides in the starting solution, concentrate, and permeate on a NOKIA LP-4900 gamma spectrometer as well as the specific activity of β-emitting nuclides on a TESLA NZR 601 beta analyzer.

We determined the effectiveness of the method with the use of the purification factor (K_{pur}), i.e., the ratio of the values of the specific radioactivity in the starting solution and in the permeate.

The quantity K_{pur} consists of two factors: the coefficient of distribution of radionuclides between the dissolved and bound (on the agent used) states and the degree of retention of the agent by the semipermeable membrane.

The first factor, in its turn, depends on the optimal conditions for performing the chemical reactions. It is therefore important to determine the working range of pH values for the agents used. In this manner we found the optimal pH range for the ^{60}Co–polymer ligand (PL) system (Fig. 1).

The second factor affecting the flow of the chemical reaction is the concentration of the binding agent. Since the mass concentrations of the radionuclides are extremely low, the main problem is to ensure that they combine with the binding agent in the solution. The probability for such compounds to form increases when the concentration of reagents, in this case the binding agent (Fig. 2), increases as well as when the intensity or the duration of the mixing process increases.

Examining Fig. 2 we can conclude that in all cases a concentration of the PL many times greater than the minimum required has practically no effect on K_{pur}.

The factor K_{pur} is apparently most sensitive to the molecular-mass spread in the PL or the wide size distribution of pores in the membranes [the latter circumstance is indirectly confirmed by the dependence of K_{pur} on the radius of the pores in the membranes (see Fig. 2)]. The summed effect of both factors is also possible.

A second series of experiments was performed with real liquid radioactive wastes with a total specific activity of γ-emitting nuclides equal to $1.85 \cdot 10^5$ Bq/liter (primarily ^{137}Cs, ^{134}Cs, ^{60}Co, ^{131}I) and salt content of ~500 mg/liter; the main ionic components in the salt component were Na^+, Ca^{2+}, Mg^{2+}, Cl^-, NO_3^-, SO_4^{2-}; and, the pH was equal to 7-9.

Into the solution we added consecutively copper hexacyanoferrate, polyacrylic acid, and starch with concentrations of 5, 10, and 10 mg/liter, respectively. In the experiments we used the principle of maximum concentration of the starting mixture in the process of extracting the permeate, samples of which we analyzed (see Table 1).

TABLE 1. Results of Purification of Real Liquid Radioactive Wastes

Activity of γ-emitting nuclides in the permeate, Bq/liter				K_{pur}			
^{137}Cs	^{134}Cs	^{60}Co	^{131}I	^{137}Cs	^{134}Cs	^{60}Co	^{131}I
<13	<13	<25	<63	>360	>100	>30	~ 14

In spite of the fact that the starting solution was concentrated 40-fold by volume, K_{pur} for each radionuclide remained constant and the concentration of radioactive contaminants in the starting liquid radioactive wastes was reduced to the normal levels.

It should be noted that the volume concentration achieved was not the limiting concentration and is determined only by the amount of suspension in the starting solution and the content of the reagents introduced.

It is intended that the concentrates obtained be boiled down, since their salt content is at the level of the starting solution. Thus, the volume of liquid radioactive wastes to be solidified and stored can be decreased at least by two orders of magnitude.

Based on the results presented we can draw the following conclusions:

– the method combining selective complexing and ultrafiltration is promising for reprocessing of liquid radioactive wastes, especially wastes with a salt content exceeding 500 mg/liter;

– in order to develop the method further, it is necessary to study the interaction of the binding agents with the membrane material, surface-active substances, and with each other;

– it is necessary to search for and synthesize new, more effective binding agents.

LITERATURE CITED

1. Patent No. 1590828, 1981 (Great Britain).
2. F. A. Cotton and G. Wilkinson, Advanced Inorganic Chemistry, Wiley (1972).

EMERGENCY SHUTDOWN OF AN AMBIPOLAR REACTOR

N. N. Vasil'ev and M. G. Kuznetsov

UDC 621.039.6

An important stage in the design of any nuclear power plant is an analysis of possible emergencies and a development of measures to localize and eliminate their effect. As far as a hybrid thermonuclear reactor is concerned, the greatest hazard seems to be related to overheating of the fuel elements of the uranium blanket (for instance, as a result of accidental failure of coolant circulation) and subsequent fuel-element containment failure and escape of fission products into the coolant circuit. Another possible accident which is specific to a thermonuclear reactor and has serious consequences is sealing failure of the circuits of the vacuum–tritium complex with escape of tritium into the reactor room. Obviously, it is such systems that largely determine the safety of a hybrid thermonuclear machine.

When accidental failure of uranium blanket cooling occurs, it is essential to "quench" the thermonuclear reaction as quickly as possible. In an ambipolar system, this can be achieved by switching off the systems of injection into the central trap and into the locking ones, as well as the system of thermal barrier pumping out and that of microwave heating of electrons. As fuel supply stops and the ambipolar barrier is destroyed, the ion density and temperature in the central trap decrease, and so does, consequently, the intensity of the thermonuclear reaction.

However, if the central trap and the locking ones are emptied too fast, there will take place a significant (though short) jump of the heat flux on the end plasma receivers which

Translated from Atomnaya Énergiya, Vol. 58, No. 4, pp. 274-275, April, 1985. Original article submitted June 8, 1984.

0038-531X/85/5804-0317$09.50

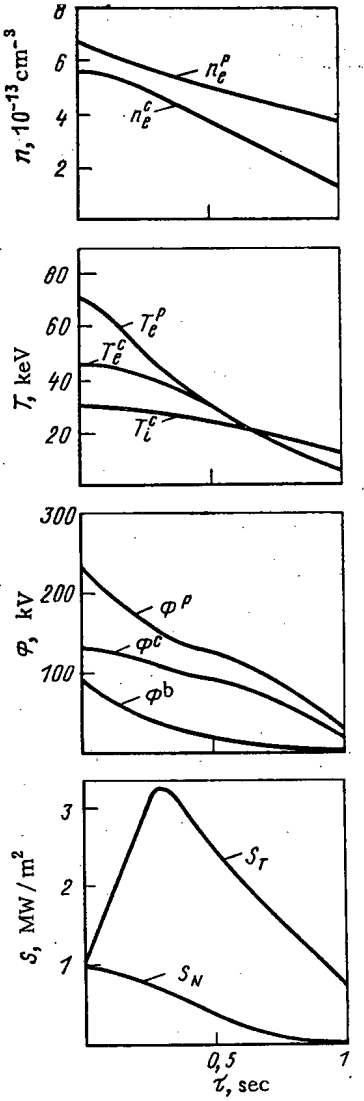

Fig. 1. Variation of plasma parameters and energy characteristics of the TROL reactor with time when the systems of injection into the central trap and into the locking ones, of pumping out thermal barriers, and of microwave heating of electrons in the locking traps are switched off instantaneously.

already operate under quite severe conditions. This can lead to burnout of the receiver tubes with all the serious consequences which follow from it. Thus, an optimal shutdown scenario for an ambipolar hybrid reactor has to be found.

The complexity of this task is due not only to the uncertainty connected with the inaccuracy of the existing physical plasma models, but also to a great number of external systems involved in the operation of an ambipolar reactor, to the possibility of adjusting the parameters of these systems over a wide range, etc. Therefore, this study started out by investigating the behavior of the energy parameters of an ambipolar reactor with thermal barriers when all the injection systems and the system of microwave heating of electrons in locking traps are instantaneously switched off. The goal of this study was not to analyze in detail the dynamics of the reactor as a whole (for example, the transient conditions in the blanket), but rather to investigate only the variation of plasma parameters and their influence upon the neutron flux on the first wall and upon the heat flux falling on the end plasma receivers.

Calculations were made with a model of energy and particle balance for an ambipolar trap described in detail in [1]. It represents a system of zero-dimensional nonstationary equations for the density and temperature of fuel ions, of helium, and of electrons. The values

of the plasma potential in the central trap and the locking ones were computed with algebraic equations for the balance of ion and electron losses at each time, while the thermal barrier was specified parametrically.

In this calculation, the power operating mode of a hybrid ambipolar reactor TROL (thermonuclear power 800 MW) [2], modified with due regard for the introduction of thermal barriers equal to a doubled temperature of flight-path electrons, was taken as rated. In this case, the injection energy and the mean plasma density in the locking traps were reduced to 500 keV and to $6.5 \cdot 10^{13}$ cm^{-3}, respectively, with an injection current of 170 A and a power of the microwave heating of electrons equal to 150 MW.

It was assumed in the calculation that when the pumping out system is instantaneously switched off, thermal barriers are destroyed both due to a decrease of the temperature of the flight-path electrons and as a result of an increased density of ion–ion collisions in a characteristic time (for the plasma parameters considered here, this time amounts to ~1 sec).

Figure 1 shows the calculated variations of density n, temperature T, and potentials Φ of plasma with time, as well as the time dependence of the neutron flux S_N on the first wall and of the heat flux S_T on the end receivers. It can be seen that the quenching time of a coolant (S_N drops to 1% of the rated value) is determined by the characteristic destruction time or thermal barriers and amounts to ~1 sec. During all this time, $nPe > n^{c}e$, $TPe \gtrsim T^{c}e$, $\Phi^{b} < \Phi^{c} < \Phi^{P}$, $T^{c}e \leq 0.5(\Phi^{P} - \Phi^{c})$. Here superscripts c, p, and b correspond to the central trap, to the locking ones, and to thermal barriers, respectively. Therefore, ambipolar confinement is preserved during the whole period of transient conditions under study, which gives us reason to believe that the physical plasma model used is correct.

The specific heat release in the fuel elements of the uranium blanket has the same time dependence as the neutron flux on the first wall (without taking into consideration the afterheat). Consequently, knowing the rated parameters of the blanket, we can easily calculate the temperature increase of the fuel-element core in the absence of heat removal. For the blanket of the TROL reactor [4], this temperature increase amounts to ~150°C. In this case, though there is no danger of fuel-element core or jacket meltdown, the fuel element can be damaged because the phase (α/β) transition temperature of uranium metal is exceeded.

The maximum value of the heat flux falling on the end plasma receivers is ~3 times greater than the rated one which corresponds to steady-state operating conditions of the reactor; obviously, the cooling system for the end receivers must be designed with a margin of safety.

Thus, the analysis shows that emergency shutdown of an ambipolar reactor is not an easy task. It is therefore essential to continue the development of models describing plasma decay in the traps of an ambipolar reactor with due regard for a series of complicating physical factors, such as an abnormally rapid destruction of thermal barriers, an intensified erosion of plasma by a neutral gas due to a deterioration of vacuum, a possible loss of stability because the anchors become less efficient, etc. Another pressing problem lies in finding an optimal shutdown scenario in order to develop requirements for appropriate emergency protection systems.

LITERATURE CITED

1. N. N. Vasil'ev and M. G. Kuznetsov, "The effect of alpha-particle confinement on the characteristics of an ambipolar reactor," At. Energ., 55, No. 3, 148-151 (1983).
2. N. N. Vasil'ev, I. N. Golovin, A. V. Nedospasov, and G. E. Shatalov, "A hybrid reactor with ambipolar plasma confinement (the TROL project)," At. Energ., 52, No. 2, 113-117 (1982).
3. M. Lontano, L. S. Pekker, and R. Pozzoli, Fiz. Plazmy, 6, 793 (1980).
4. N. N. Vasil'ev et al., Issues in Nuclear Science and Technology [in Russian], Thermonuclear Fusion Series, No. 1(9) (1982), p. 24.

YIELD OF FRAGMENTS FROM PHOTODISSOCIATION OF ^{242}Pu

Vo Dak Bang, Yu. S. Zamyatnin,
Chan Dyk Tkhiep, Chan Dai Ngiep,
Fan Tkhu Khyong, and Le Tkhi Kat Tyong

UDC 539.173.3

There are few published papers on the photodissociation of ^{242}Pu. The angular distribution of the fission fragments produced by near-threshold (5-10 MeV) bremmstrahlung was measured in [1] with glass detectors in order to study the structure of the fission barrier. The data on the mass distribution of the fragments from the photodissociation of this nuclide were not published. On the other hand, interest in nuclear data on the yield of fragments from fission of nuclides is continuing in connection with the development of the theory of nuclear fission and the solution of applied problems. In this work we determined for the first time the post-neutron yields of fragments from the photodissociation of ^{242}Pu by bremmstrahlung from electrons with energies of 18.1 ± 0.2 MeV and 20.7 ± 0.3 MeV as well as the parameters of the mass distribution of the fragments.

The target consisted to 3 ± 0.3 mg of plutonium dioxide enriched up to 94.7% ^{242}Pu. We deposited a thin layer of plutonium on an aluminum substrate 70 μm thick with a diameter of 55 mm. The diameter of the active spot was equal to 20 mm. We used the technique described, for example, in [2] for collecting the fragments escaping from the layer of the fissioning material, followed by γ spectrometry of the undissociated mixture of fission fragments. We placed the foil-collector consisting of highly pure (99.999%) aluminum 0.1 mm thick at a distance of 1 mm from the ^{242}Pu layer. To eliminate any effects from the fissioning of the ^{241}Pu impurity by thermal neutrons, we surrounded the entire assembly with a layer of cadmium 0.5 mm thick. We neglected the fission by fast neutrons because of its negligible contribution (<0.1%). For the irradiation, we used an MT-22 microtron [3]. The bremmstrahlung was generated in a tungsten target 2 mm thick. The residual electrons were absorbed in aluminum foil 35 mm thick. An average beam current of 10 μA was maintained with a stability of ±5%. We measured the spectra with the help of a spectrometric system consisting of a Ge(Li) detector with a volume of 28 cm^3 and an LP-4900 (NOKIA ELECTRONIKS) multichannel analyzer. The energy resolution of the system was equal to 3 keV according to the 662-keV line of ^{137}Cs, the irradiation time was 5 h for the 18.1-MeV electrons and 6 h for the 20.7-MeV electrons. We measured the γ spectra in the automatic mode with the spectra recorded one after another on a magnetic tape. We selected the cooling and measuring times depending on the decay scheme of the chain with the nuclide under study and we varied them in the range 0.5-1470 h and 0.5-10 h, respectively. We identified and calculated the intensities of the peaks with the help of the ACTIV program [4], adapted to the MINSK-32 computer. We performed a higher precision analysis of the spectra using the KATOK [5] program on a PDP-11/70 computer.

We calculated the relative yields on the SDS-6500 computer using the RICH 1 program, in which the FUMILI subprogram [6], which performs least-square calculations, was used. The technique used to calculate the relative yields was the same as that described in [2]. The data on the half-lives of the nuclides, the absolute quantum yields of the γ lines, and their errors are taken from [2, 7-9]. We scaled the values of the relative cumulative yields of the identified nuclides to the total yields of the chain with a given mass. At the same time, we calculated the parameter Z_p in the Gaussian distribution of the independent yields under the assumption that the charge distribution in the fissioning nucleus and in the fragments remained unchanged, taking into account the deviation of the set of experimentally measured values of Z_p from this law [10]. The value of the width of the Gaussian distribution σ, equal to 0.657, was found by extrapolating the experimental data on the photodissociation of ^{235}U and ^{238}U at 20 MeV [11] to the mass 242.

The absolute values of the yields of the products from the fission of ^{242}Pu by bremmstrahlung with a limiting energy of 20.7 MeV, presented in Table 1, were obtained with normalization to 200% of the area under the mass-distribution curve, constructed from the values of the total yields. We normalized the yields with 18.1 MeV, which are also presented in

Translated from Atomnaya Énergiya, Vol. 58, No. 4, pp. 275-277, April, 1985. Original article submitted June 25, 1984.

 0038-531X/85/5804-0320$09.50

TABLE 1. Total Yield of Fragments Produced by Fission of ^{242}Pu by Bremmstrahlung with a Limiting Energy of 18.1 MeV and 20.7 MeV, %

Mass number	Nuclide	18,1 MeV	20,7 MeV	Mass number	Nuclide	18,1 MeV	20,7 MeV
85	^{85m}Kr	0,76±0,05	0,82±0,05	127	^{127}Sb	—	0,87±0,09
87	^{87}Kr	1,04±0,12	1,35±0,09	129	^{129}Sb	1,51±0,16	1,63±0,18
88	^{88}Kr, ^{88}Rb	1,26±0,28	1,53±0,28	131	^{131}I	3,49±0,33	3,52±0,25
91	^{91}Sr	2,61±0,18	2,67±0,18	132	^{132}Te, ^{132}I	3,78±0,21	4,03±0,33
92	^{92}Sr, ^{92}Y	2,94±0,47	3,01±0,46	133	^{133}I	6,30±1,04	6,26±0,65
93	^{93}Y	—	3,61±0,22	135	^{135}I	5,81±0,87	6,01±0,55
95	^{95}Zr, ^{95}Nb	3,72±0,62	—	140	^{140}Ba, ^{140}La	4,49±0,66	4,49±0,55
97	^{97}Zr, ^{97}Nb	4,61±0,17	4,62±0,18	141	^{141}Ce	4,38±0,45	4,60±0,46
99	^{99}Mo, ^{99}Tc	5,87±0,82	5,86±0,54	143	^{143}Ce	3,69±0,26	3,57±0,25
103	^{103}Ru	5,76±0,25	—	147	^{147}Nd	2,04±0,13	2,08±0,17
105	^{105}Rh	5,11±0,62	5,11±0,55	149	^{149}Nd	1,61±0,12	1,46±0,11
112	^{112}Ag	0,85±0,13	0,94±0,08	153	^{153}Sm	1,03±0,08	1,19±0,15
115	^{115m}In	—	0,35±0,05				

TABLE 2. Parameters of the Mass Distribution of the Fragments from Photodissociation of ^{242}Pu

Parameter	18,1 MeV	20,7 MeV
P	—	$\geqslant 17$
$\bar{A}_L$, amu	98,7±0,3	98,9±0,3
$\bar{A}_H$, amu	140,4±1,0	139,9±1,1
$HWHH_L$, amu	16,0±0,4	17,3±0,5
$HWHH_H$, amu	14,3±0,4	15,5±0,4

Table 1, to the total yield of the peak fragments at 20.7 MeV, which remained virtually constant as a function of the energy [12].

Figure 1 shows the mass distribution of the fragments from the photodissociation of ^{242}Pu at 18.1 MeV and 20.7 MeV, as well as the fissioning of ^{241}Pu by thermal neutrons [13]. All distributions have a "double-hump" form, indicating the asymmetrical fissioning of ^{242}Pu. With the exception of the mass range 133-135, the mass-distribution curves are smooth. A weak fine structure, noted previously in [14] in the fissioning of ^{241}Pu by thermal neutrons and in the spontaneous fissioning of ^{242}Pu in [15], owing to the effect of the closed neutron shell N = 82 is observed in the range 133-135. The parameters of the mass distribution are presented in Table 2. The mean-weighted value of the masses of the light $\bar{A}_L$ and of the heavy $\bar{A}_H$ fragments remain virtually constant as a function of the excitation energy, which agrees with the result of [12] for the photodissociation of ^{235}U and ^{238}U with an excitation energy of E* = 9.7-19.9 MeV. However, in a wider range of variation of E*, as an analysis of the totality of our data and the results of [15] shows, $\bar{A}_L$ decreases slowly, while $\bar{A}_H$ increases with increasing E* with the coefficients $\Delta\bar{A}_L/\Delta E^* \cong -0.33$, $\Delta\bar{A}_H/\Delta E^* \cong +0.26$, respectively. To calculate these parameters, we estimated the average energy of excitation of the ^{242}Pu nucleus with electron energies of 18.1 and 20.7 MeV, which turned out to be equal to 12.0 and 13.3 MeV.

This phenomenon can apparently be explained by the increase in the competition between the emissive fission and the smoothing of the fine structure with increasing E*. With the transition from 18.1 MeV to 20.7 MeV the half-width at half-height (HWHH) both for the light and heavy peaks increases approximately by 8%, which agrees with the data in [13-16]. The values of HWHH which we obtained for the peak of light fragments are 12% greater than for the peak of heavy fragments, which confirms the role of emissive fission [17], which does not occur at E* = 6.3 MeV [14]. In accordance with this explanation, a somewhat greater broadening is observed at 20.7 MeV than at 18.1 MeV. Our value of the peak-to-trough ratio P agrees well with the overall systematic behavior of this parameter presented in [18].

In conclusion the authors thank A. G. Belov, Ts. Vylov, V. B. Brudanin, G. V. Buklanov, and S. P. Tret'yakova for assistance.

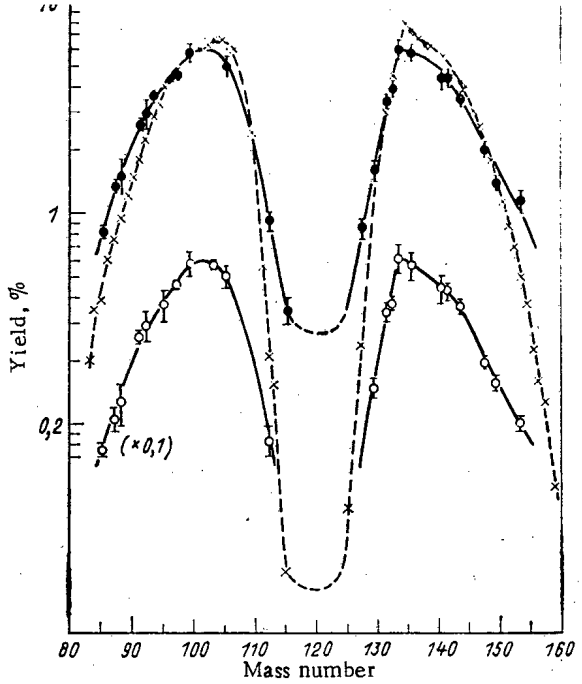

Fig. 1. Mass distribution of the fragments from the fission of ^{242}Pu by bremmstrahlung from 20.7 MeV (•) and 18.1 MeV (o) electrons and from fissioning of ^{241}Pu by thermal neutrons (×) [13].

LITERATURE CITED

1. N. S. Rabotnov et al., Yad. Fiz., 11, 508 (1970).
2. H. Thierens et al., Nucl. Instrum. Methods, 134, 299-308 (1976).
3. A. G. Belov, P. G. Bondarenko, Ch. Shinmane, and M. Vognar, The MT-22 Microtron, Report No. R9-82-301, Joint Institute of Nuclear Research, Dubna (1982).
4. V. B. Zlokazov, "ACTW – programs for automatic processing of γ spectra," Report No. R10-82-105, Joint Institute of Nuclear Research, Dubna (1982).
5. V. I. Gadzhokov et al., "Pointwise processing of discrete nuclear emission spectra with the help of an automatically controlled iterative process," Report No. R10-12724, Joint Institute of Nuclear Research, Dubna (1979); No. E10-12352, Dubna (1979).
6. I. N. Silin, in: Statistical Methods in Experimental Nuclear Physics [in Russian], Atomizdat, Moscow (1976), p. 319.
7. J. Blachot and C. Fiche, At. Data Nucl. Data Tables, 20, 242 (1977).
8. Table of Isotopes, N.Y. (1978).
9. J. Dickens and J. McConnel, Phys. Rev., 24, 192 (1981).
10. A. Wahl et al., in: Proc. Second Int. Symp. on the Physics and Chemistry of Fission, Vienna (1969), p. 813.
11. D. De Frenn et al., Phys. Rev. C, 26, 1356 (1982).
12. E. Jacobs et al., ibid., 19, 422 (1979); 21, 237 (1980).
13. E. Crouch, At. Data Nucl. Data Tables, 19, No. 5, 417-532 (1977).
14. H. Farrar et al., Can. J. Phys., 42, 2063 (1964).
15. E. Allaert et al., Nucl. Phys. A, 380, 61-71 (1982).
16. F. Caitucoli et al., Nucl. Phys. A, 369, 15 (1981).
17. M. Ya. Kondrat'ko et al., At. Energ., 53, No. 3, 164 (1982).
18. V. M. Gorbachev, Yu. S. Zamyatnin, and A. A. Lbov, in: Interaction of Radiation with the Nuclei of Heavy Elements and Nuclear Fission [in Russian], Atomizdat, Moscow (1976), p. 314.

DETERMINATION OF THE SENSITIVITY OF THERMOLUMINESCENT DETECTORS TO THERMAL NEUTRONS

Yu. N. Zhilov, V. G. Erkin, O. V. Lebedev,
V. A. Kuchumov, and G. A. Tyurin

UDC 539.12.08

Individual thermoluminescent dosimeters of the albedo type with detectors based on ^{6}LiF and ^{7}LiF [1] are used widely for the dosimetric monitoring of personnel working in conditions of the action of neutron and γ-radiation. The first ones record thermal neutrons scattered by the person's body as a result of moderation in it of fast and intermediate neutrons, and the second record γ-radiation. The sensitivity to thermal neutrons is the most important characteristic of the detectors, determining their application for dosimetry in mixed fields. In the present paper, the sensitivity to thermal neutrons is obtained for thermoluminescent detectors with the natural content of lithium isotopes supplied by V/O "Izotop" (TLD-0-05), and also ^{6}LiF (TLD-6-05) and ^{7}LiF (TLD-7-05) detectors corresponding to Technical Specification (TU) 6-02-2-679-82.

The TLD-0-05 detectors contain 7.5% ^{6}Li and 92.5% ^{7}Li, TLD-6-05 contain 88% of ^{6}Li and 12% ^{7}Li, and TLD-7-05 contain 0.1% ^{6}Li and 99.9% ^{7}Li. They are prepared by the method of crystallization from a melt in vacuo and have a diameter of 5 × 1 mm. The sensitivity to thermal neutrons was determined by irradiating the detectors in an isotropic field of thermal neutrons with an effective flux density of $(6.2 \pm 0.2)\cdot 10^3$ cm$^{-2}\cdot$sec^{-1}, which was generated by (Pu + Be)-sources in a moderator of hydrogeneous plastic. The flux density of the thermal neutrons was measured from the activation of gold foil by the method of cadmium ratios [2]. The flux density of the fast neutrons and the dose intensity of the γ-radiation at the location of the detectors amounted to $(2.4 \pm 0.9)\cdot 10^3$ cm$^{-2}\cdot$sec^{-1} and $(9 \pm 0.9)\cdot 10^{-6}$ rad/sec (1 rad = 0.01 Gy). Prior to irradiation, the detectors were subjected to thermal treatment: 1 h at 400°C, 17 h at 80°C. The thermoluminescence was recorded with a "Kharshou-2000D" instrument by the integral method. The thermoluminescence light sum, due to thermal neutrons, was found by the difference between the total light sum and its components due to γ-radiation. The contribution of fast neutrons to the thermoluminescence of LiF was found to be insignificant and therefore was not taken into acount.

For comparison of the characteristics of different thermoluminescent detectors, the sensitivity to thermal neutrons usually is used, expressed as the dose of γ-radiation which is required to produce the same light sum as by the action of a thermal neutron fluence at the detector of 10^{10} cm^{-2} [3]. When determining the sensitivity it is necessary to correct the experimentally recorded light sum (S_0) by taking account of self-screening and depression effects [4], due to the absorption of thermal neutrons according to the reaction ^{6}Li(n, α)^{3}H. The coefficients of self-scrrening and depression (see Table 1) were calculated with certain simplifying assumptions [5], allowing an analytical procedure to be used [6] with an accuracy acceptable for this purpose. Starting from the values obtained, after inserting a correction for scattering of the neutrons within the sample, the coefficient of reduction of the thermal neutron flux density (ΔF) was calculated, representing the ratio of the average flux density within the detector to the unperturbed flux in the same medium [6]. The coefficient ΔF was used for correcting the light sum resulting from the thermal neutrons: $S = 0.886\cdot S_0/\Delta F$, where 0.886 is a coefficient for averaging the light sum over a Maxwellian thermal neutron distribution. The dose of γ-radiation necessary for generating the light sum S is the quantity characterizing the required sensitivity.

The sensitivity of detectors to thermal neutrons, expressed in terms of the exposed dose of γ-radiation, is given below:

Translated from Atomnaya Énergiya, Vol. 58, No. 4, pp. 277-278, April, 1985. Original article submitted July 11, 1984.

0038-531X/85/5804-0323$09.50

TABLE 1. Coefficients of Self-Screening (G), Depression (H) and Reduction of Flux Density (ΔF) of Thermal Neutrons

Detector	G	H	ΔF
TLD-6-05	0,287	0,932	0,278
TLD-7-05	0,919	0,995	0,986
TLD-0-05	0,576	0,963	0,572

Detector	D, R
TLD-6-05	2365 ± 245
TLD-7-05	1,8 ± 0,9
TLD-0-05	221 ± 10
TLD-100	324 ± 15
TLD-600	2000*
TLD-700	1,2*
TLD-100	310*

*Literature data.

The literature data are also shown here [7] concerning the sensitivity to thermal neutrons of detectors of the firm "Kharshou": TLD-600 (95.6% ^{6}Li), LTD-700 (0.007% ^{6}Li) and TLD-100 with the natural content of the isotopes. Contradictory data about the sensitivity of detectors of the same type are given in the papers of different authors. For example, for TLD-600, these values amount to 870-2400 R (1 R = $2.58 \cdot 10^{-4}$ C/kg) [7]. Some authors, obviously, have not taken account of the role of self-screening and depression effects, which can lead to a lower sensitivity to thermal neutrons by comparison with the actual sensitivity. Therefore, the generalized literature data are given in the table for those papers in which the sensitivity was determined with the introduction of the corresponding correction of the experimental values. For TLD-100 the sensitivity was obtained experimentally and amounted to 324 ± 15 R, which agrees well with the literature data and indicates the validity of the chosen procedure of the investigations.

The comparison of the results shown above in Table 1 confirms that with respect to sensitivity to thermal neutrons, TLD-6-05 is not inferior to the widely used TLD-600 detectors. The lower limit of recording of thermal neutrons by TLD-6-05 detectors for the measurement equipment used amounts to a fluence of $\sim 4 \cdot 10^4$ cm^{-2}, which corresponds to an equivalent dose of 0.4 mrem (0.4 μSievert). The sensitivity to thermal neutrons for TLD-7-05 detectors, designed for recording γ-radiation, is almost three orders of magnitude lower than for the TLD-6-05. This same ratio of sensitivity to thermal neutrons is characteristic for the TLD-600 and TLD-700 detectors. For detectors with the natural content of lithium isotopes, the sensitivity to thermal neutrons is an order of magnitude lower than for the TLD-6-05, which corresponds to the ratio of the ^{6}Li concentrations in these detectors.

Thus, the considerable difference in sensitivity to thermal neutrons of the TLD-6-05 and TLD-7-05 detectors allows them to be used jointly for the separate recording of thermal neutrons and γ-radiation in mixed fields. These detectors may be found useful in individual neutron dosimeters of the albedo type for monitoring the radiation safety of personnel.

LITERATURE CITED

1. E. Piesh, Int. J. Appl. Radiat. Isotop., 33, No. 11, 1061 (1982).
2. V. P. Yaryna et al., in: Metrology of Neutron Measurements in Nuclear-Physics Facilities [in Russian], Vol. 2, Moscow (1976), p. 17.
3. K. Ayyangar, A. Lakshmanan, B. Chandra, and K. Ramadas, Phys. Med. Biol., 19, No. 5, 665 (1974).
4. Y. Horowitz, B. Shahar, S. Mordechal, and A. Dubi, Rad. Res., 69, 402 (1977).
5. R. Fleming, Int. J. Appl. Radiat. Isotop., 33, No. 11, 1263 (1982).
6. N. A. Damburg, L. L. Pelekis, and L. F. Protasova, in: Neutron Activation Analysis [in Russian], Zinatne, Riga (1966), p. 15.
7. V. Horowitz, Phys. Med. Biol., 26, No. 4, 765 (1981).

RADIATIVE CAPTURE CROSS SECTION OF ^{58}Fe AT A NEUTRON ENERGY OF 0.5-2.0 MeV

Yu. N. Trofimov

UDC 539.172.4

A natural mixture of iron isotopes contains 0.33% ^{58}Fe. During neutron irradiation of the structural steels of the reactors, ^{59}Fe forms due to radiative neutron capture of ^{58}Fe. ^{59}Fe has a high-energy γ-spectrum with a long half-life (45.54 days). For calculating radiation shielding of the reactors, the error in the cross section of the ^{58}Fe(n, γ)^{59}Fe reaction must be within 15% in the neutron energy range 0-15 MeV. However, at the present time there are no data on the radiative capture cross section of fast neutrons by the ^{58}Fe nuclei.

In the present work we measured the cross section of the ^{58}Fe(n, γ)^{59}Fe reaction in the neutron energy range 0.5-2.0 MeV in relation to the reference (standard) cross sections of the ^{180}Hf(n, γ)^{181}Hf and ^{58}Ni(n, p)^{58}Co reactions. Specimens were made by placing the ^{58}Fe-enriched iron in powder form between two thin polyethylene tapes with a thickness of 8 mg/cm^2. The isotopic composition of the enriched iron is as follows (%): 91.9 ^{58}Fe, 8.07 ^{57}Fe, and 0.03 ^{56}Fe. The irradiated specimen weight was 195 mg, and the spot diameter was 6 mm.

Neutrons were obtained from the ^{3}H(p, n)^{3}He reaction by bombarding the tritium–titanium targets with the protons accelerated using an electrostatic accelerator of the V. G. Khlopin Radium Institute. The integral neutron flux was measured using the method of activation detectors of ^{180}Hf. Two detectors measuring 6 mm in diameter and 0.2 mm in thickness were placed up against the specimen from both sides. The activation difference between the short-range (close) and the long-range detector did not exceed 15%. The specimen and the ^{180}Hf detectors were placed at a distance of 12 mm from the neutron source, and were subjected to radiation for a period of 24 h. Besides hafnium, we used ^{58}Ni as a detector, whose activation product exhibits a long half-life. Table 1 shows the main characteristics of the nuclear products of the experimental and the reference reactions.

The energy and the intensity of the γ-peaks were measured using a Ge(Li)-spectrometer with a detector having a capacity of 38 cm^3 and a resolution of 3 keV for the 1332-keV line. Calibration of the spectrometer was carried out using a set of standard γ-nuclides (OSGI) and the standard γ-sources of the D. I. Mendeleev All-Union Scientific-Research Institute of Metrology.

Table 2 gives the measured values of the cross sections of the ^{58}Fe(n, γ)^{59}Fe reaction and the used values of the cross sections of the reference reactions. It can be seen that there is an insignificant reduction in the radiative neutron-capture cross section of ^{58}Fe in the 0.5-2.0 MeV energy range. The correction for the unsteadiness of the neutron flux is small owing to the closeness of the half-life periods of ^{59}Fe and ^{181}Hf. The corrections for the neutrons forming from the (p, n) reaction on the structural elements of the accelerator, for the self-absorption of γ-radiation in the specimen, and for the miscounts of the analyzer (because of frontal pulse pile-up) were negligibly small. Based on the activation of ^{115}In in the (n, n') and (n, γ) reactions, we controlled the background originating from the neutrons scattered and decelerated in the structural elements of the accelerator. According to our evaluation, this background amounted to 3 ± 1% of the main neutron flux.

TABLE 1. Characteristics of the Nuclear Products of the Reactions under Study and the Reference Reactions

Reaction	Half-life, days	E_γ, keV	Quantum output, % [1, 2]
^{58}Fe (n, γ) ^{59}Fe	45,54±0,05	1099,25	55,5
^{180}Hf (n, γ) ^{181}Hf	42,4±0,1	482,0	86
^{58}Ni (n, p) ^{58}Co	70,79±0,04	810,75	99,45

Translated from Atomnaya Énergiya, Vol. 58, No. 4, pp. 278-279, April, 1985. Original article submitted July 9, 1984.

0038-531X/85/5804-0325$09.50

TABLE 2. Cross Sections of the $^{58}Fe(n, \gamma)$-^{59}Fe Reaction and the Reference Reactions

E_n, MeV	$\pm\Delta E_n$, MeV	$\sigma\pm\Delta\sigma$, 10^{-31} m^2		
		$^{58}Fe(n, \gamma)$	$^{180}Hf(n, \gamma)$ [3]	$^{58}Ni(n, p)$ [2]
0,5	0,13	3,0±0,3	42	—
1,0	0,12	2,7±0,3	45	—
1,5	0,10	2,5±0,3	40	—
2,0	0,08	2,6±0,3	32	—
2,0	0,08	2,5±0,3	—	38

The total error in the measured cross sections is equal to 10-12% and is due mainly to the error in the reference cross section. Table 2 shows the characteristic scatter in the values of the neutron energy which is caused by the energy losses of protons in the titanium–tritium targets and by the solid angle of the specimen relative to the neutron source.

LITERATURE CITED

1. N. G. Gusev and P. P. Dmitriev, Quantum Radiation of Radioactive Nuclides [in Russian], Atomizdat, Moscow (1977).
2. BNL/NCS-50.446, ENDF/B IV Dosimetry File, N.Y. (1975).
3. H. Beer and R. Macklin, Phys. Rev. C, 26, No. 4, 1404 (1980).

TOTAL NEUTRON CROSS SECTION OF ^{101}Ru AND ^{102}Ru IN THE NEUTRON ENERGY RANGE 0.01-1750 eV

V. A. Anufriev, S. I. Babich,
N. G. Kocherygin, and V. N. Nefedov

UDC 621.039.556

The magnitude of the resonance parameters of ruthenium isotopes is of considerable interest for reactor design (calculations) because up to 5% of all the fission fragments are due to them.

In order to study the interaction of neutrons with the nuclei of ^{101}Ru and ^{102}Ru, we used two specimens highly enriched in ^{101}Ru and ^{102}Ru. The specimen characteristics are given in Table 1.

We studied the interaction of neutrons with ^{101}Ru and ^{102}Ru using the time-of-flight method on an SM-2 neutron spectrometer [1] having a rotor-interrupter with a rectangular slot measuring $(1.5\cdot10)\ 10^{-6}$ m^2 in cross section.

Neutron transmission of the specimens was measured in the 0.01-1700 eV neutron energy range. In the 0.01-5 eV energy range we employed a working regime of the spectrometer in which the rotor-interrupter was maintained at 350 rpm and the selected channel width of the AI-4096 time-delay analyzer was equal to 32 μsec. In the 5-1700 eV energy range, the transmission of the specimens was determined maintaining the rotor-interrupter at 6660 rpm and the channel width of the time-delay analyzer at 2 μsec.

We used a 92 m flight base and a neutron detector made from a battery of the SNM-17 helium counters. The statistical error in the measurements did not exceed 1%. When calculating the energy dependence of transmission on a BÉSM-6, we introduced corrections for the spectrometer background and the miscounts in the analyzer channels.

Based on the obtained transmission curves, the resonance parameters were calculated according to the "shape" method using the single-level Breit–Wigner formula. The width of the resolution function at a rotor speed of 350 and 6660 rpm was found to be 1 μsec/m and 56 nsec/m, respectively. For identifying and calculating the resonance parameters of ^{101}Ru and

Translated from Atomnaya Énergiya, Vol. 58, No. 4, pp. 279-280, April, 1985. Original article submitted July 30, 1984.

 0038-531X/85/5804-0326$09.50

TABLE 1. Specimen Characteristics

Isotope	Specimen 1		Specimen 2	
	content, %	specimen thickness, nuclei/b ($1\ b = 10^{-28}\ m^2$)	content, %	specimen thickness, nuclei/b
^{99}Ru	0,3	$5,92 \cdot 10^{-5}$	0,1	$7,6 \cdot 10^{-5}$
^{100}Ru	0,5	$9,86 \cdot 10^{-5}$	0,1	$7,6 \cdot 10^{-5}$
^{101}Ru	92,7	$1,826 \cdot 10^{-2}$	0,4	$3,09 \cdot 10^{-4}$
^{102}Ru	6,0	$1,183 \cdot 10^{-3}$	99,2	$7,61 \cdot 10^{-2}$
^{104}Ru	0,4	$7,89 \cdot 10^{-5}$	0,4	$3,09 \cdot 10^{-4}$

TABLE 2. Parameters of the Resonance Levels of ^{101}Ru

E_0, eV	g	Γ, meV	Γ_γ, meV	$2g\Gamma_n$, meV	E_0, eV	g	Γ, meV	Γ_γ, meV	$2g\Gamma_n$, meV
13,60±0,05	0,5	—	—	0,004±0,001	338,8±2,0	0,6	—	—	31±6
13,94±0,05	0,5	—	—	0,009±0,001	375,7±0,6	0,6	—	—	251±25
15,90±0,03	0,6	223,7±18,1	220±20	4,28±0,25	425±3	0,6	—	—	146±25
25,06±0,07	0,5	—	—	0,013±0,003	452±5	0,6	—	—	233±30
36,41±0,07	0,5	—	—	0,038±0,07	476±6	0,4	—	—	23±7
38,66±0,24	0,5	—	—	0,013±0,008	527±5	0,6	—	—	114±34
42,0±0,1	0,6	193,1±18,2	180±19	16,14±1,20	574±5	0,5	—	—	27±20
47,07±0,26	0,5	—	—	0,022±0,013	617±7	0,5	—	—	76±38
51,76±0,01	0,6	238,0±26,0	236±26	2,10±0,06	657±10	0,5	—	—	178±100
61,26±0,01	0,4	236±32	231±32	3,93±0,23	770±10	0,5	—	—	62±22
66,2±0,2	0,4	274±33	228±36	28,5±2,5	840±10	0,5	—	—	67±30
100,1±0,2	0,6	—	—	9,05±0,62	926±15	0,5	—	—	330±100
112,2±0,4	0,4	—	—	8,15±0,45	997±15	0 5	—	—	290±100
140,7±0,6	0,6	—	—	2,95±0,26	1040±20	0,5	—	—	470±150
150,5±0,3	0,5	—	—	0,42±0,13	1140±25	0,5	—	—	80±40
156,6±1,0	0,4	—	—	10,54±0,79	1240±30	0,5	—	—	43±20
196,3±1,0	0,6	—	—	64,3±4,9	1295±30	0,5	—	—	420±150
242,1±1,0	0,6	—	—	26,2±4,9	1410±40	0,5	—	—	1215±300
249,4±2,1	0,4	—	—	3,98±1,22	1600±50	0,5	—	—	900±300
308,3±2,0	0,6	—	—	182,5±14,3	1720±50	0,5	—	—	100±50

^{102}Ru, we considered the resonances of ^{99}Ru, ^{100}Ru, and ^{104}Ru according to the published parameters [2], and the relative contribution of the ^{101}Ru and ^{102}Ru resonances – according to the parameters obtained in the present work.

From the neutron transmission curves of the specimens in the 0.01-5 eV energy range we obtained the total cross sections of ^{101}Ru and ^{102}Ru at the thermal point ($E_0 = 0.025$ eV). It was found that $\sigma_{tot} = 11.2 \pm 0.4$ b for ^{101}Ru and $\sigma_{tot} = 10.4 \pm 0.6$ b for ^{102}Ru. The resonance parameters of ^{101}Ru and ^{102}Ru were determined based on the neutron transmission of the specimens in the 4-1700 eV energy range. The obtained data are given in Tables 2 and 3.

Based on the Γ_γ values for five resonances of ^{101}Ru and for three resonances of ^{102}Ru, we found the average Γ_γ values to be equal to 219 ± 19 meV and 172 ± 46 meV, respectively. These values were used in the calculation of other resonances.

The present data (see Tables 2 and 3) were compared with the previously published data [3-5]. We note that in the transmission measurements of the earlier investigations [3-5] specimens of different thickness values were used with a natural mixture of ruthenium isotopes.

Owing to the presence of highly enriched preparations of ^{101}Ru and ^{102}Ru (see Table 1), we could make specimens thicker than those employed in the earlier studies [3-5]: about 3 times thicker in case of ^{101}Ru and 10 times thicker in case of ^{102}Ru. Consequently, in the present work, the parameters of seven resonance levels of ^{101}Ru were additionally identified in the energy range up to 150 eV and calculated, and in case of ^{102}Ru, in addition to the three known resonances, the parameters of another 11 resonance levels were determined in the energy range up to 1700 eV.

However, the insufficient resolution of the spectrometer used in the present work did not permit us to resolve closely spaced resonances having an energy exceeding 150 eV. Thus, for example, Popov et al. [4] identified 33 resonance levels for ^{101}Ru in the 190-1000 eV

of ^{102}Ru

E_0, eV	Γ, meV	Γ_γ, meV	Γ_n, meV
9,802±0,003	128±8	128±8	0,0093±0,0002
19,01±0,03	154,1±92,7	254±93	0,0040±0,0007
42,15±0,01	135±37	135±37	0,10±0,01
165,13±0,24	—	—	0,69±0,10
211,8±0,6	—	—	0,49±0,13
413±1	—	—	8,2±7,1
452,2±0,8	—	—	6,1±1,1
629±10	—	—	16,5±12,7
877±10	—	—	13±6
970±15	—	—	45±24
1261±30	—	—	721±100
1350±30	—	—	47±23
1410±30	—	—	184±40
1580±40	—	—	158±30

energy range using a spectrometer having a resolution of 7 nsec/m, whereas, in the present work we could identify only 20 levels.

The value of the force function was determined for ^{101}Ru based on the resonance parameters in the energy range up to 660 eV, and was found to be $(5.47 \pm 0.15)\cdot 10^{-5}$. Within the errors in determination, this value agrees with that reported earlier [4]. The force function for ^{102}Ru was found to be $(2.21 \pm 0.66)\cdot 10^{-5}$. Based on the data of Table 3, the average distance between the levels and the average normalized neutron width were also found out: $\overline{D}$ = (112 ± 20) eV and $\overline{\Gamma_n^0}$ = (2.48 ± 0.75) meV.

Based on the parameters of the resonance levels presented in Tables 2 and 3, we computed the resonance integrals of capture I_γ = (108 ± 15) b for ^{101}Ru and I_γ = (5.5 ± 0.5) b for ^{102}Ru.

LITERATURE CITED

1. N. G. Kocherygin, S. I. Babich, and S. N. Nikol'skii, Neutron Interrupter with Four Synchronously Rotating Rotors Suspended in a Magnetic Field [in Russian], Preprint NIIAR-28(387), Dimitrovgrad (1979).
2. BNL-325, 3rd ed. (1973).
3. N. Priesmeyer and H. Yung, in: Proc. Internat. Conf. on Nuclear Cross Section for Technology, Knoxville (1971), p. 688.
4. A. B. Popov, K. Tshchetsyak, and Khvan Chen Gu, "Neutron resonance parameters of ruthenium," Yad. Fiz., 29, No. 3, 561 (1979).
5. H. Bolotin, Nucl. Phys., 42, 676 (1963).

AN INTEGRATED BENCHMARK FOR ATTENUATION OF NEUTRONS WITH AN ENERGY OF 14 MeV BY LEAD LAYERS

S. Antonov, G. Voikov,
K. Ilieva, and I. Iordanova

UDC 621.039.572.4

The integrated experiments on the transmission (passage) of neutrons having an energy of 14 MeV through highly inhomogeneous systems permit one to evaluate the reliability of the numerical algorithms and also the degree of sufficiency of the neutron (nuclear)-physical data for describing the complex inhomogeneous shield of the future thermonuclear reactors.

In the present work we carried out a numerical study of the attentuation of the total neutron flux passing through an iron collimator (neutron tube) and lead barriers located just (directly) behind the collimator. Our previous experimental results [1] served as a basis for comparison. The choice of the decelerating material (moderator) is due to the increasing interest in lead as a neutron multiplier (breeder) in the blanket of the thermonuclear reactors [2-4].

In order to carry out the experiments we used a neutron source based on a tritium target which is bombarded with an accelerated deuterium ion beam.

At a 1.5 mA current of the deuterium ions, the neutrons forming from the T(d, n)^{4}He reaction and having an energy of 14.9 MeV emerge isotropically with an intensity of 10^{10} sec^{-1}. The cylindrical iron collimator (length 130 cm, internal diameter 10 cm, and external diameter 12 cm) was positioned just behind the target. The collimator was located in the wall made of a mixture of iron shots (pellets) and polyethylene. Behind the collimator we placed the lead plates measuring 40 × 40 × d cm. The detector is a flat-response counter in the form of a cylinder measuring 37.5 cm in diameter and 42 cm in length. It was placed at a distance of 82 cm from the collimator end.

The calculations were carried out using two models: a unidimensional model based on the method of discrete ordinates (ANISN [5]) and a three-dimensional model based on the Monte Carlo method (MORSE [6]). In order to evaluate the energy dependence of the cross sections and the neutron fluxes, we used a 25-group approximation [7] based on the SUPERTOG program and the ENDF/B IV and ENDL data files.

According to the unidimensional description of the experiment (ANISN), we obtained the neutron fluxes from the unidirectional source behind the aforementioned lead layers. In this case, we took account of the fact that the neutrons approach the detector at a solid angle arc tg 0.2 corresponding to the experimental conditions.

Using the three-dimensional model (MORSE) we considered the actual geometric conditions of the experiment: the neutrons having an energy of 14 MeV emerge isotropically from the surface of a disc (ring) of radius 5 cm located at the collimator entrance (front portion), and reach the detector after passing through the collimator and the lead barriers. The detector is approximated to a ring measuring 20 cm in radius situated perpendicular to the axis of measurement at the central point of the detector.

Figure 1 shows the experimental and the numerical results on the attenuation (relative to the flux without a layer) of the neutron flux having an energy of 14 MeV. The mean deviations of the computed values based on the MORSE program and the data files of ENDL and ENDF are 6.4 and 8.5%, respectively; the mean deviation based on the ANISN program and the aforementioned data files is almost identical, and is equal to 9.6%.

Comparison of the numerical values obtained on the basis of the ENDF and ENDL files shows a virtual coincidence with those obtained from the calculations carried out accortding to ANISN. A more striking difference in the data based on MORSE can be attributed to higher

Institute of Nuclear Research and Nuclear Energy, Bulgarian Academy of Sciences, Sofia.
Translated from Atomnaya Énergiya, Vol. 58, No. 4, pp. 280-281, April, 1985. Original article submitted August 9, 1984.

0038-531X/85/5804-0329$09.50

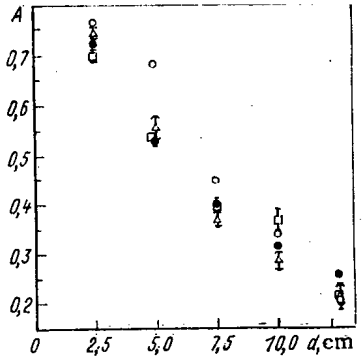

Fig. 1. Attenuation of neutron flux A as a function of the layer thickness d: o) experiment; Δ) MORSE, ENDF; □) MORSE, ENDL; •) ANISN.

sensitivity of the method with respect to the scattering matrix and the large statistical scatter associated with this.

We note that in spite of the smallness of statistics (data) employed when calculating with MORSE (10^4 histories per draw and 15 min computer time on IBM 370/145) and the associated difficulties in adequately modeling the entire system, the obtained results show a satisfactory agreement with the experimental values.

LITERATURE CITED

1. I. Iordanova, K. Ilieva, V. Khristov, T. Troshev, N. Sokolinova, and O. Penchev, Dokl. BAN, 3, No. 37, 313 (1984).
2. S. Rozhkov and G. Shatalov, in: US–USSR Sym. on Fusion–Fission Reactors, Livermore (1976), p. 143.
3. V. Blinkin and V. Novikov, in: Proc. Conf. on Engineering Problems in Fusion Reactors, Vol. 2, Leningrad (1977), p. 187.
4. Nuclear Data for Fusion reactor Technology. IAEA-TEC, DOC-223, Vienna (1979).
5. ANISN-W Code. WANL-PR-(LL)-034, Vol. IV (1970).
6. M. Emmet, The MORSE Monte Carlo Transport Code System. ORNL-4972 (1972).
7. G. Voykov, V. Gadjokov, and S. Minchev, L26P3S34, IAEA-INDC(BUL)-007/GV, Vienna (1983).
8. G. Voykov, V. Gadjokov, and K. Ilieva, Modification of SUPERTOG, IAEA-INDC(BUL)-6/GV, Vienna (1982).

DETECTORS FOR SPECTROMETRY OF THE X-RAY EMISSION FROM GERMANIUM OBTAINED BY THE HYDRIDE METHOD

G. G. Devyatykh, G. N. Flerov,
Yu. A. Nechuneev, A. V. Gusev,
Yu. P. Kharitonov, Yu. S. Tsyganov,
and V. A. Gavva

UDC 546.289:539.1.074

Until recently, the principal instruments by means of which the numerous problems associated with the spectrometry of ionizing radiations were resolved were silicon surface-barrier and silicon and germanium lithium-drift semiconductor detectors. With the appearance of high-purity germanium, the advantages and versatility of semiconductor detectors (SCD) based on this material are becoming even more obvious.

Compared with other types of detectors, SCD have the following advantages: high sensitivity per unit volume, mechanical stability, relatively low grid bias, high radiation stability, etc.

In order to prepare the detectors, high-purity germanium is used, with a concentration of noncompensated charge carriers of 10^{10}-10^{11} atoms per cm^3. These detectors are stable at room temperature, tolerate repeated thermal cycling from the temperature of liquid nitrogen to room temperature, and allow relatively high-temperature thermal processing to be carried out (up to 120°C) for annealing radiation defects [1].

The principal factor determining the quality of the detectors is the degree of purity of the germanium. The production of germanium suitable for the preparation of detectors with a high resolution is a complex problem. Several methods exist. The most promising, in our opinion, is the hybride method [2].

The present paper is devoted to the investigation of certain characteristics of p–n structures, prepared on a base of germanium obtained by the hydride method. The purpose of the paper is to estimate the degree of purity of the germanium and its applicability for the preparation of detectors with a high energy resolution. Monocrystals of the p type were used, with a uniform distribution of the electrophysical characteristics over the length of the crystal. The concentration of noncompensated charge carriers in the samples used for the preparation of the detectors amounted to $\sim 7 \cdot 10^{10}$ atoms per cm^3, and mobility was not less than 35,000 $cm^2/(V \cdot sec)$. In order to prepare the detectors from the monocrystal, plates with a thickness of 5-5.5 mm were cut out with a diamond disk. Circular blanks were cut out with a diameter of 10-12 mm, by means of brass punches. The flats were ground on glass successively with M-20, M-14, and M-5 micropowders. After polishing, the samples were thoroughly cleaned, degreased, and etched by the procedure described in [3]. Ohmic contact was obtained by the vaporization in vacuo of a thin layer of gold, and the n^+ contact was obtained by vaporization of metallic lithium with subsequent diffusion at T = 340°C during 10 min. The residues of lithium oxide were removed by means of an aqueous solution of ethyl alcohol, and the lateral surface of the sample was etched twice in a mixture of nitric and fluoric acids during 5 min.

On completion of diffusion of the lithium in the samples by means of the procedure described in [3], a protective groove was cut out, the width of which overlapped the boundary of diffusion of the lithium. The depth of the groove was 2/3 the thickness of the sample. Having protected the electrodes by means of a plastic adaptor, the groove was twice etched during 3 min in a mixture of high-purity nitric and fluoric acids. In order to investigate the characteristics of the detectors obtained, a cryostat used for spectrometric measurements was adapted. The design of the cryostat provided for the elimination of background noise, which has a significant effect on the limiting energy resolution of the detector. The detector was installed in the cryostat with a preamplifier cooled by a cascade. The volt–ampere and volt–capacity characteristics were investigated on the detectors obtained, and

Translated from Atomnaya Énergiya, Vol. 58, No. 4, pp. 281-283, April, 1985. Original article submitted September 24, 1984.

0038-531X/85/5804-0331$09.50

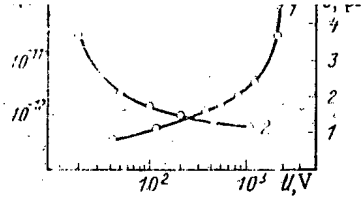

Fig. 1. Volt–ampere (a) and volt–capacity (b) characteristics of the detector.

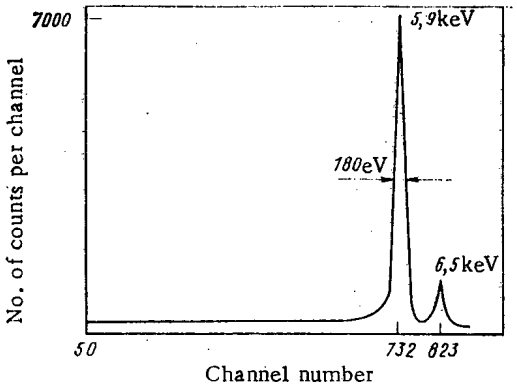

Fig. 2

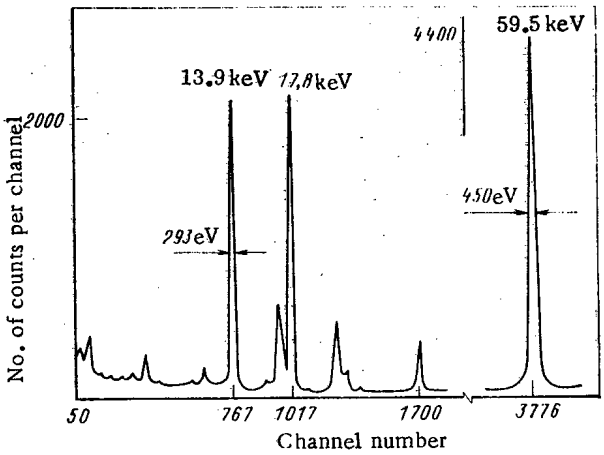

Fig. 3

Fig. 2. Emission spectrum of ^{55}Fe, obtained by means of a germanium detector: U_c = 1300 V, S = 0.25 cm^2; W = 4.5 mm.

Fig. 3. Emission spectrum of ^{241}Am, obtained by means of a germanium detector: U_c = 1300 V, S = 0.25 cm^2; W = 4.5 mm.

the emission spectra of ^{55}Fe and ^{241}Am were obtained. Typical volt–ampere and volt–farad characteristic curves are shown in Fig. 1, from which it can be seen that with increase of the reverse bias, the capacity of the p–n junction decreases sharply, but with a voltage of >500 V the capacity is almost unchanged. The depth of the sensitive region W was calculated by the equation [4]

$$W = (2\varepsilon U/gN)^{1/2},$$

where ε is the dielectric permeability; U, bias voltage; N, concentration of noncompensated charge carriers; and g, charge of the electron. A calculation showed that for our detectors, with a reverse bias of 900 V, the depth of the sensitive region is equal to the geometric size of the samples. The concentration of noncompensated charge carriers, obtained when investigating the volt–capacity characteristics [4], coincides well with the above stated values, obtained by investigation of the Hall effect.

From an analysis of the volt–ampere characteristics, it follows that with a change of the bias voltage from 300 to 1000 V, the reverse currents do not exceed 10^{-11} A. This corresponds to a current noise of ≦100 eV.

The apparatus spectra of ^{55}Fe and ^{241}Am are shown in Figs. 2 and 3. It can be seen from the figures that according to the ^{55}Fe line, corresponding to E = 5.9 keV, the energy resolution amounts to 180 eV, for ^{241}Am according to the 13.9 keV line it is equal to 293 eV, and according to the 59.5 keV line it amounts to 450 eV. In the region of "soft" radiation energy, the energy resolution depends markedly on the type of the charge-sensitive preamplifier. In our case, a preamplifier was used with a sink connection. Amplifiers with an optoconnection obviously would have allowed the resolution of the detectors to be improved.

Thus, the characteristics of the detectors obtained confirm the excellent quality and high purity of the germanium hydride. The energy resolution of the detectors is found at the level of the best samples supplied by foreign firms. The results of the investigation allow the conclusion to be drawn about the applicability of germanium hydride for the preparation of ionizing radiation detectors with a high resolution.

spectrometric measurements.

LITERATURE CITED

1. R. Baertsch, IEEE Trans. Nucl. Sci., 19, No. 3, 275 (1971).
2. G. G. Devyatykh, "Some problems of the production of elements of high purity through their volatile compounds," in: Production and Analysis of High-Purity Substances [in Russian], Gorki (1974), pp. 5-12.
3. B. N. Osipenko et al., Detectors of Ultrapure Germanium for the Spectrometry of γ-Radiation, Prepared in the Laboratory of Nuclear Problems of the JINR [in Russian], Preprint JINR 13-83-669 (1983).
4. L. S. Berman, Capacity Methods of Investigation of Semiconductors [in Russian], Nauka, Leningrad (1972).

EFFECT OF HEAT RELEASE IN THE COOLANT ON THE STABILITY OF A WATER-COOLED–WATER-MODERATED REACTOR

S. I. Vdovin and E. F. Sabaev

UDC 621.039.577.14

It is known that in boiling reactors at quite high power and steam content, self-exciting power fluctuations originate [1-3]. The instability mechanism of the coolant in these reactors is related with the strong dependence of the reactivity on the steam content and the inertia of the heat exchange in the core [3, 4], and also with the interaction of neutron-physical and thermohydraulic processes [5, 6]. A large steam coefficient of reactivity and a quite high frequency of the power fluctuations with instability (of the order of 1 Hz), as noted in [6], lead to a significant stabilizing effect of the less inertial processes of steam formation, which previously had not been taken into consideration, in view of the smallness of their relative magnitude (surface boiling [6]).

The effect on the neutron-physical instability of heat release in the coolant, which in these reactors also is the moderator, is being considered further. It is known that ~2-3% of the power [7] is released directly into the coolant during thermalization of the fast neutrons and attenuation of the γ-radiation. The characteristic time constant of these processes (delayed γ-emission is not taken into account) is much less than the inertia of the heat exchange in the core, i.e., the release of heat in the coolant omits one of the principal inertial links in the feedback chain: neutron flux–fuel element temperature–steam content–reactivity–neutron flux.

In order to estimate the effect of heat release on the coolant we shall use the exact kinetic equations. We shall describe the change of temperature of a fuel element by a simple inertial link with a periodic function $1/(1 + Tp)$. Assuming that the enthalpy and velocity of the water at the core inlet are constant and the change of temperature of the coolant is much less than the change of temperature of the fuel, the characteristic equation for investigating the neutron-physical instability can be written in the form

$$p\left(\frac{l}{\beta}+\sum_{i=1}^{6}\frac{\beta_i/\beta}{\lambda_i+p}\right)=\frac{1-\varepsilon}{1+Tp}\left|k_g-k_TW(p)\right|-\varepsilon k_TW(p), \qquad (1)$$

where p is the Laplace transform parameter; T is the time constant of the fuel element; ε is the relative fraction of heat released in the coolant, and $-k_TW(p)$ is the transfer function from the change of heat flow in the coolant to the change of reactivity. With the normalization $W(0) = 1$, the parameters $(1 - \varepsilon)k_g$ and $-k_T$ are numerically equal to the reactivity, in units of β,* injected (in linear approximation) by the power effect of the fuel and the density

*β is the effective fraction of delayed neutrons.

Translated from Atomnaya Énergiya, Vol. 58, No. 4, pp. 283-284, April, 1985. Original article submitted September 24, 1984.

0038-531X/85/5804-0333$09.50

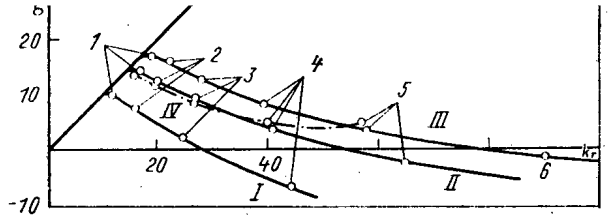

Fig. 1. D-partition boundaries: I) $\varepsilon = 0$; II) $\varepsilon = 0.02$; III) $\varepsilon = 0.03$; boundary IV is constructed from the approximate relations (3) for $\varepsilon = 0.02$; figures at the points are the values of ω, rad/sec.

effect of reactivity of the coolant for a change of power by 100% of the initial steady-state value, i.e., these parameters are the static coefficients of amplification of the feedbacks in the reactor.

We shall carry out the investigation of the stability of the stationary regime by means of the method of D-partition of the plane of the real parameters k_T and k_g [8]. Assuming in Eq. (1) $p = j\omega$, we obtain the system of equations defining the boundary of the D-partition $k_T(\omega)$ and $k_g(\omega)$:

$$\begin{aligned} -k_T(\omega)\,[\mathrm{Re}W - \varepsilon T\omega \mathrm{Im}W] + (1-\varepsilon)\,k_g(\omega) &= \omega^2\left[\sum_{i=1}^{6}\frac{\beta_i/\beta}{\lambda_i^2+\omega^2} - T\left(\frac{l}{\beta}+\sum_{i=1}^{6}\frac{\beta_i/\beta}{\lambda_i^2+\omega^2}\lambda_i\right)\right];\\ -k_T(\omega)\,[\mathrm{Im}W + \varepsilon T\omega \mathrm{Re}W] &= \omega\left[T\omega^2\sum_{i=1}^{6}\frac{\beta_i/\beta}{\lambda_i^2+\omega^2} + \frac{l}{\beta} + \sum_{i=1}^{6}\frac{\beta_i/\beta}{\lambda_i^2+\omega^2}\lambda_i\right]. \end{aligned} \qquad (2)$$

Figure 1 shows the boundaries of D-partition, separating the region of stability for different values of ε. For this, the transfer function $W(p)$ is constructed in accordance with perturbation theory for an increment of reactivity, the transfer of heat over the height of the core is calculated by a homogeneous model without taking account of phase slippage and surface boiling, and the values of the steady-state energy distribution over the height of the core are taken from [9]. Despite the simplicity of this model, it was used in a number of papers in order to explain the power oscillations, and good agreement with the experimental data was obtained [10]. The region of stability in the plane of the coefficients of amplification k_T and k_g is located to the left of the corresponding D-partition curve and below the singular straight line $k_T = (1 - \varepsilon)k_g$. The principal parameters of the calculated regime are derived later and correspond approximately to a similar operating regime of [2].

Pressure, MPa	3.5
Height of core, m	2
Time constant of fuel element T, sec	6
Coolant velocity at the core inlet, m/sec	0.5
Coolant preheating in the core, kcal/kg (kJ/kg)	41 (172)
Underheating of water at core inlet, kcal/kg (kJ/kg)	7.5 (31)

It follows from the figure that by taking account of the release of 2-3% of heat in the coolant, the boundary value of k_T for $k_g = -1$ is increased by a factor of 1.9-2.7, and the phase frequency ω is increased by a factor of 1.4-1.7. Therefore, with a working value of the power coefficient of reactivity with respect to the fuel k_g^* of approximately -1, the heat release in the coolant exerts a significant stabilizing effect.

In the case of a more total feedback (with a more rigid description of the heat transfer), the stabilizing effect of the heat release in the coolant can be estimated by means of perturbation theory. We denote by $k_{T0}(\omega)$ and $k_{g0}(\omega)$ the D-partition boundary constructed without taking account of the release of part of the heat directly in the coolant ($\varepsilon = 0$). Taking account of the smallness of this heat release, we estimate to a first approximation with respect to ε the correction introduced by it at the position of the boundary of the region of stability. Assuming that $\omega \sim 1\ \mathrm{sec}^{-1}$, we obtain from Eq. (2)

$$\begin{aligned} (k_T - k_{T0})/\varepsilon &= k_{T0}(k_{g0} + T\lambda - 1);\\ (k_g - k_{g0})/\varepsilon &= (k_{g0} + T\lambda)(k_{g0} + T\lambda - 1) + 1 + (T\omega)^2, \end{aligned}$$

where $\sum_{i=1}^{n} \ldots$ hence, it follows that $\kappa_g - \kappa_{g_0} > \varepsilon(1, \omega)$, i.e., the D-partition boundary is displaced strongly upward, increasing the region of stability (see Fig. 1).*

Thus, the "instantaneous" release of even an insignificant part of the heat (2-3% of the power) in the coolant exerts a significant stabilizing effect on the stability of a boiling reactor, especially in the case of a high steam content at the core outlet, which must be taken into consideration when analyzing the dynamics of boiling reactors.

LITERATURE CITED

1. J. Harrer et al., in: Proceedings of the Second Geneva Conference. Selection of Reports of Foreign Scientists [Russian translation], Vol. 4, Atomizdat, Moscow (1959), p. 177.
2. V. A. Afanas'ev et al., At. Energ., 24, No. 4, 368 (1968).
3. I. Ya. Emel'yanov, P. A. Gavrilov, and B. N. Seliverstov, Control and Safety of Nuclear Power Reactors [in Russian], Atomizdat, Moscow (1975).
4. F. M. Mitenkov and B. I. Motorov, Mechanisms of Unstable Processes in Thermal and Nuclear Power Generation [in Russian], Énergoizdat, Moscow (1981).
5. S. Zivi and R. Rait, in: Kinetics and Regulation of Nuclear Reactors [in Russian], Atomizdat, Moscow (1967), p. 187.
6. P. A. Leppik, S. P. Pavlov, and V. I. Plyutinskii, At. Energ., 52, No. 6, 379 (1982).
7. A. M. Weinberg and E. P. Wigner, Physical Theory of Neutron Chain Reactors, Univ. of Chicago Press (1958).
8. Yu. I. Neimark, Stability of Linearized Systems [in Russian], Order of the Red Banner Military-Aviation Engineering Academy, Leningrad (1949).
9. I. N. Sokolov et al., Teploenergetika, No. 5, 62 (1968).
10. G. A. Sankovskii et al., At. Energ., 25, No. 6, 514 (1968).

*The first approximation with respect to ε may prove to be inadequate for determining the displacement of the boundary of the region of stability for large values of ω.

EFFECT OF NEUTRON FIELD PARAMETERS ON THE YIELD OF ^{252}Cf

A. V. Klinov, A. V. Mamelin, and Yu. G. Toporov

UDC 621.039.8.002:621.039.554

Efficient production of ^{252}Cf in nuclear reactors requires a sound choice of parameters for the neutron field in which the parent material is irradiated. Among these, the spectral characteristics are of prime importance. The sensitivity of ^{252}Cf yield to the neutron spectrum is due to large differences between the thermal cross sections and resonance integrals of several nuclides in the buildup chain (Fig. 1): for some, the resonance integrals exceed the thermal cross sections by more than a factor of 10 [1] (see Table 1). On this basis it is concluded in [2-4] that ^{252}Cf can be effectively produced using "hard" neutron spectra. This conclusion relies on a comparison of the ^{252}Cf yields calculated for different irradiation times in neutron fields whose hardness varieswhile either the total neutron flux density [3] or the fission rate [4] remains constant. Such conditions do not obtain in actual practice, and the problem is to choose the most appropriate irradiation channel in terms of both spectrum hardness and absolute neutron flux density.

This study attempts to determine the basic behavior of the ^{252}Cf yield indexes in the most general case, when the thermal and epithermal neutron flux density are varied together with the irradiation time. The parent material used is a mixture of heavy isotopes of curium [5], and the optimization criterion is the ^{252}Cf yield.

The buildup of ^{252}Cf was calculated with a CONUS computer program [6]. The relative content of ^{246}Cm in the parent material was 20%, and that of ^{248}Cm was 2%. The nuclear reaction rates were found by the formula

$$b_i = \sigma^r_{0,i}\Phi + I^r_{\text{eff},i}\varphi,$$

Translated from Atomnaya Énergiya, Vol. 58, No. 4, pp. 284-286, April, 1985. Original article submitted October 22, 1984.

0038-531X/85/5804-0335$09.50

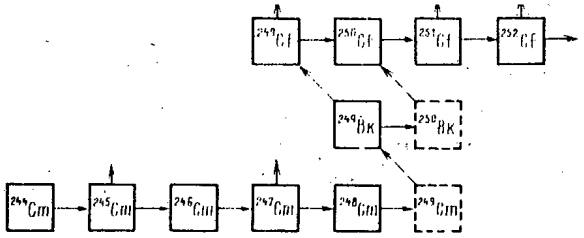

Fig. 1. ^{252}Cf buildup chain: vertical arrows denote fission; dashed arrows, β^--decay; horizontal arrows, radiative neutron capture; short-lived nuclides ($T_{1/2}$ < 10 h) are in dashed boxes.

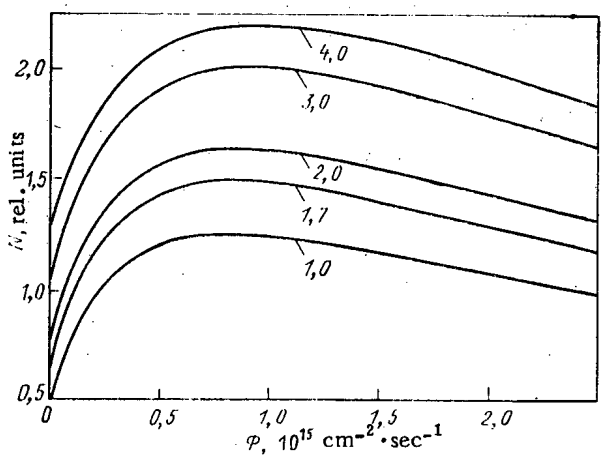

Fig. 2. Yield of ^{252}Cf for an irradiation time of 250 days, plotted as a function of the thermal neutron flux density (the curves are labeled with the values of φ, 10^{14} $cm^{-2} \cdot sec^{-1}$).

where $\sigma_{0,i}^{r}$ is the cross section of the r-th reaction of the i-th nuclide with neutrons at an energy of 0.0253 eV, Φ is the thermal neutron flux density, $I_{eff,i}^{r}$ is the effective resonance integral of the r-th reaction of the i-th nuclide, and φ is the epithermal neutron flux density per unit lethargy interval.

The thermal neutron flux density varied between 0 and $2.5 \cdot 10^{15}$ $cm^{-2} \cdot sec^{-1}$, and the epithermal between 1 and $4 \cdot 10^{14}$ $cm^{-2} \cdot sec^{-1}$. In all instances the irradiation time ranged up to the value corresponding to maximum ^{252}Cf yield.

Figure 2 shows the ^{252}Cf yield plotted against the thermal neutron flux density for a constant irradiation time. The numbers next to the curves are the values of φ, 10^{14} $cm^{-2} \cdot sec^{-1}$. The curve pattern remains the same when the irradiation time is varied. This is depicted in Fig. 3, which gives the ^{252}Cf yield calculated by varying the thermal neutron flux density and irradiation time at a constant φ. The calculation results are generalized in Fig. 4, where the thermal neutron flux density maximizing the ^{252}Cf yield is plotted as a function of the irradiation time for different φ.

The findings show that increasing φ to the limit of the range under consideration is accompanied by an increase in the yield; this tendency is maintained even if $\varphi > 4 \cdot 10^{14}$ $cm^{-2} \cdot sec^{-1}$.

If φ is constant, on the other hand, for any given irradiation time there is a particular thermal neutron flux density (or neutron spectrum hardness) at which the ^{252}Cf yield reaches a maximum. Increasing Φ further does not improve the yield, and has no effect at best. It is also inadvisable to "harden" the neutron spectrum so much that Φ would be reduced.

The reason for this behavior becomes apparent from an inspection of Table 1. The rate of progress of curium nuclei along the buildup chain is limited by the interaction rate of

TABLE 1. Thermal Cross Sections and Resonance Integrals of Nuclides, barns*

Nuclide	Cross section for 2200 m·sec^{-1} neutron velocity		Resonance integral at infinite dilution (E ≥ 0.625 eV)	
	$\sigma_{n,\gamma}$	$\sigma_{n,f}$	$I_{n,\gamma}$	$I_{n,f}$
^{244}Cm	10,0	1,5	585,0	17,1
^{245}Cm	383,0	2161,0	104,0	766,0
^{246}Cm	1,4	0,17	119,0	10,0
^{247}Cm	58,0	72,3	500,0	761,0
^{248}Cm	2,89	0,11	251,0	14,0
^{249}Bk	1600,0	0	4000,0	0
^{249}Cf	495,0	1720,0	777,0	1863,0
^{250}Cf	1701,0	0	11600,0	0
^{251}Cf	2849,0	4801,0	1600,0	5400,0
^{252}Cf	20,4	32,0	43,5	110,0
^{253}Cf	12,0	1100,0	12,0	2000,0

*1 barn = 10^{-28} m^2.

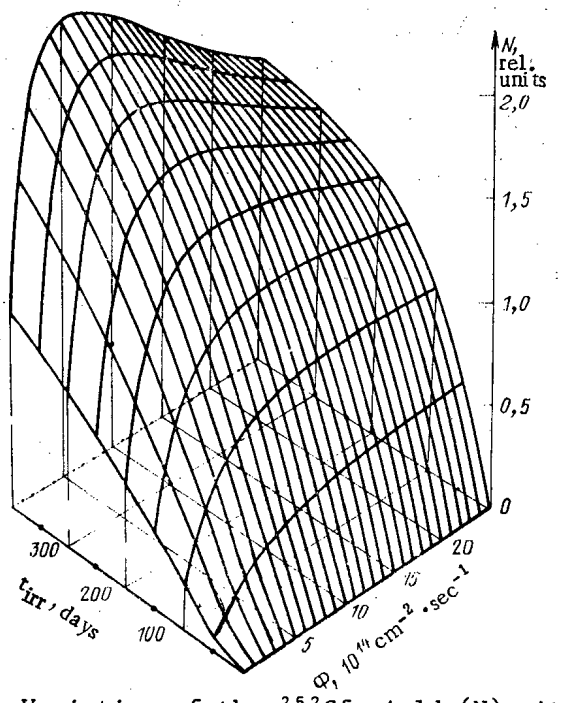

Fig. 3. Variation of the ^{252}Cf yield (N) with the irradiation time and thermal neutron flux density ($\varphi = 1.3 \cdot 10^{14}$ cm^{-2}·sec^{-1}).

neutrons with the nuclides having the smallest constants – ^{246}Cm and ^{248}Cm. Since the resonance integrals of these nuclides exceed their thermal cross sections by a factor of about 100, the buildup rate of transcurium nuclei is essentially controlled by the thermal neutron flux density. However, both the thermal and epithermal flux densities contribute comparably to the ^{252}Cf burnup rate. There is, consequently, a region within which a reduction of Φ (at constant φ and irradiation time) will appreciably decrease the ^{252}Cf burnup rate almost without affecting the production rate, and thus led to an increased yield. On the other hand, when the thermal neutron flux density drops below a certain limiting value, the resultant decrease in the ^{246}Cm and ^{248}Cm buildup rate and ^{249}Cm burnup rate [7] produces a net reduction of the ^{252}Cf yield. Within the range considered, the optimal value is largely determined by the irradiation time and varies only very little with φ (see Fig. 4).

The results obtained are not all-inclusive and may be modified in individual cases – for instance, if the isotropic composition of the parent curium is changed. Nonetheless, the relationships derived among the basic irradiation parameters may be useful for optimizing the irradiation channel characteristics in the production of ^{252}Cf.

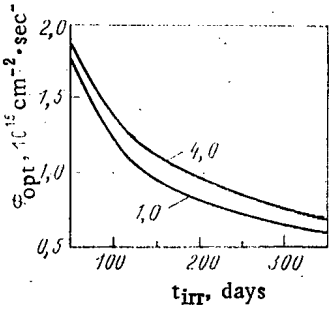

Fig. 4. Optimal thermal neutron flux density Φ_{opt} maximizing the ^{252}Cf yield, plotted as a function of the irradiation time (the curves are labeled with the values of φ, 10^{14} $cm^{-2} \cdot sec^{-1}$).

LITERATURE CITED

1. R. Benjamin et al., USERDA Report DP-1394 (1975).
2. L. Epel, J. Chernick, B. Manowitz, and W. Winche, "Transuranium element production in epithermal reactors," Trans. Am. Nucl. Soc., 8, No. 1, 57 (1965).
3. A. K. Krasin et al., Izv. Akad. Nauk BSSR, Ser. Fiz.-Energ. Nauk, No. 3, 5 (1975).
4. J. Zamyatin et al., in: Proc. of the Paris Symposium of the Intern. Symp. on ^{252}Cf Utilization, CONF-760436 (1976), Vol. 2, p. 25.
5. L. King, in: Proc. of the Paris Symposium of the Intern. Symp. on ^{252}Cf Utilization, CONF-760436 (1976), Vol. 2, p. 1.
6. Yu. N. Polyakov, "A computer program for radionuclide formation and burnup in a nuclear reactor," NIIAR Preprint 37(552), Dimitrovgrad (1982).
7. Yu. G. Toparov et al., "Operating conditions for berkelium-249 production and some of its applications," NIIAR Preprint 50(503), Dimitrovgrad (1981).

How To Comply With The New Copyright Law

Participation in the Copyright Clearance Center (CCC) assures you of legal photocopying at the moment of need.

Libraries everywhere have found the easy way to fill photocopy requests legally and instantly, without the need to seek permissions, from more than 3000 key publications in business, science, humanities, and social science. You can:

Fill requests for multiple copies, interlibrary loan (beyond the CONTU guidelines), and reserve desk without fear of copyright infringement.

Supply copies from CCC-registered publications simply and easily.

The Copyright Clearance Center is your one-stop place for on-the-spot clearance to photocopy for internal use.

Its flexible reporting system accepts photocopying reports and returns an itemized invoice. You send only one convenient payment. CCC distributes it to the many publishers whose works you need.

And, you need not keep any records, the CCC computer will do it for you. Register now with the CCC and you will never again have to decline a photocopy request or wonder about compliance with the law for any publication participating in the CCC.

To register or for more information, just contact:

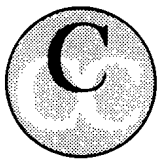

Copyright Clearance Center
21 Congress Street
Salem, Massachusetts 01970
(617) 744-3350

a not-for-profit corporation

NAME _____ TITLE _____

ORGANIZATION _____

ADDRESS _____

CITY _____ STATE _____ ZIP _____

COUNTRY _____ TELEPHONE _____

CHANGING YOUR ADDRESS?

In order to receive your journal without interruption, please complete this change of address notice and forward to the Publisher, 60 days in advance, if possible.

(Please Print)

Old Address:

name

address

city

state (or country) zip code

New Address

name

address

city

state (or country) zip code

date new address effective

name of journal

THE LANGUAGE OF SCIENCE
Plenum
PUBLISHING CORPORATION

233 Spring Street, New York, New York 10013

MEASUREMENT TECHNIQUES
Izmeritel'naya Tekhnika
Vol. 27, 1984 (12 issues) $520

MECHANICS OF COMPOSITE MATERIALS
Mekhanika Kompozitnykh Materialov
Vol. 20, 1984 (6 issues) $430

METAL SCIENCE AND HEAT TREATMENT
Metallovedenie i Termicheskaya Obrabotka Metallov
Vol. 26, 1984 (12 issues) $540

METALLURGIST
Metallurg
Vol. 28, 1984 (12 issues) $555

PROBLEMS OF INFORMATION TRANSMISSION
Problemy Peredachi Informatsii
Vol. 20, 1984 (4 issues) $420

PROGRAMMING AND COMPUTER SOFTWARE
Programmirovanie
Vol. 10, 1984 (6 issues) $175

PROTECTION OF METALS
Zashchita Metallov
Vol. 20, 1984 (6 issues) $480

RADIOPHYSICS AND QUANTUM ELECTRONICS
Izvestiya Vysshikh Uchebnykh Zavedenii, Radiofizika
Vol. 27, 1984 (12 issues) $520

REFRACTORIES
Ogneupory
Vol. 25, 1984 (12 issues) $480

SIBERIAN MATHEMATICAL JOURNAL
Sibirskii Matematicheskii Zhurnal
Vol. 25, 1984 (6 issues) $625

SOIL MECHANICS AND FOUNDATION ENGINEERING
Osnovaniya, Fundamenty i Mekhanika Gruntov
Vol. 21, 1984 (6 issues) $500

SOLAR SYSTEM RESEARCH
Astronomicheskii Vestnik
Vol. 18, 1984 (6 issues) $365

SOVIET APPLIED MECHANICS
Prikladnaya Mekhanika
Vol. 20, 1984 (12 issues) $520

SOVIET ATOMIC ENERGY
Atomnaya Énergiya
Vols. 56-57, 1984 (12 issues) $560

SOVIET JOURNAL OF GLASS PHYSICS AND CHEMISTRY
Fizika i Khimiya Stekla
Vol. 10, 1984 (6 issues) $235

SOVIET JOURNAL OF NONDESTRUCTIVE TESTING
Defektoskopiya
Vol. 20, 1984 (12 issues) $615

SOVIET MATERIALS SCIENCE
Fiziko-khimicheskaya Mekhanika Materialov
Vol. 20, 1984 (6 issues) $445

SOVIET MICROELECTRONICS
Mikroélektronika
Vol. 13, 1984 (6 issues) $255

SOVIET MINING SCIENCE
Fiziko-tekhnicheskie Problemy Razrabotki Poleznykh Iskopaemykh
Vol. 20, 1984 (6 issues) $540

SOVIET PHYSICS JOURNAL
Izvestiya Vysshikh Uchebnykh Zavedenii, Fizika
Vol. 27, 1984 (12 issues) $520

SOVIET POWDER METALLURGY AND METAL CERAMICS
Poroshkovaya Metallurgiya
Vol. 23, 1984 (12 issues) $555

STRENGTH OF MATERIALS
Problemy Prochnosti
Vol. 16, 1984 (12 issues) $625

THEORETICAL AND MATHEMATICAL PHYSICS
Teoreticheskaya i Matematicheskaya Fizika
Vol. 58-61, 1984 (12 issues) $500

UKRAINIAN MATHEMATICAL JOURNAL
Ukrainskii Matematicheskii Zhurnal
Vol. 36, 1984 (6 issues) $500

Send for Your Free Examination Copy

Plenum Publishing Corporation, 233 Spring St., New York, N.Y. 10013
In United Kingdom: 88/90 Middlesex St., London E1 7EZ, England
Prices slightly higher outside the U.S. Prices subject to change without notice.

I [AN JOURNALS IN THE PHYSICAL [D MATHEMATICAL SCIENCES

AVAILABLE IN ENGLISH TRANSLATION

AL(LOGIC
Alge
Vol. es) $360

AST
Astro
Vol. s) $420

AUT(ID REMOTE CONTROL
Avtom... ...elemekhanika
Vol. 45, 1984 (24 issues) $625

COMBUSTION, EXPLOSION, AND SHOCK WAVES
Fizika Goreniya i Vzryva
Vol. 20, 1984 (6 issues) $445

COSMIC RESEARCH
Kosmicheskie Issledovaniya
Vol. 22, 1984 (6 issues) $545

CYBERNETICS
Kibernetika
Vol. 20, 1984 (6 issues) $445

DIFFERENTIAL EQUATIONS
Differentsial'nye Uravneniya
Vol. 20, 1984 (12 issues) $505

DOKLADY BIOPHYSICS
Doklady Akademii Nauk SSSR
Vols. 274-279, 1984 (2 issues) $145

FLUID DYNAMICS
Izvestiya Akademii Nauk SSSR, Mekhanika Zhidkosti i Gaza
Vol. 19, 1984 (6 issues) $500

FUNCTIONAL ANALYSIS AND ITS APPLICATIONS
Funktsional'nyi Analiz i Ego Prilozheniya
Vol. 18, 1984 (4 issues) $410

GLASS AND CERAMICS
Steklo i Keramika
Vol. 41, 1984 (6 issues) $590

HIGH TEMPERATURE
Teplofizika Vysokikh Temperatur
Vol. 22, 1984 (6 issues) $520

HYDROTECHNICAL CONSTRUCTION
Gidrotekhnicheskoe Stroitel'stvo
Vol. 18, 1984 (12 issues) $385

INDUSTRIAL LABORATORY
Zavodskaya Laboratoriya
Vol. 50, 1984 (12 issues) $520

INSTRUMENTS AND EXPERIMENTAL TECHNIQUES
Pribory i Tekhnika Eksperimenta
Vol. 27, 1984 (12 issues) $590

JOURNAL OF APPLIED MECHANICS AND TECHNICAL PHYSICS
Zhurnal Prikladnoi Mekhaniki i Tekhnicheskoi Fiziki
Vol. 25, 1984 (6 issues) $540

JOURNAL OF APPLIED SPECTROSCOPY
Zhurnal Prikladnoi Spektroskopii
Vols. 40-41, 1984 (12 issues) $540

JOURNAL OF ENGINEERING PHYSICS
Inzhenerno-fizicheskii Zhurnal
Vols. 46-47, 1984 (12 issues) $540

JOURNAL OF SOVIET LASER RESEARCH
A translation of articles based on the best Soviet research in the field of lasers
Vol. 5, 1984 (6 issues) $180

JOURNAL OF SOVIET MATHEMATICS
A translation of Itogi Nauki i Tekhniki and *Zapiski Nauchnykh Seminarov Leningradskogo Otdeleniya Matematicheskogo Instituta im. V. A. Steklova AN SSSR*
Vols. 24-27, 1984 (24 issues) $1035

LITHOLOGY AND MINERAL RESOURCES
Litologiya i Poleznye Iskopaemye
Vol. 19, 1984 (6 issues) $540

LITHUANIAN MATHEMATICAL JOURNAL
Litovskii Matematicheskii Sbornik
Vol. 24, 1984 (4 issues) $255

MAGNETOHYDRODYNAMICS
Magnitnaya Gidrodinamika
Vol. 20, 1984 (4 issues) $415

MATHEMATICAL NOTES
Matematicheskie Zametki
Vols. 35-36, 1984 (12 issues) $520

continued on inside back cover